République Algérienne Démocratique et Populaire
Ministère de l'Enseignement Supérieur et de la Recherche Scientifique
Université 8 Mai 1945 Guelma

Faculté : Sciences et Technologie
Département : Génie civil et d'Hydraulique
Laboratoire de domiciliation : Génie civil et d'Hydraulique

THÈSE

EN VUE DE L'OBTENTION DU DIPLOME DE DOCTORAT EN 3ème CYCLE

Domaine : **Sciences et Technologie** Filière : **Génie civil**
Spécialité : **Structures**

Présentée par

GUENDOUZ Ilies

Intitulée

Contribution à la modélisation par MEF des structures en FGM

Soutenue le : 08/11/2023 Devant le Jury composé de :

Nom et Prénom	Grade	Université	
Mr NAFA Zahereddine	Professeur	Univ. 8 Mai 1945- Guelma	Président
Mr GUENFOUD Mohamed	Professeur	Univ. 8 Mai 1945- Guelma	Encadreur
Mr BENMARCE Abdelaziz	Professeur	Univ. 8 Mai 1945- Guelma	Examinateur
Mr BOUZIANE Salh	Professeur	Univ. 20 Aout 1955- Skikda	Examinateur
Mr KHEBIZI Mourad	MCA	Univ. Frères Mentouri Constantine	Invité
Ms ZIOU Hassina	MRA	CNERIB	Invité

Année Universitaire : 2022/2023

بسم الله الرحمن الرحيم

 https://orcid.org/0000-0002-6920-3135

Dedication

I dedicate my dissertation work to All my family members and many friends. A special feeling of gratitude to my loving parents, Ali and Ourida Saoudi whose words of encouragement and push for tenacity ring in my ears. I will always appreciate all they have done.

I dedicate this work and give special thanks to my best friend Mr Herabi Ayyoub for being there for me throughout the entire doctorate program.

Thanks

My most distinguished thanks go to my thesis director Pr Guenfoud Mohamed, I deeply appreciate how you have been continuously encouraging and guiding me in the last three years, and also how you have always been so friendly and supportive of all of my efforts and struggles. Working under your supervision has been very enjoyable and I have learned and grown a lot.

I also thank Pr. Khebizi Mourad for the fruitful discussions we had throughout my thesis work. Sincere thanks to Pr Abdelkrim Kadid for proofreading (university of Batna 2), Special thanks also to Pr Rached El Fatmi for his contribution to the CSB project (the National School of Engineers of Tunis (ENIT)).

I thank my colleagues and all the personnel of university of guelma 8 mai 1945.

My sincere thanks to my family, friends and anyone who has contributed in any way to the completion of this work.

Finally, I would like to express my deepest thanks to all the members of the jury

Abstract

In this work, we present a torsional-bending analysis of different homogeneous or FGM beams using a refined beam theory built on 3D Saint-Venant's solution (RBT/SV) and taking into account the edge effects. In this theory, the displacement models include Poisson's effects, out-of-plane deformations and distortions extracted from 3D Saint-Venant's solution. These modes, which reflect the mechanical behavior of the cross-section, lead to a beam theory that actually corresponds to the cross-section type (shape and materials). To implement this approach, a tool called CSB (Cross-Section and Beam analysis) is provided and is based on a first cross-section analysis solved by 2D-FEM computations to get the sectional deformation modes, and then the equilibrium beam problem is solved by 1D-FEM computation according to the displacement model. The results obtained for RBT models are systematically compared with other models in the literature, 3D-FEM which we also consider as a reference, and those provided by the full Saint-Venant beam theory (SVBT) calculations. The results clearly show the efficiency of RBT by greatly improving the internal solution, and at the same time, a detailed 3D solution is obtained in the edge region.

Résumé

Dans ce travail, nous présentons une analyse en torsion-flexion de différentes poutres homogènes ou FGM en utilisant une théorie de poutre raffinée construite sur la solution 3D de Saint-Venant (RBT/SV) et prenant en compte les effets de bord. Dans cette théorie, les modèles de déplacement incluent les effets de Poisson, les déformations hors-plan et les distorsions extraites de la solution 3D de Saint-Venant. Ces modes, qui traduisent le comportement mécanique de la section, conduisent à une théorie de poutre qui correspond effectivement au type de section (forme et matériaux). Pour mettre en œuvre cette approche, un outil appelé CSB (Cross-Section and Beam analysis) est fourni et est basé sur une première analyse de section résolue par des calculs 2D-FEM pour obtenir les modes de déformation de la section, puis le problème d'équilibre de la poutre est résolu. Par calcul 1D-FEM selon le modèle de déplacement. Les résultats obtenus pour les modèles RBT sont systématiquement comparés avec d'autres modèles de la littérature, 3D-FEM que nous considérons également comme référence, et ceux fournis par les calculs de la théorie complète des poutres de Saint-Venant (SVBT). Les résultats montrent clairement l'efficacité de RBT en améliorant considérablement la solution interne, et en même temps, une solution 3D détaillée est obtenue dans la région de bord.

ملخص

في هذا العمل ، نقدم تحليل الانحناء الالتوائي لروافد مختلفة متجانسة أو متدرجة وضيفيا باستخدام نظرية شعاع مصقولة مبنية على حل سان فونوه ثلاثي الابعاد و مع مراعاة تأثيرات الحافة. في هذه النظرية ، تشتمل نماذج الإزاحة على تأثيرات بواسون والتشوهات خارج المقطع العرضي والتشوهات المستخرجة من حل سان فونوه ثلاثي الابعاد. هذه الأنماط التي تعكس السلوك الميكانيكي للمقطع العرضي ، تؤدي إلى نظرية الرافدة التي تتوافق في الواقع مع نوع المقطع العرضي (الشكل والمواد). لتنفيذ هذا النهج ، يتم توفير أداة تسمى CSB (تحليل المقطع العرضي والشعاع) وتعتمد على تحليل المقطع العرضي الأول الذي تم حله بواسطة حسابات 2D-FEM للحصول على أوضاع التشوه المقطعي ، ومن ثم يتم حل مشكلة الرافدة بواسطة حساب 1D-FEM وفقًا لنموذج الإزاحة. تتم مقارنة النتائج التي تم الحصول عليها لنماذج RBT بشكل منهجي مع النماذج الأخرى في الأدبيات، 3D-FEM التي نعتبرها أيضًا مرجعًا ، وتلك التي توفرها حسابات نظرية شعاع سان فونوه ثلاثي الابعاد الكاملة. تظهر النتائج بوضوح كفاءة RBT من خلال تحسين الحل الداخلي بشكل كبير ، وفي الوقت نفسه ، يتم الحصول على حل ثلاثي الأبعاد مفصل في منطقة الحافة.

.

Contents

List of tables

List of Figures

1 GENERAL INTRODUCTION

1.1 Introduction

The study of materials and their properties is an important area of research. Since ancient times, the driving force behind the discovery of new materials has been a great motivation for the development of human needs. These are related, on the one hand, to the problems man has to solve for his material life and, on the other hand, to his intellectual need to know and understand the world around him. Scientists introduce the field of materials science using familiar objects that represent the main families of metals, ceramics and polymers. By explaining their properties, how materials are created and the processes involved in making objects, they show how materials science brings together engineering and technology with physics, chemistry and biology. They also show how materials influence construction, architecture, communications, media and fine art.

The development of composite materials has made it possible to combine specific properties of various materials in a single part. In order to optimise these properties locally, for example by combining a high stiffness material with the surface of tough material, the problem of the interface arises. This sudden transition of compositions can generate locally high-stress concentrations. The solution of a continuous transition of the desired properties, through a compositional gradient, makes it possible to reduce this singularity through the use of Functionally Graded Materials (FGMs) (see Fig.1.1).

Functionally graded materials are among the most widely used and widespread inhomogeneous complex materials during the past few decades, due to their great advantages of microstructures, spatially structure, and properties through the irregular distribution of the reinforcement phase [1]. As a new composite material, functionally graded materials have a tremendous ability to reduce stress concentration and alleviate thermal stress, these unique features make it a preferred material for use in various new structures. There are many uses of functionally graded materials in many fields, e.g., the automotive and aircraft sectors, in the field of civil and mechanical engineering, as well as in various elements of machines [2]. The mechanical properties of functionally graded materials differ through a continuous gradient of two or more com- ponents (often between metal and ceramic) in one direction (through length or thickness) or two directions (length and thickness). Various and efficient structural finite elements (beams, plates, and shells) require suitable homogenization procedures in order to reach the maximum rigidity of the shear, bending, transverse, and torsional shear properties [3, 4]. It should be noted that a huge number of papers dealing with modeling and simulation

of the static and dynamic problems of functionally graded material beams can be found in many pieces of literature's works.

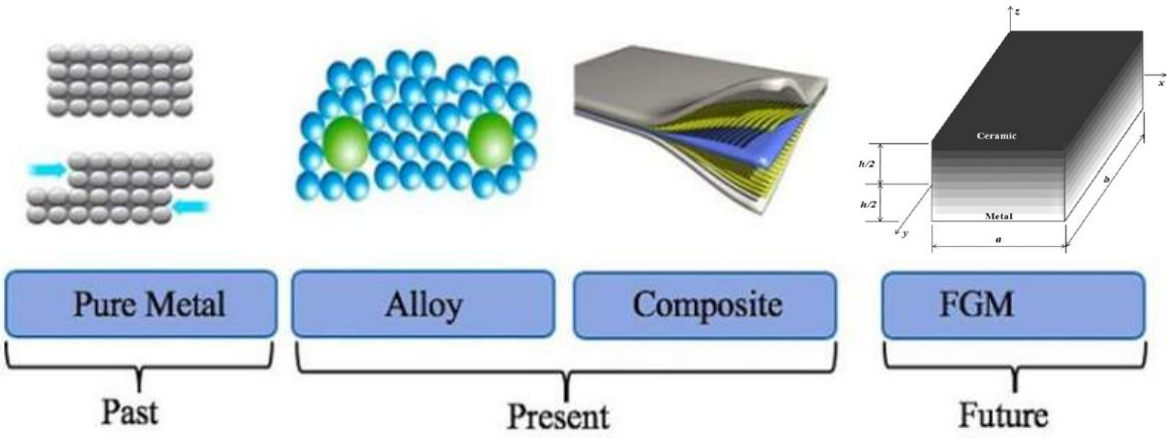

Fig 1. 1: History of engineering materials leading to FGM development

Thus, the use of beams with increasingly thin and heterogeneous sections (composites) is a trend in new construction technologies for reasons of economy, performance, and service. The purpose of a heterogeneous or FG composite beam is to benefit from the qualities of each of its constituent materials. As a result, it is crucial to be able to track the 3D state of each material (mechanical, thermal, etc.) because each one must be evaluated in accordance with its own criteria.

A beam is practically assimilated to a one dimensional medium (1D) within the framework of the assumptions generally accepted in the classical beam theory (RDM). This extremely simplistic view has the advantage of being simple, but it is insufficient to describe the spatial character (3D) of the real mechanical behavior of a thin profile or a heterogeneous beam.

When talking about the classical references in beam theories, i.e. those whose results are widely used, there are four names that appear systematically: Saint-Venant, Bernoulli, Timoshenko and Vlasov. Their theories were established for the isotropic homogeneous case. All current construction standards are based on computations inherent to these classical theories.

Nevertheless, the classical beam theories Challenges such as the constant concern for optimization and cost reduction (rational use of materials, lightening of structures), the working of parts under increasingly severe service conditions, as well as other criteria of various considerations, impose on engineers more precise analyses and more accurate models. In addition, the use of composite materials is increasing for performance reasons. Indeed,

modern composite materials (FGMs) are known to have interesting mechanical properties such as: controllable elastic constants, high mass resistance ratios, good fatigue resistance, and other criteria related to environmental behaviour like corrosion for example. And in contrast to homogeneous beams, the mechanical behaviour of composite beams is difficult to understand (structural couplings due to material anisotropies and arrangements, large cross-sectional deformation effects), and their calculation becomes complex.

All of these factors combined express the necessity of developing more accurate models that meet current challenges and needs. And despite the availability of more advanced computational techniques such as 3D finite element method (3D FEM), beam models retain their advantages in many applications due to their low computational cost and ease of implementation. Beam theories are still the preferred modeling method for slender structures.

In order to improve on the predictions of classical theories that suppose that the cross-section is undeformable, it is necessary to develop new beam models that can now account for certain phenomena that the classical models are unable to analyse. This can be achieved through higher order beam theories which have a richer kinematics and allow the cross-section to be deformed. The following displacement field ξ is considered:

$$\boldsymbol{\xi} = \underbrace{\boldsymbol{u} + \boldsymbol{\omega} \wedge \boldsymbol{GM}}_{\text{mouvement rigide de section}} + \underbrace{\sum \eta_i \boldsymbol{\mathcal{M}}^i}_{\text{enrichissement}}$$

with $\boldsymbol{u}$ and $\boldsymbol{\omega}$ respectively translations and rotations of the current section, $\boldsymbol{GM}$ location vector in the section plane, η_i new kinematic parameters and $\boldsymbol{\mathcal{M}}^i$ section deformation modes; the vectors are noted in **bold type**. Classical beam theories are limited to the rigid solid motion of the cross-section. Higher order beam theories move beyond the classical models and allow the cross-section to deform according to a set of deformation modes $\boldsymbol{\mathcal{M}}^i$.

Among the pioneers was the Vlasov's model [5] which, by adding a cross-sectional warping term, allowed the torsional behaviour of thin open profiles to be computed correctly and to account for the phenomenon of non-uniform warping. The concept of enriching the kinematics seems simple, and the approach proves successful. This is evidenced by the large number of papers published on beam theories in the last decades. The main difficulty is to find a systematic way to derive the appropriate cross-sectional deformation modes $\boldsymbol{\mathcal{M}}^i$ for any given problem. The results of these theories depend essentially on this new term of enrichment. The key feature in the development of such beam models is to keep a good compromise between the simplicity of the model, its scope and its accuracy.

1.2 Objective

This study is particularly concerned with the problems of beam equilibrium analysis of any cross-section made of functionally graded materials (FGMs). The goal is to extend the Cross Section & Beam analysis (CSB) project by calculating FGM beams using higher order models based on the 3D Saint-Venant's solution (RBT/SV). In these models, the displacement models include Poisson's effects, out-of-plane deformations and distortions. For a given section, the sectional displacement modes are derived from the computation of the particular 3D SV's solution. These modes, which reflect the mechanical behavior of the cross-section, lead to a beam theory that actually corresponds to the cross-section type in terms of shape and material. In addition, the focus is on boundary conditions by connecting to a detailed 3D solution close to the edges.

1.3 Thesis organization

Apart from this introduction (Chapter 1) and the conclusion (Chapter 6), this document is divided into 4 chapters:

The second chapter covers the position of the problem through a general representation of composite materials (structures), and the cracking mechanisms of composites with emphasis on the delamination phenomenon. Then, we move on to functionally graded materials (FGMs) and discuss their history, the direction of their research and development, the areas of their application, and finally the functioning of their mechanical properties.

The third chapter recalls the state of the art by presenting the different approaches to beam theories. This will be an opportunity to situate the classical beam theories of Bernoulli and Timoshenko in relation to that of Saint-Venant (at least for the isotropic homogeneous case). In the first place, particular attention is attributed to the approach of Saint-Venant in which are included: the 3D SV problem, the 3D SV solution, the 1D SV beam theory and the SV Principle, as well as to the mechanical characteristics of the section, which are fundamental to understand the mechanics of a section or a beam, Vlasov's hindered torsion is also taken into account in this chapter.

The fourth chapter presents the RBT/SV models as a whole (kinematic modelling, generalized quantities, equations of motion). The different strong formulations of the problem concerning the generalized stress-displacement and displacement unknowns are presented. in addition, it proposes a computational method whose objective is to better model the edge conditions and

thus obtain a detailed solution close to the edges and, sometimes, a better approximation of the inner solution.

The fifth chapter is devoted to the validation of the proposed RBT/SV models. For this purpose, a wide range of FGM beams subjected to different mechanical behaviours (bending, torsion, and bending-torsion) are treated. The numerical and 3D results obtained with homogeneous and FGM beams are systematically compared to other models in the literature and to those provided by the full Saint-Venant Beam Theory (SVBT) computations.

2 Composite materials and functionally graded materials

2.1 Introduction

Composite materials offer considerable advantages over traditional materials. They offer many functional advantages: mechanical and chemical resistance, lightness, reduced maintenance, freedom of shape. Their characteristics make it possible to increase the service life of certain equipment. They also improve design possibilities by allowing the creation of complex shapes that can fulfil several functions and making structures lighter.

The development of advanced composite materials has reached a new level due to the wealth of experience and knowledge in design, testing and manufacturing. they offer designers and manufacturers new possibilities to combine materials, functions and shapes in the design. this extends the technical possibilities and better satisfies the sometimes contradictory needs (weight - function) that are difficult for traditional homogeneous materials to meet.

The world of composite materials has changed by revealing materials that are different from conventional heterogeneous materials. A composite material is defined as a structural material consisting of two or more constituents that are combined at the macroscopic level and are insoluble in each other. It should be understood that the above composite material is not the by-product of any chemical reaction between its two or more constituents. One of its constituents is called the reinforcing phase, in which the reinforcing phase material is incorporated, the reinforcing phase material may be in the form of fibres, particles or flakes (e.g., glass fibres). And the other is called the matrix. The matrix phase materials are usually continuous (e.g., epoxy resin). The reinforcement phase is strong and hard and may not be light, while the matrix phase is light but weak.

Functionally graded materials (FGMs) are part of the composite materials and are designed to meet various functionalities, where they are able to survive in a harsh working environment, without losing their properties. FGMs are characterised by a compositional gradient from one material to another, which is completely different from conventional composite materials. As a new composite material, functionally graded materials have a tremendous ability to reduce stress concentration and alleviate thermal stress, these unique features make it a preferred material for use in various new structures. FGMs are used in many fields such as automotive, power generation, aerospace, structural and bioengineering.

2.2 Structure of composite materials

Composite materials consist of two or more components. The principal components refer to the reinforcement (fiber) and the matrix, or the reinforcement phase and the matrix phase. The reinforced phase is a continuous or chopped filament of high strength and rigidity. It is

considered the basic phase because it bears the external loads to which the composite materials are exposed, and it is dispersed and surrounded by a matrix. The matrix phase is the coherent material surrounding the reinforcement phase, whose role is to support and protect the reinforcement phase from external loads to which the compound is exposed. So, the adhesion between the fiber and the matrix is very critical.

The properties of the composite materials depend on the reinforcement and its chemical and physical surface states, including the type, properties, and distribution of the composite materials. In addition, their properties depend on the compound methods and environmental conditions [6][7].

2.2.1 Matrix phase

The matrix is a homogeneous base material that forms the bulk of a composite material layer, where it has many functions, including aggregating the fibers together, thus transferring load (in particular transverse stress, intraluminal shear stress and bearing stress) across the interface to the reinforcing fibers from external sources. The matrix dominates certain properties of the composite, such as stiffness and transverse strength. These properties allow the composite material to withstand many conditions, such as abrasion resistance, temperature resistance and chemical resistance, as well as dominating external characteristics such as appearance. Matrix materials can be ceramics, metals or polymers. Due to the ease of manufacturing highly complex parts with low manufacturing costs for the capital investment, polymeric matrices are the most common and productive [8].

2.2.2 Reinforcing phase (Fibers)

It is a natural or man-made substance It has a longitudinal shape. Fibers are often used in the manufacture of other materials, that are usually responsible for the anisotropy of the composite. The strongest engineering materials often incorporate fibers such as carbon fiber and ultra-high-molecular-weight polyethylene. As this fiber provides strength and stiffness, reduce thermal expansion, it is also used to reduce and increase the physical properties such as electric conductivity, thermal conductivity. In any composite, it highlights not only the physical properties, but also the cost. where Fiber reinforcements tradeoff between performance and cost [8]. The fibers can be classified into continuous or discontinuous fibers in order to obtain maximum strength and stiffness. Moreover, there are a wide variety of fiber forms that are used to compose the material and meet the requirements of different processing methods (Fig.2.1).

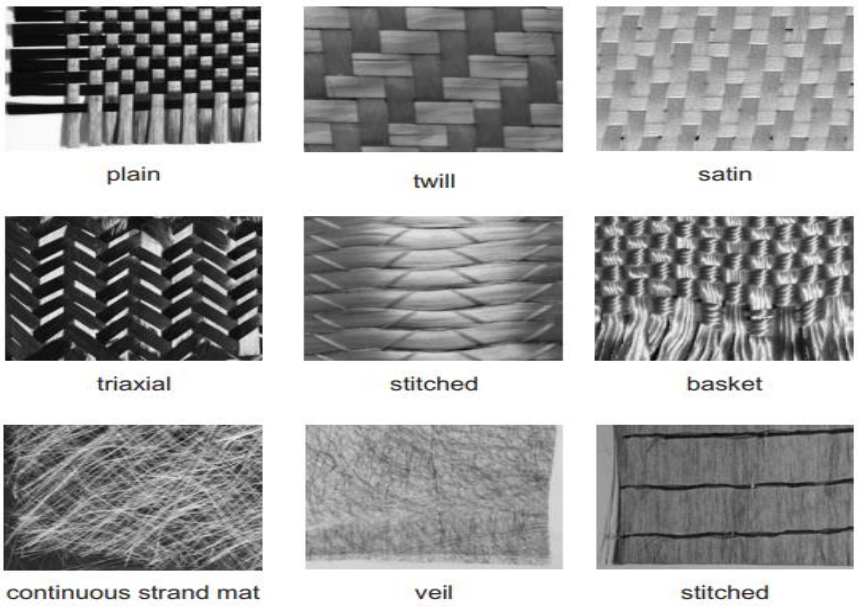

Fig 2. 1: Fiber forms [8]

2.3 Classification of Composite Materials

Material composite are usually classified according to the shape of the reinforcement and the type of the matrix [6]. According to the shape of reinforcement, it can be divided into four classes as follows (Fig.2.2).

- Laminated composite
- Continuous fiber composite
- Fine composite
- Shortcut fiber composite

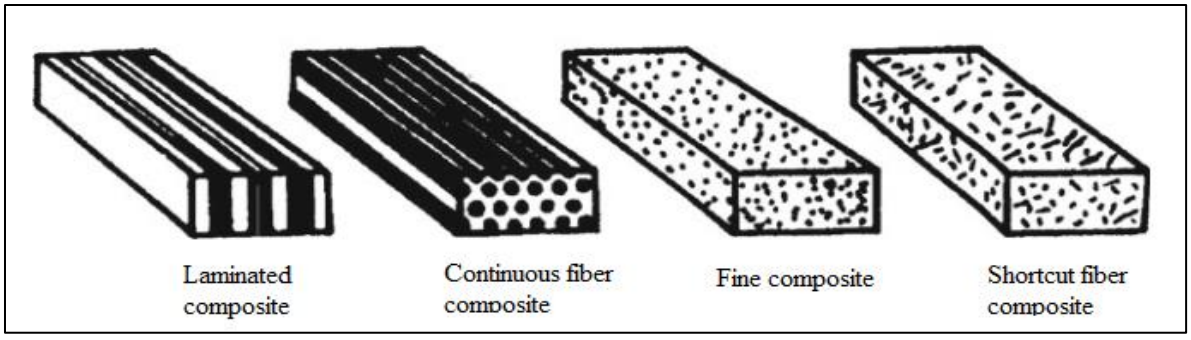

Fig 2. 2: Diagram of structures of composite materials [6]

Composite materials can also be divided into three categories by the nature of the matrix as follows:

- Polymer matrix composite (PMC)
- Metal matrix composite (MMC)

- Ceramic matrix composite (CMC)

2.4 Advantages and disadvantages of composites materials

Composite materials are widely used for the primary structures of industrial, commercial, aerospace and marine structures. Composite parts, therefore, have both advantages and disadvantages compared to the metal parts they are intended to replace [9].

2.4.1 Advantages of composite materials

- Weight reduction – savings in the range 20% - 50% are often quoted.
- Mechanical properties can be tailored by 'lay-up' design, with tapering thicknesses of reinforcing cloth and cloth orientation.
- High impact resistance – Kevlar (aramid) armor shields planes, too – for example, reducing accidental damage to the engine pylons which carry engine controls and fuel lines.
- High damage tolerance improves accident survivability.
- 'Galvanic' - electrical – corrosion problems which would occur when two dissimilar metals are in contact (particularly in humid marine environments) are avoided. Here non-conductive fiberglass plays an important role.

2.4.2 Disadvantages of composite materials

- Some higher recurring costs,
- Higher nonrecurring costs,
- Higher material costs,
- Non-visible impact damage,
- Repairs are different than those to metal structure,
- Isolation needed to prevent adjacent aluminum part galvanic corrosion.

2.5 The interface and the interphase

The interface is the two-dimensional boundary between the fiber and matrix (i.e., a boundary between two layers of different chemistry and/or microstructure). It is quite critical to control composite properties because fiber-matrix interaction occurs through the interface. This interaction be able to happen through three mechanisms (Fig.2.3 showing some examples of the various interactions at the fiber-matrix interface)[10]:

- Mechanical coupling interlocking of the two materials
- Physical coupling or electrostatic interaction
- Covalent bonding between the fiber and the matrix

However, these boundaries are rarely free of chemical interaction, so it is also possible to define a region called interphase, which is the volume of material affected by the interaction at the interface.

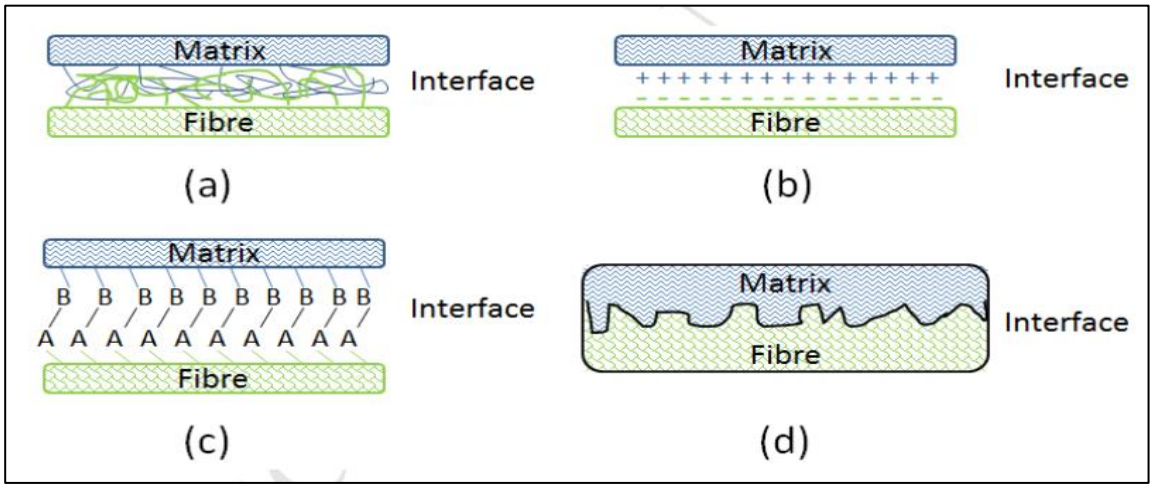

Fig 2. 3: Fiber-matrix interfacial bonding mechanisms: (a) molecular entanglement following interdiffusion, (b) electrostatic adhesion (c) chemical bonding and (d) mechanical interlocking [11]

Interphase is a three-dimensional region where coating/fiber and matrix diffused into each other's domain and form a flexible, three-dimensional polymer network. Fig.2.4 Illustrates a schematic diagram of a composite interphase, with a cross-section of fiber–reinforced composite (left) and a detail of the region at the fiber surface (right). The main objective of this 3D network is to provide a lattice that the matrix molecule can penetrate and come in close proximity to fibers. Interphase can form on the surface of the fiber, in order to control the properties of this interface, surface treatments are often used on the fiber prior to its use in composite structures. Surface treatment generally involves surface oxidation of the fiber, either electrolytically or using gas or liquid chemicals. this provides some functionality on the fiber surface by increasing the surface area and the number of reactive groups on the surface, and can improve adhesion in terms of mechanical interlocking and physicochemical interactions.

Interphase consider is responsible for transferring the load from the matrix to the fibers. As for the formation of interphase region and the resulting properties are some of the areas that poorly understood yet.

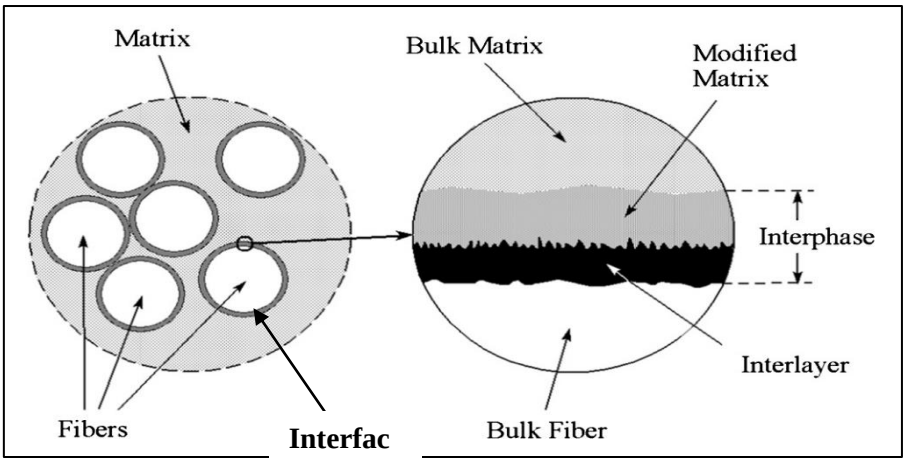

Fig 2. 4: Schematic illustration of a composite interphase [12]

2.6 Delamination and FGMs

2.6.1 Delamination

One of the main advantages of high fiber reinforced composite laminates is the ability to orient the fibers in all layers to achieve properties. often stiffness and strength, adapted to the loads in the intended directions. For example, a laminated plate may have twice the tensile stiffness in one direction than the other. Despite excellent in-plane properties, laminates have a problem unique to laminate materials: inter-laminar failure. This failure mechanism is characterized by decohesion between the laminate plies. It is generally called "delamination".

A laminate under load shows different stages of degradation. In the most "traditional" defect evolution scenario [13], the matrix and the fiber/matrix interface are the first to degrade (Fig. 2.5.a). Thus, the first defects are fiber/matrix decohesion and matrix microcracking. Then, these defects develop stably at the layer scale by coalescence (Fig. 2.5.b), the microdefects join to form transverse cracks. Transverse cracks can reach the ply interface and cause delamination under inter-laminar stresses (Fig. 2.5.c). These defects and their evolution depend on the number of plies, stacking, size and shape of the structure, and the loading considered.

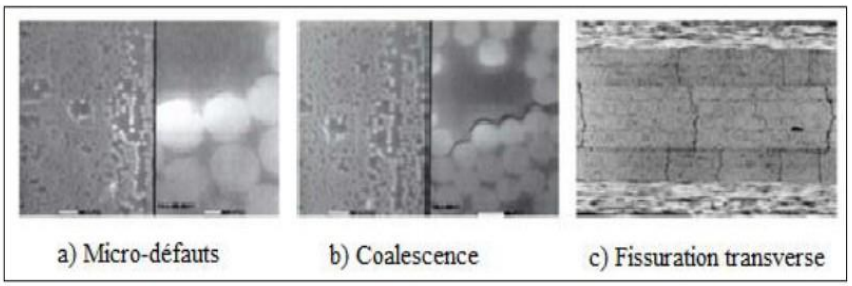

Fig 2. 5: Defects evolution [8]

The major micro-mechanisms of damage that join delamination are schematically given in (Fig.2.6). They include:

- Damaged zone: The concentration of high stresses around the crack tip results in a damaged zone where plastic deformation and/or matrix microcracks are located.
- Lateral cracks: After the crack has passed, microcracks in the damaged area can develop into lateral cracks in the matrix around the delamination plane.
- Fiber Bridging: The presence of cracks below or above the delamination plane promotes the creation of fiber bridges between the two delaminated surfaces. Some fiber bridges break down during the delamination process.

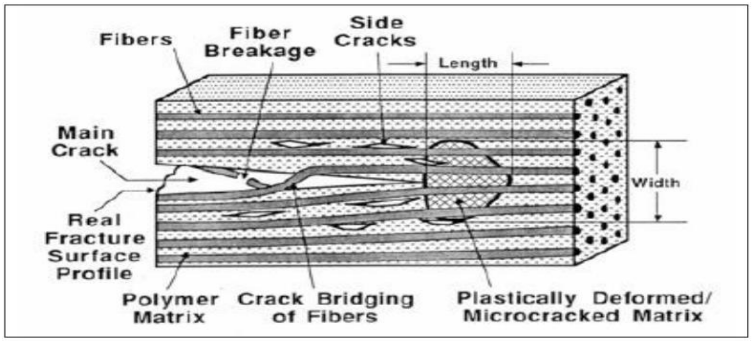

Fig 2. 6: Mechanisms of damage accompanying delamination

[14]

Advances in composite materials have made it possible to assign specific qualities to separate materials within a single component. The local optimization of these characteristics, for example by attaching a substance of high hardness to the surface of a strong material, creates the interface problem.

This abrupt change in composition can result in localized high stress concentrations. The solution of a continuous change in desired properties, through a compositional gradient, mitigates this singularity through the use of functionally gradient materials (FGMs).

2.6.2 Functionally graded materials (FGMs)

Functionally graded materials (FGMs); a type of composite material produced by continuously changing the volume fractions in thickness, length, or both directions to achieve a well-defined profile. These types of materials (FGM), have attracted a lot of interest in recent times due to the advantages of reduced disparity in material properties and stress reduction.

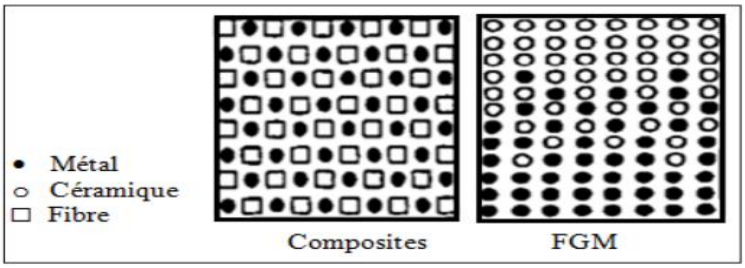

Fig 2. 7: Composite and FGM configurations

The concept of functionally graded material was developed in the National Aerospace Laboratory of Japan in 1984 by M. Niino and his colleagues in Sendai. The aim is to develop materials to be used as thermal barriers in space constructions and fusion reactors [15].

FGMs can be used for different applications, such as gas turbines, thermal barrier coatings for ceramic engines, optical thin films, etc... [16]

Generally, FGMs are made from isotropic materials such as ceramics and metals [17].

Functionally graded material was at first classified by researchers under conventional composite materials depending on the used combinations of constituents. There are several material combinations that may be employed to create FGMs. Metal–metal, metal–ceramic, ceramic–ceramic or ceramic–polymer are the most common as displayed in Fig.2.8 [18].

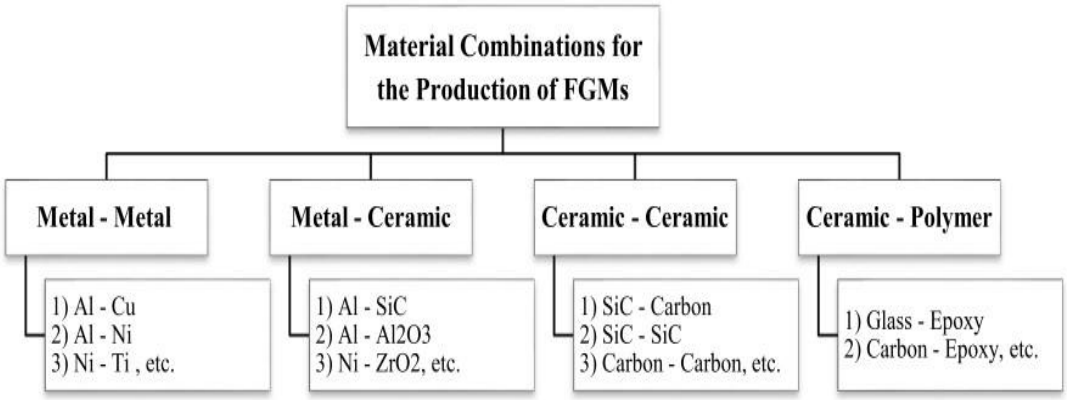

Fig 2. 8: Examples of possible material combinations used in FGMs [18]

Functionally graded materials are composites with macroscopically heterogeneous characteristics. The continuous change in the composition in the microstructure of the material distinguishes FGMs from conventional composite materials [15]. This results in a gradient that will define the properties of FGMs in several cases.

2.6.2.1 Functionally graded material performance evaluation

Functionally graded materials differ from conventional materials because they have a unique performance, so a set of systems for evaluating their performance must be established.

However, researchers around the world have yet to produce a set of accurate and rigorous performance evaluation techniques, which has severely hampered the continued development of FGMs.

FGMs was first suggested in the aerospace industry for the study and development of ultra-high temperature structural materials. As a result, scientists around the world have conducted a series of studies and research on mechanical properties, thermal fatigue properties, thermal insulation properties, thermal stress and thermal shock resistance. However, today, the performance evaluation of functionally graded materials is still in its infancy. The establishment of a systematic evaluation system is an essential part of the future development of FGMs.

2.6.2.2 Functionally graded materials research direction

At present, research into FGMs is still at an advanced stage. Although a considerable number of high-performance gradient composites have been developed and deployed in recent years, some critical issues remain unresolved.

In the future, the development of Functionally graded materials will be in the following directions:

- Further exploration of the microstructure, phase composition of gradient materials and phase transformation, and a full understanding of the microscopic mechanism.
- Extend the notion and principle of functionally graded material to other disciplines (other fields).
- additional functionally graded materials in order to provide a unified method for assessing the performance of FGMs

Classifications of functionally graded materials (FGMs):

<u>according to the case during FGM processing</u>

In the case of FGMs processing, methods can be classified into three categories: liquid state processes, solid state processes, and deposition processes. Fig.2.9 illustrates the many processing techniques that fall into these categories. The production of functionally graded materials by various routes and in various cases affects the characteristics of the end result depending on the mechanical loading, thermal influences, inertial forces and pressure that occur during industrialisation.

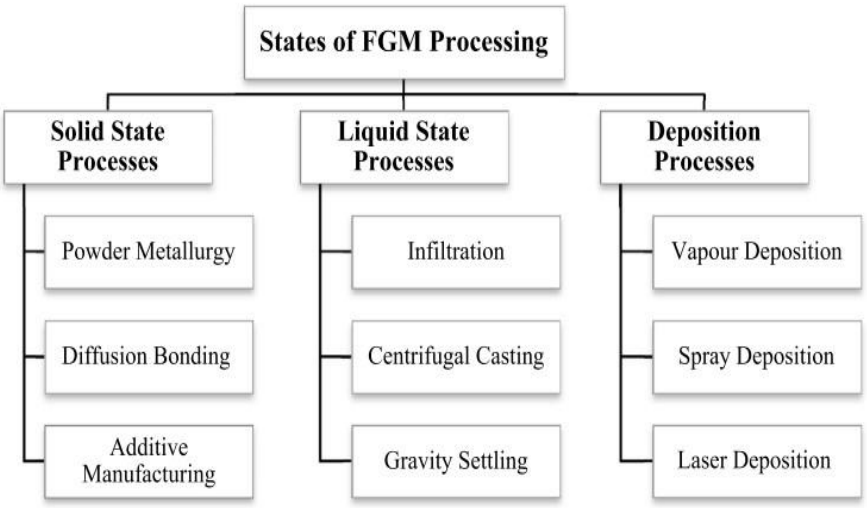

Fig 2. 9: Classification of FGMs according to case during manufacturing [18]

<u>According to FGM structure</u>

Functionally graded materials can be in general classified into two main groups: continuous graded material and discontinuous graded material as shown in Fig.2.10.

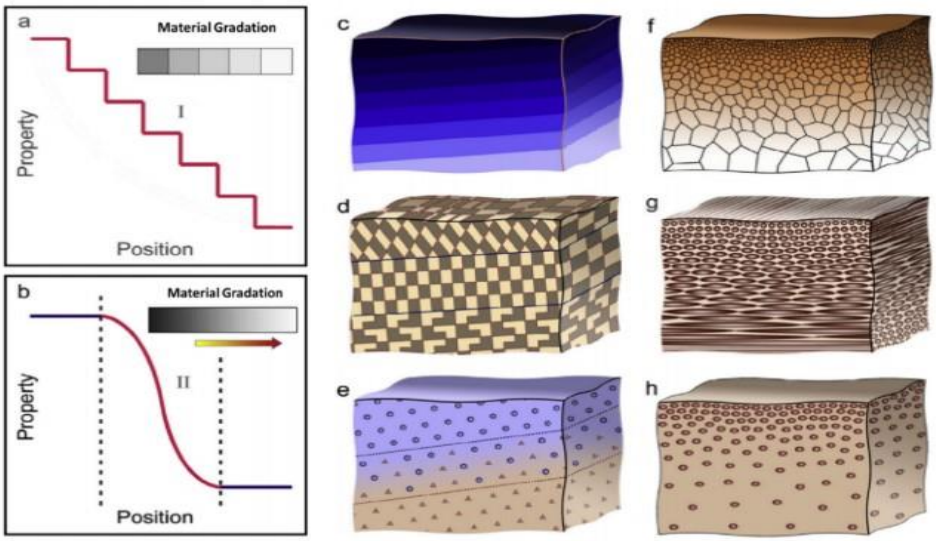

Fig 2. 10: FGMs with different shapes of gradient [19]. (a) Discrete/ discontinuous FGMs with interface. (b) Continuous FGMs with no interface. (c), (f) Composition gradient. (d, g) Orientation gradient. (e, h) Fraction gradient

<u>According to the type of FGM gradient</u>

Functionally graded materials may be divided into three gradient groups: microstructure, composition, and porosity. as shown in Fig.2.11 [19].

The composition type of FGM gradient is determined by the material's composition, which changes from one component to the next, resulting in various phases with diverse chemical structures. These many stages of manufacturing are determined by the synthetic amount and the conditions under which the reinforced materials are manufactured.

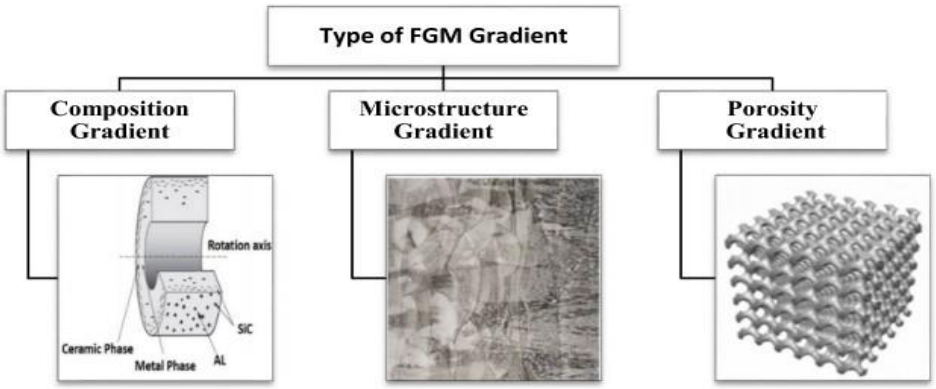

Fig 2. 11: Example of three different types of FGM gradient

<u>According to the functionally graded material scale and dimensions</u>

"Thin FGMs" are manufactured by various methods such as chemical vapor deposition (CVD), physical vapor deposition (PVD), self-propagating high-temperature synthesis (SHS) techniques, and thermal spray deposition like laser cladding. whereas "Bulk FGMs" are manufactured by solid freeform techniques, powder metallurgy centrifugal casting, gravity settling (Fig.2.12).

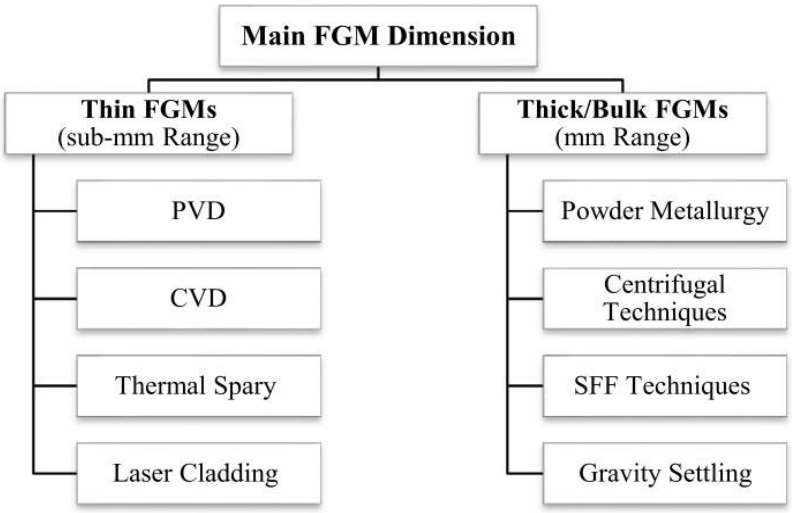

Fig 2. 12: FGMs classification based on the main FGM dimension [18]

2.6.2.3 According to the field of applications

Functionally graded materials play a role in industrial production through the process of improving productivity and material requirements, as these materials (FGMs) are used in many fields such as aerospace, automotive, biology, electromagnetics, civil engineering, etc. through an artificial mixture of organic and inorganic materials such as minerals and ceramics. Fig.2.13 gives an overview of the classification according to the main application areas.

Aerospace field

Functionally graded materials with high-temperature resistance, thermal fatigue resistance, thermal shock resistance and corrosion resistance can be applied to aircraft engine parts and heat resistant surfaces of the space shuttle [20]. The side of the combustion chamber wall of the spacecraft engine during work has to withstand high temperatures and thermal corrosion of more than 2000 K, the material (FGM) has excellent thermal insulation properties, while the other side has a low temperature that cools the liquid hydrogen. Functionally graded materials are able to withstand large temperature differences in temperature gradient conditions caused by thermal stress and mechanical loading, so that the materials can work for a long time.

Nuclear energy field

The corrosion resistance, high strength and heat resistance of FGMs offer a reliable guarantee for the development of the next generation nuclear industry. Nuclear weapons storage, nuclear power and nuclear power generation are extremely dangerous. When an accident occurs, it has catastrophic consequences. Therefore, it is necessary to protect it and ensure its safety. In the application of the nuclear fusion reactor (NFR), a good thermal stress relaxation effect is demonstrated, which makes the NFR safer. As a heat resistant, high strength and shielding material, FGMs offer significant superiority in nuclear furnace wall materials and nuclear furnace construction materials [21].

Biological field

Functionally graded material is found in many natural structures, including the shell of a layered structure, the layered human skin, and the strong and durable animal skeleton. The medical advancement of functionally graded material allows for more rapid and better makes medical assistance to patients. the FGM has the characteristics of high specific modulus, high

specific strength, biocompatibility and abrasion resistance. According to this, the artificial joint produced allows the artificial prosthesis and the patient's own skeleton to have a high binding force and be durable while also demonstrating good biocompatibility [22]. Because of its exceptional qualities, functionally graded material has a promising future in biological sectors such as artificial bones, heart and teeth.

Electromagnetic field

Special structures have unique properties due to the graded distribution of functionally graded materials. The gradient structure in the electromagnetic field has both the electromagnetic gradient function and the piezoelectric gradient function, which also can be used to produce electromagnetic shielding materials, ultrasonic oscillators, ceramic filters, and so on [23]. As well as can be used the functionally graded materials on disks, electromagnets, permanent magnets, electromagnets, and oscillators in order to decrease the size and mass of the corresponding devices and progress their performance [24].

Optical field

Ordinary glass has a high hardness but a high brittleness. The service life of the glass is substantially shortened due to the unpredictability of the external environment. Concurrently, At the same time, the transmittance of ordinary glass cannot be adjusted in response to changes in the environment, which will have an influence on manufacturing, work, and living. Therefore, enhancing the mechanical and optical qualities of glass has emerged as a critical area of research [25]. By enhancing functionally graded materials with rare earth elements and materials, the optical properties of glass can be changed according to the environment, where specialized scientists (Optical field) have managed to prepare materials such as optical fiber lenses, glass lasers, discolored glass, and anti-reflection films.

Energy sector

Functionally graded materials play an important role in the field of energy because they have special properties that depend on heat resistance, thermal shock resistance, corrosion resistance. In the case of a power generating system, for example, the use of gradient thermoelectric energy conversion material prevents the emitter from cracking in a high-temperature operating environment of 1860 C° and significantly decreases the thermal stress of the system. Meanwhile, the application of the heat release substrate to the system's low-temperature electrode demonstrates strong thermal conductivity and an exothermic radiation rate [26].

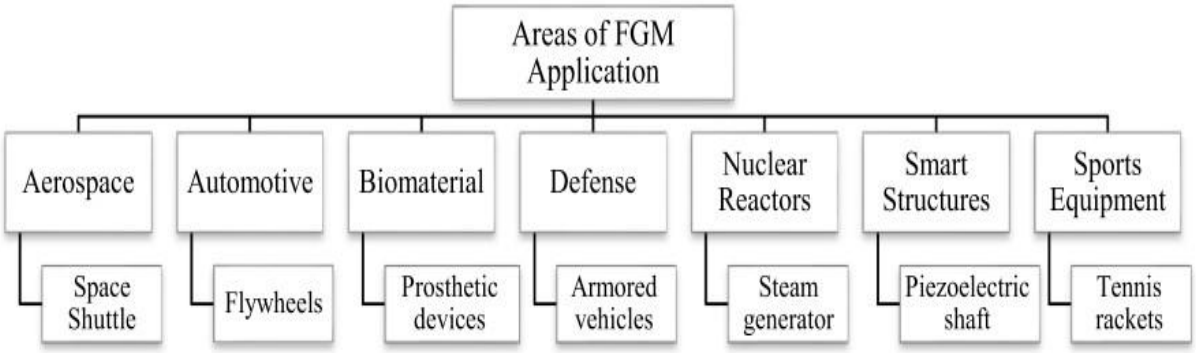

Fig 2. 13: Functionally graded materials: fields of application and examples

2.6.2.4 Possible classifications of FGMs' production methods

Classifications of functionally graded material (FGM) production methods have been proposed based on the degree of control achievable over the property gradient, the complexity of the product shape and wall thickness, the equipment and manufacturing costs, the residual stresses developed due to the FGM production method, the assessed environmental impact and the specific energy consumption throughout the whole life cycle (In Fig.2.14 a circle represents the possible classifications of FGM production methods).

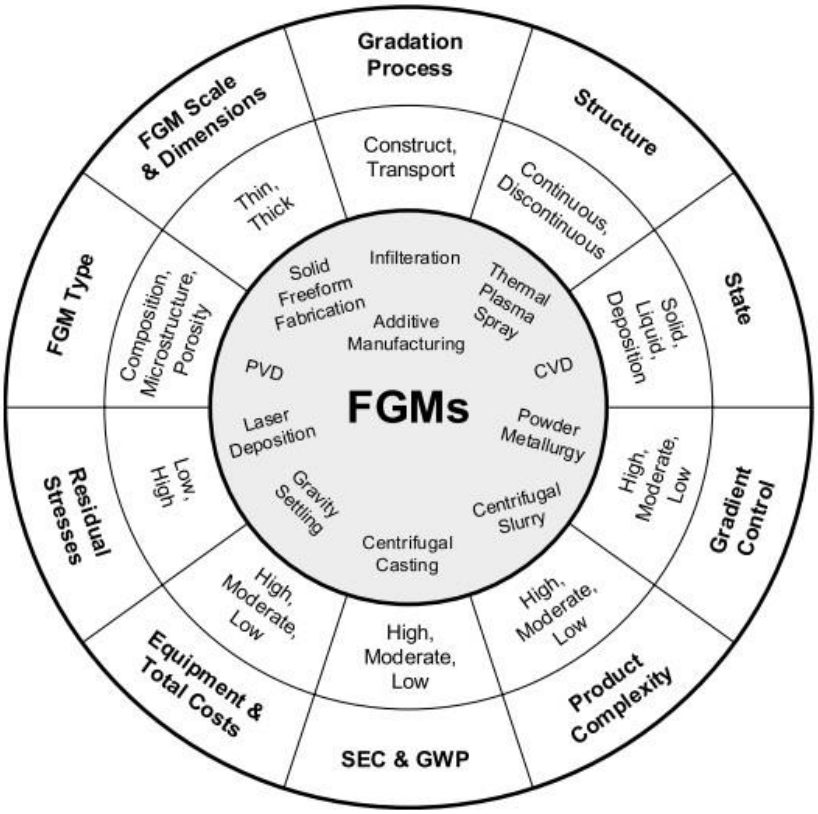

Fig 2. 14: Possible classifications of FGM production methods [18]

2.6.2.5 Effective properties of functionally graded material

Functionally graded materials are composed of two materials with different properties. A detailed description of a present graded microstructure is in general not available, except for information on the volume fraction distribution. when the volume fraction of each phase gradually changes along the gradation direction, this makes the functional functionally graded materials substances change.

Therefore, we have two possible approaches for FGM as models: For the first, a piecewise difference of the volume fraction of the metal or ceramic is assumed, and the FGM is made to be laid down with the same volume fraction in each part, i.e., quasi-homogeneous ceramic-metal layer (Fig.2.15.a); For the second, a continuous variation of the volume fraction of the metal or ceramic is assumed (Fig.2.15.b).

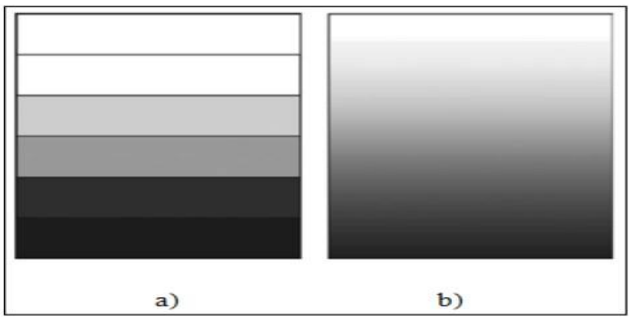

Fig 2. 15: Analytical model for a functional gradient material layer: a) first approach; b) second approach

The continuous difference in properties (Fig.2.16) is applied when the upper surface is exposed to high temperature while the lower surface is exposed to low temperature. In this case, the top surface is made of full ceramic and the bottom surface is made of full metal, with a gradual transition between the two.

Ceramics are known to be fragile and very vulnerable to small defects. But this material has wonderful qualities which are as follows:

- Good corrosion resistance and low chemical reactivity,
- High modulus of elasticity and high hardness
- High tensile strength
- Good wear resistance and low friction coefficient
- Retention of properties at high temperatures
- Low coefficient of thermal expansion and Low thermal conductivity

The characteristics of the metal are given as follows:

- Good mechanical resistance

- High thermal conductivity
- Very good toughness

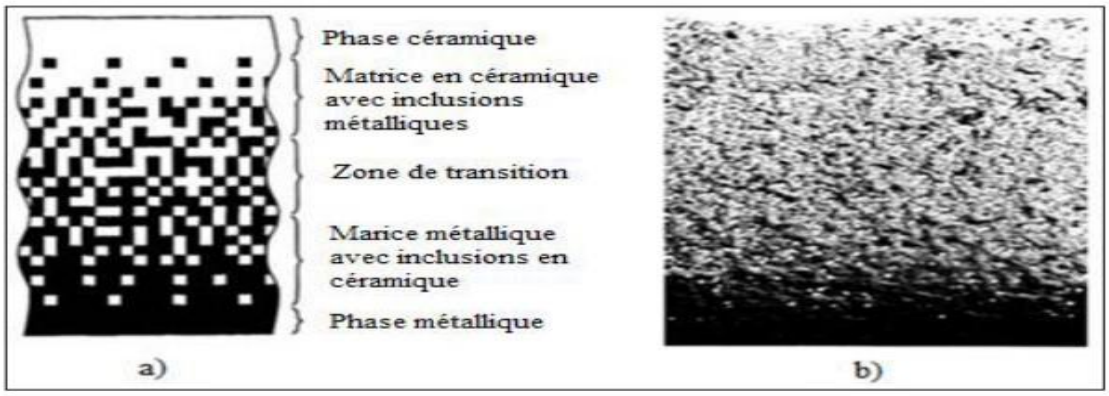

Fig 2. 16: Continuous variation of the microstructure: a) (schematic); b) (photo)

Functional gradient materials (FGM) consist of the association of two (usually ceramic and metal) or more materials with various structural and functional properties with an ideally continuous transition of the composition structure, and porosity distribution between different materials in order to optimize the performance of the structure they comprise.

FGM materials are distinguished by their non-uniform microstructures and spatially graded macro-properties. The multiphase composition across the thickness is one of the crucial characteristics to be established during the manufacture of these materials. The positional dependence of the properties is reflected in the consideration of the law of mixtures corresponding to the Voigt model.

$$P_F = \sum_{i=1} P_i V_{Fi} \tag{2-1}$$

P_i is the material properties and V_{Fi} is the volume fraction of the constituent material i with the sum of the volume fractions of all constituent materials gives unit 1:

$$\sum_{i=1} V_{Fi} = 1 \tag{2-2}$$

In actuality, the majority of FGM constructions are two-component in nature: ceramic and stainless steel in general (Fig.2.17). Using a basic rule of combination of constituent material properties P_{i}; where i= m, c as:

$$P_{\mathrm{i}} = P_c V_c + P_m V_m \tag{2-3}$$

$$V_c + V_m = 1 \tag{2-4}$$

The variation of volume fractions can be used to define an FGM. To explain volume fractions, most studies employ the power function, exponential function, or sigmoid function. The connections between the particles must be tough enough on the inside to withstand breaking and tough enough on the exterior to withstand wear.

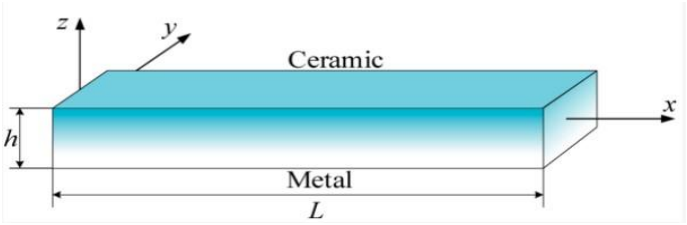

Fig 2. 17: FGM beam model

Consider an FG beam as shown in Figure.2.17 b and h represent the width and the thickness of the beam, respectively. the length of the beam is L. The Young's modulus varies continuously along with the thickness of the beam with a power-law distribution. The properties of the material vary in a continuous manner according to the thickness (such as young's modulus and Poisson's ratio) on the upper and lower faces of the beam.

Ziou et al [27] reported that the effect of the Poisson's ratio on the distortions is negligible compared to that of Young's modulus. Therefore, Poisson's ratio can be assumed as constant. However, Young's modulus in the thickness direction of the FGM beam varied according to the exponential function (E-FGM), the power-law (P- FGM), or the sigmoid function (S-FGM).

Material properties of the P-FGM beam

Based on the power-law distribution function, the young's modulus E (y) (Khebizi et al [28], Guendouz et al [29] and Guenfoud [30]) and the material density $\rho(y)$ varying continuously through thickness can be expressed as:

$$E(z) = E_b + (E_t - E_b) \times \left(\frac{2y + h}{2h}\right)^P \tag{2-5}$$

E_t and E_b are Young's modulus on the top $(z = h/2)$ and bottom $(z = -h/2)$ FGM beam surface, P and h are the exponent of the power-law and beam's thickness, respctively.

$$\rho(y) = \rho_b + (\rho_t - \rho_b) \times \left(\frac{2y + h}{2h}\right)^P \tag{2-6}$$

ρ_t and ρ_b are the material density top and bottom beam surfaces, respectively.

The Variation of Young's modulus in the thickness direction of the P-FGM beam is shown in (Fig.2.18) by Ilies et al [31]. It is clear that the latter changes rapidly near the lower surface, and increases rapidly near the upper surface.

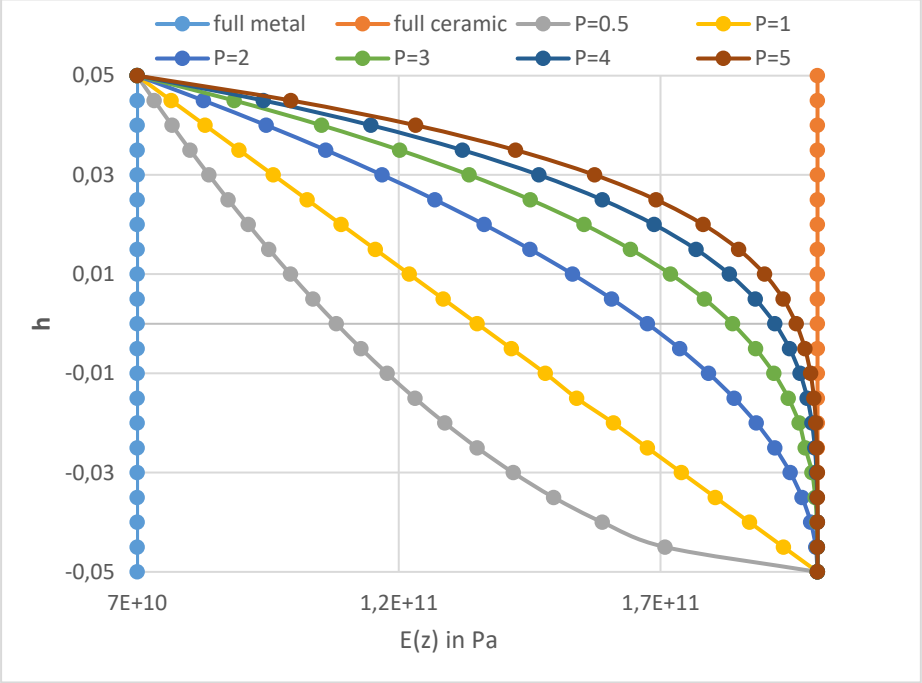

Fig 2. 18: Variation of Young's modulus through the thickness of P–FGM beam

Material properties of the S-FGM beam

To provide a suitable stress distribution across all surfaces, Chi et al [32] determined the volume fraction of the FGM beam using two power-law functions. The following are the definitions of the two power-law functions:

$$V_c(z) = \frac{1}{2}\left(\frac{h/2 + z}{h/2}\right)^p \quad \text{pour} : -h/2 \le z \le 0 \tag{2-7}$$

$$V_m(z) = 1 - \frac{1}{2}\left(\frac{h/2 - z}{h/2}\right)^p \quad \text{pour} : 0 \le z \le h/2 \tag{2-8}$$

Using the law of mixtures, Young's modulus of the S-FGM beam can be calculated by:

$$E(z) = V_c(z)E_c + [1 - V_c(z)]E_m \text{ Pour} : -h/2 \le z \le 0 \tag{2-9}$$

$$E(z) = V_m(z)E_c + [1 - V_m(z)]E_m \text{ Pour} : 0 \le z \le h/2 \tag{2-10}$$

(Fig.2.19) Illustrates that the variation of the volume fraction described by equations (2-7) and (2-8) resembles sigmoid distributions, and this FGM beam is referred to as (S- FGM beam).

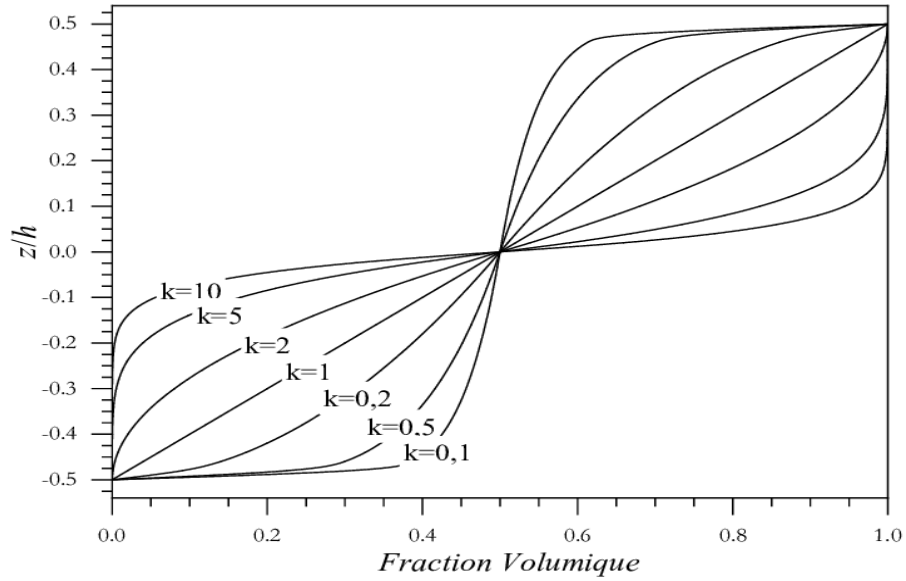

Fig 2. 19: Variation of the volume fraction through the thickness (S-FGM)

Material properties of the E-FGM beam

For the exponential distribution (E–FGM), the young's modulus is given by Khebizi et al [28]:

$$E(y) = A \times e^{B\times\left(y+\frac{h}{2}\right)} \text{ where } A = E_b \text{ , } B = \frac{1}{h}\ln\left(\frac{E_t}{E_b}\right) \tag{2-11}$$

The Variation of Young's modulus in the thickness direction of the E-FGM beam is shown in Figure.2.20 by Ilies et al [33].

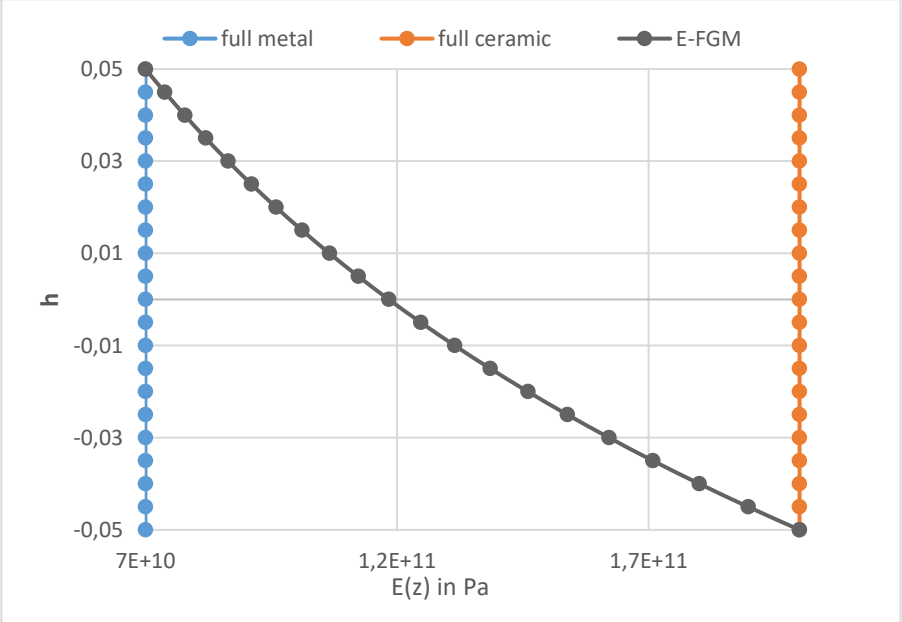

Fig 2. 20: Variation of Young's modulus through the thickness of E–FGM beam

2.7 Conclusion

In this chapter, an overview is given of composite materials and the role of the different phases (fibre, interface, matrix...) with their advantages and disadvantages. The failure mechanisms of composites are then discussed with emphasis on the delamination phenomenon. After that, a new topic was introduced, called functionally graded materials (FGMs), on which we focus in this thesis. This part includes the history, development, properties and design of FGMs as well as their different fields of application in special civil engineering structures.

3 About beam theories

3.1 Introduction

A beam is a 3D medium slender in one direction: the axis or mean line of the beam. A beam theory is a simplified (1D) theory that allows one to describe with a certain approximation (at least sufficient in the engineering sense) the real 3D equilibrium state of the beam.

The beam theory consists of two basic components, The set of 1D equations, where the only space variable is along the mean line of the beam. The 1D solution of these equations provides the description of the global 1D behavior in terms of section displacements and internal forces. And The set of formulas that allow, from the 1D solution, to go back to the 3D solution in terms of displacement and (especially) stress.

When talking about classical beam theories, Timoshenko and Bernoulli are systematically put forward, depending on whether or not one wishes to account for shear forces. “Classical” means a beam theory where the external and internal actions are reduced to a force and a moment at the current section. in addition, among the classical beam theories, which are very rich in definition, the Saint Venant (SV) approach has a privileged place in the understanding of the mechanics of sections and beams. The 3D SV’s solution problem has the fundamental property of being representative of the exact solution away from the edges. It is now established that the exact solution tends asymptotically towards the 3D SV’s solution when moving away from the edges. Moreover, a 1D beam theory is derived from the 3D SV’s solution, which we will call the Saint Venant Beam Theory (SVBT). This theory has the particularity of allowing us to systematically go back to the 3D SV’s solution, which represents the exact solution far from the edges. In addition, for the torsion of thin open sections of common lengths, Vlasov's hindered torsion (used in steel constructions) is considered in the last part of the chapter.

3.2 Recall and classification

3.2.1 Beam theories

A beam is a three-dimensional (3D) solid body with one dimension (1D) fixed relative to the other two dimensions. Beam theories exploit this geometrical characteristic of slenderness to propose simplified approximations.

Beam theories are models of the continuous medium that allow simplifying the resolution of the mechanical problem and to provide approximations of the required solution. This simplification consists in transforming the 3D equilibrium problem into a problem whose unknowns depend on only one space variable. The resolution of this simplified one-

dimensional problem leads to a set of results that is used to generate the approximation of the initial three-dimensional problem.

The one-dimensional in a beam theory only solves the problem in the mathematical sense. Once found, the one-dimensional solution is used to recover the three-dimensional approximation. In particular, for beam theories built on a displacement model, this is made possible by modelling the motion of the current section and introducing generalised coordinates that vary along the beam axis.

It is quite obvious that there is a difference between the exact solution obtained from the three-dimensional model and the approximate solution obtained from a beam model. The quality of a beam theory can be evaluated through this difference.

3.2.2 Classification of beam theories

From the different beam modelling approaches, three main approaches are identified

- The Saint-Venant beam theory deduced from the Saint-Venant 3D solution.
- Beam models obtained from kinematic or/and static hypotheses.
- Beam models obtained through asymptotic development methods.

In our study, we are specifically interested in beam theories built on kinematic assumptions as well as the beam theory derived from the 3D Saint-Venant solution. Indeed, our study is based on a higher-order beam theory built on the 3D Saint-Venant solution. It is nevertheless useful to briefly recall the main ideas associated with the asymptotic development methods, knowing also and especially that some asymptotic results are in direct relation with the results of the Saint-Venant solution.

3.3 Asymptotic approach

3.3.1 Asymptotic development method

Asymptotic development methods provide a rigorous mathematical means of modelling beams. First introduced for the study of shell and plate behaviour during the 1960s and 1970s, these methods make use of one or more parameters that are supposed to tend to zero and characterise the problem being addressed [34].

The first parameter ϵ which is suggested by the beam geometry and introduced by default represents the beam slenderness defined by $\epsilon = \frac{L_s}{L}$ with L the length of the beam and L_s the characteristic length of the section. The approximate solution is an asymptotic expansion series of type:

$$\varepsilon = \varepsilon_0 + \varepsilon_1\epsilon + \varepsilon_2\epsilon^2 + \varepsilon_3\epsilon^3 + \cdots \text{ (higher order terms)}$$
$$\boldsymbol{\sigma} = \sigma_0 + \sigma_1\epsilon + \sigma_2\epsilon^2 + \sigma_3\epsilon^3 + \cdots \text{(higher order terms)} \quad (3\text{-}1)$$

With ε the strain field and $\boldsymbol{\sigma}$ the stress field of the beam. Vector and tensor quantities are noted in "**Bold Type**".

Asymptotic development methods have served two different purposes:

1. Model Validation & Justification
2. Model development

In terms of model justification, an example is the fact that when an expansion to order 4 is performed, the results of classical beam theories are found. As a result, these techniques once more support the presumptions regarding the displacement and stress fields' shapes. For model building, this depends on the order of approximation chosen. But this has not always been successful. Indeed, several obstacles are encountered when trying to identify terms of power order greater than or equal to 5. For instance, one of the difficulties is properly defining the boundary conditions and the appropriate induced functional spaces. A summary of the state of the art and an implementation of the method can be found in the book by Trabucho and Viano [34].

Recent works based on asymptotic approaches include those of Ferradi et al [35], Kim and Wang [36]

3.3.2 Variational asymptotic method

Another way, this time fruitful and important for the computation of beams, is the variational asymptotic method (VAM) presented by Berdichevsky [37] for plates, and developed by Hodges, Yu, Volovoi and their colleagues [[38][39][40][41][42]] for beams.

Under the assumption of small deformations, this method divides the three-dimensional elasticity problem into a linear two-dimensional problem posed on the cross-section and a nonlinear one-dimensional problem posed on the "beam axis" [43]. The asymptotic development is then carried out on the expression of the deformation energy as a function of small parameters inherent to the beam studied.

To implement VAM, two calculation codes are suggested:

- Variational Asymptotic Beam Sectional Analysis (VABS) provides 2D-FEM analysis of the section to determine its behavior [44].
- The Geometrically Exact Beam Theory (GEBT) provides the 1D-FEM analysis of the 1D beam problem [45].

VABS is able to determine the outcomes of traditional theories as well as the Saint-Venant solution without using kinematic assumptions.

3.4 Classical beam theories

The term "classical beam theories" refer to the Euler-Bernoulli model and the Timoshenko model. In the Anglo-Saxon literature, the term "engineering beam theories" is also used. The principal assumption of these models is that the current cross-section S_z has a rigid solid motion.

3.4.1 Euler-Bernoulli beam theory

This is a classical beam theory that deals with the case of small deformations of a beam only subjected to lateral loads. Under this theory, the cross-section of the beam remains perpendicular to the deformed axis and no rotation is allowed between them. Such rotation is caused by the shear deformation of the beam, which is not considered.

It also implies that the cross-section of the beam is extremely rigid in its plane and remains plane after a stress deformation. The formulation of the stiffness matrix in Euler-Bernoulli beam theory considering two degrees of freedom, i.e., displacement and rotation at each node for a cantilever beam with a point load at the end is as follows:

$$K = \begin{bmatrix} \frac{12E}{l^3}I & \frac{6E}{l^2}I & -\frac{12E}{l^3}I & \frac{6E}{l^2}I \\ \frac{6E}{l^2}I & \frac{4E}{l}I & -\frac{6E}{l^2}I & \frac{2E}{l}I \\ -\frac{12E}{l^3}I & -\frac{6E}{l^2}I & \frac{12E}{l^3}I & -\frac{6E}{l^2}I \\ \frac{6E}{l^2}I & \frac{2E}{l}I & -\frac{6E}{l^2}I & \frac{4E}{l}I \end{bmatrix} \tag{3-2}$$

3.4.2 Timoshenko beam theory

This theory includes both shear deformation and rotation, which makes the behavior of short beams adequately described. Therefore, it permits the effect of rotational inertia between the cross-section and the bending axis of the beam, although the plane sections remain plane. It considers the average shear deformation through the thickness of the beam.

The formulation of the stiffness matrix in the Timoshenko beam theory considers two degrees of freedom, i.e., displacement and rotation at each node for a cantilever beam with a point load at the end, considering the shear factor, that is used in the analytical solution is given by:

$$K = \begin{bmatrix} \frac{12EI}{l^3(\phi+1)} & \frac{6EI}{l^2(\phi+1)} & -\frac{12EI}{l^3(\phi+1)} & \frac{6EI}{l^2(\phi+1)} \\ \frac{6EI}{l^2(\phi+1)} & \frac{EI(\phi+4)}{l(\phi+1)} & -\frac{6EI}{l^2(\phi+1)} & \frac{EI(-\phi+2)}{l(\phi+1)} \\ -\frac{12EI}{l^3(\phi+1)} & -\frac{6EI}{l^2(\phi+1)} & \frac{12EI}{l^3(\phi+1)} & -\frac{6EI}{l^2(\phi+1)} \\ \frac{6EI}{l^2(\phi+1)} & \frac{EI(-\phi+2)}{l(\phi+1)} & -\frac{6EI}{l^2(\phi+1)} & \frac{EI(\phi+4)}{l(\phi+1)} \end{bmatrix} \quad (3\text{-}3)$$

In the equations of the above stiffness matrix, K is the stiffness, E is the modulus of elasticity of the beam, I is the moment of inertia, L is the length of the beam, ϕ is the shear flexibility where ϕ = 12ϒ, ϒ is the shear rotation, where ϒ = (EI / AGL2).

Considering the shear factor k, ϕ = (12EI / kAGL2), k is the shear factor, G is the shear modulus, where G = [E/(2v +2)] and v is the fish ratio that is considered in the Timoshenko beam theory. The next figure shows the difference between these theories in case of deformation.

3.4.3 The difference between Euler-Bernoulli beam theory and Timoshenko beam theory

The Timoshenko beam theory is of higher order than the Euler-Bernoulli theory and is known to be better at predicting the transverse response of the beam. However, the superiority of the Timoshenko model is more noticeable for beams with a small aspect ratio. It is demonstrated that using a controller based on Euler-Bernoulli theory to suppress beam vibrations may lead to instability caused by unintentional excitation of unmodeled modes.

The beam elements are designed on the principle of the Timoshenko beam, which is a first-order shear deformation theory: the cross-section shear strain is constant, i.e., the cross-sections remain flat and undeformed after deformation.

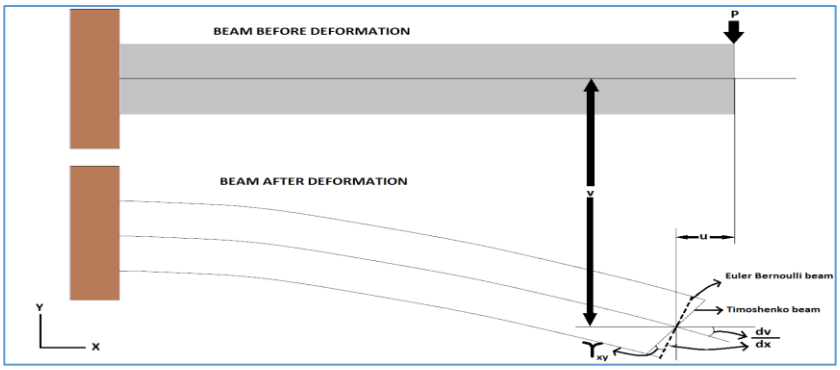

Fig 3. 1: Deformation of Timoshenko beam compared to Euler beam

In Figure.3.1 u and v are the displacements of the beam in the X and Y directions as a result of the applied load P and we can see that each deformation is in agreement with their theories, where the Euler-Bernoulli beam is rigid and the Timoshenko beam is flexible. The Timoshenko beam theory considers the shear rotation ϒxy, unlike the Euler-Bernoulli beam theory.

The deformation equations are as follows:

- Euler-Bernoulli Beam Theory: $u - y(dv/dx)$
- Timoshenko Beam Theory: $u + y(-dv/dx + \Upsilon xy)$

The transverse shear stress is not considered in Euler-Bernoulli beams because the bending is supposed to act in such a way that the cross-section normal to the neutral axis remains normal to the neutral axis after bending. In the case of Timoshenko beams, the cross-section is initially normal to the neutral axis but does not remain normal after bending.

For normal stress, Euler-Bernoulli beam elements work well, as they are able to capture bending-dominated deformation fields. When the beam is not thin and undergoes bending-dominated deformation, the Timoshenko elements are weak in catching the normal stress, and the classical beam elements are weak in catching the shear deformation. However, the difference between these two beam theories will be modest if the length to thickness ratio of the beam is significant.

3.4.4 3D displacement models according to Timoshenko/Bernoulli

The expression of the displacement field results from the Timoshenko/Bernoulli (T/B) kinematic model which states that the section is undeformable and that the motion of the beam is reduced to the translation and rotation of the current section:

$$\boldsymbol{U}_{T/B}(x,y,z) = \boldsymbol{u}(z) + \boldsymbol{\omega}(z) \wedge \boldsymbol{GM} \tag{3-4}$$

Where (x, y, z) are the coordinates of a point in the beam, (u) and (ω) are the cross-section translation and rotation vector, respectively. X the in-section vector position, $\boldsymbol{G}$ is the center of the current section and**,** the position of a point $\boldsymbol{M}$ of the beam is denoted **GM.**

It follows that the solution 1D $[\boldsymbol{u}^e(z), \boldsymbol{\omega}^e(z)]$ makes it possible to go back, in accordance with the initial kinematics, to the following 3D displacement field:

$$\boldsymbol{\xi}^e_{T/B}(x, y, z) = \boldsymbol{u}^e(z) + \boldsymbol{\omega}^e(z) \wedge \boldsymbol{GM} \tag{3-5}$$

3.4.5 Limitations of classical theories

The first limitation of the classical theories is the assumption that the straight section is undeformable. Regarding the consequences of this assumption, it can be shown that:

- the distribution of shear strains and stresses is uniform over the cross-section
- the torsional rigidity is equal to the polar inertia of the section, which is only true for a circular cross-section

We cite Carrera et al. [46] and Han et al. [47] as two examples of studies that compare the various classical beam theories in greater detail.

3.5 Principle of Saint-Venant (solution of Saint-Venant)

In the literature on beam theories, the terms Saint-Venant's principle and Saint-Venant's solution are frequently used. They have played a significant role in the theory of elasticity in general as well as beam modeling for a very long time. Indeed, by combining an interior solution with an edge solution, research on the Saint-Venant principle has made it possible to characterize the structure of the linearized 3D solution [48] [49].

The 3D Saint-Venant solution is the first reference when one wishes to analyse the beams behaviour of any shape, homogeneous or heterogeneous. This reference position can be explained by:

- Its asymptotic character since it represents the inner 3D solution far from the extremities.
- the determination of a set of operators that characterise the mechanical behaviour of the section (and of the beam it generates), which we call the mechanical characteristics of the section.

In addition to the section operators, the 3D Saint-Venant solution is written in terms of generalized quantities which are solutions of a system of 1D equations. The Saint-Venant

beam theory proposed by Ladevèze and Simmonds [38] exploits this feature to generate a 1D theory capable of providing the interior solution.

3.5.1 The Saint Venant problem

The SV problem takes into account the linearized 3D equilibrium of elastic straight beam of composite section with anisotropic phases.

We start from the console beam of a constant (unspecified) section S, z-axis and length L shown in Figure.3.2 The beam recessed in Z = 0 is subjected to a surface force H, and in Z = L a volume force f. A point M is identified by $M = ZZ + GM$, where G is the centre of inertia of the section and GM belongs to S. Finally, we denote [x, y] as the axes of inertia of the section.

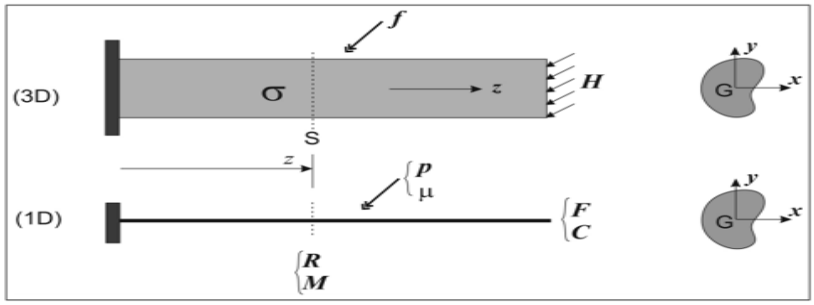

Fig 3. 2: Three-dimensional beam and one-dimensional modelling.

as shown in Figure Fig.3.2 The equilibrium equations are written as follows:

$$\begin{cases} \operatorname{div}(\boldsymbol{\sigma}) + \boldsymbol{f}_{\text{vol}} = 0 & \text{sur } \Omega \quad (3\text{-}6\ a) \\ \boldsymbol{\sigma} = \boldsymbol{C} : \boldsymbol{\varepsilon}(\boldsymbol{\xi}) & \text{sur } \Omega \quad (3\text{-}6\ b) \\ \boldsymbol{\varepsilon}(\boldsymbol{\xi}) = \frac{1}{2}(\nabla^t \boldsymbol{\xi} + \nabla \boldsymbol{\xi}) & \text{sur } \Omega \quad (3\text{-}6\ c) \\ \boldsymbol{\sigma}(\boldsymbol{n}) = \boldsymbol{f}_{\text{lat}} & \text{sur } S_{\text{lat}} \quad (3\text{-}6\ d) \end{cases}$$

$$\begin{cases} \boldsymbol{\sigma}(-e_z) = \boldsymbol{f}_0 & \text{sur } S_0 \quad (3\text{-}6\ e) \\ \boldsymbol{\sigma}(e_z) = \boldsymbol{f}_L & \text{sur } S_L \quad (3\text{-}6\ f) \end{cases}$$

$\boldsymbol{\xi}(x, y, z)$ displacement fields in Ω

$\varepsilon(x, y, z)$ linear strain fields in Ω

$\boldsymbol{\sigma}(x, y, z)$ stress fields in Ω

$\boldsymbol{C}(x, y)$ elastic behavior tensor

3.5.2 3D Saint-Venant's solution

The 3D SV's solution is the unique z-polynomial solution which verifies all equations (3.6) only in terms of resultants (force and moment):

$$\left.\begin{aligned} \int_{S_0} \boldsymbol{\sigma} \cdot (-e_z) dS &= \int_{S_0} \boldsymbol{H}_0 dS \\ \int_{S_L} \boldsymbol{\sigma} \cdot \boldsymbol{z} dS &= \int_{S_L} \mathbf{f}\, dS \\ \int_{S_0} \boldsymbol{GM} \wedge \boldsymbol{\sigma} \cdot (-e_z) dS &= \int_{S_0} \boldsymbol{GM} \wedge \boldsymbol{H}_0 dS \\ \int_{S_L} \boldsymbol{GM} \wedge \boldsymbol{\sigma} \cdot \boldsymbol{z} dS &= \int_{S_L} \boldsymbol{GM} \wedge \boldsymbol{H}_L dS \end{aligned}\right\} \quad (3\text{-}7)$$

Through the punctual actions (1D) [***F; C***] and linear [***p; μ***]**,** the 3D external actions **f** and **H** are modelled as follows:

$$\mathbf{F} = \int_S \mathbf{H} dS \quad (3\text{-}8\ a)$$

$$\mathbf{C} = \int_S \mathbf{GM} \wedge \mathbf{H} dS \quad (3\text{-}8\ b)$$

$$\mathbf{p} = \int_S \mathbf{f} dS \quad (3\text{-}8\ c)$$

$$\boldsymbol{\mu} = \int_S \mathbf{GM} \wedge \mathbf{f} dS \quad (3\text{-}8\ d)$$

At the right of the current section (normal z), Internal Behaviour (1D) is defined by:

$$\boldsymbol{R} = \int_S \boldsymbol{\sigma} \cdot \boldsymbol{z} dS = \begin{bmatrix} T_x \\ T_y \\ N \end{bmatrix} \quad (3\text{-}9\ a)$$

$$\boldsymbol{M} = \int_S \boldsymbol{GM} \wedge \boldsymbol{\sigma} \cdot \boldsymbol{z} dS = \begin{bmatrix} M_x \\ M_y \\ M_t \end{bmatrix} \quad (3\text{-}9\ b)$$

where **R** results from internal actions, **M** is the moment of inner actions, and **σ** is the tensor of the 3D stress state in the beam. The internal forces $(T_x, T_y, N, M_x, M_y, M_t)$ are designated by the shear forces, the normal force, the bending moments and the torsional moment, respectively and are identified by their components in [x, y, z].

The (1D) movement of section S is represented by translation and rotation of the section (u, w). According to SV' solution, the equilibrium equations for this problem are written as follows.

Equilibrium equations (1D):

$$\begin{aligned} \mathbf{R}' &= \mathbf{0} \\ \mathbf{M}' + \mathbf{z} \wedge \mathbf{R} &= \mathbf{0} \end{aligned} \tag{3-10}$$

The behaviour law (1D):

$$\begin{bmatrix} \mathbf{R} \\ \mathbf{M} \end{bmatrix} = \mathbf{\Gamma} \begin{bmatrix} \mathbf{u}' + \mathbf{z} \wedge \boldsymbol{\omega} \\ \boldsymbol{\omega}' \end{bmatrix}; \text{ and } \mathbf{\Lambda} = \mathbf{\Gamma}^{-1} \tag{3-11}$$

The boundary conditions:

$$\begin{bmatrix} \mathbf{u}(0) \\ \boldsymbol{\omega}(0) \end{bmatrix} = \begin{bmatrix} \mathbf{0} \\ \mathbf{0} \end{bmatrix}; \begin{bmatrix} \mathbf{R}(\mathrm{L}) \\ \mathbf{M}(\mathrm{L}) \end{bmatrix} = \begin{bmatrix} \mathbf{F} \\ \mathbf{C} \end{bmatrix} \tag{3-12}$$

where $(\cdot)'$ denotes the derivative in relation to z and the one-dimensional behaviour model is determined by the stiffness operator Γ (matrix 6×6), as the latter depends on the nature of the section only (shape, material). The flexibility operator is indicated by $\mathbf{\Lambda} = \mathbf{\Gamma}^{-1}$.

3.5.3 SV's solution properties (1D and 3D)

One-dimensional solution:

In equilibrium, the system of Eqs. (3-10), (3-11) and (3-12) provides a unique solution:

$$[\mathbf{u}^{\mathrm{e}}(\mathrm{z}), \boldsymbol{\omega}^{\mathrm{e}}(\mathrm{z})] \ , \qquad [\mathbf{R}^{\mathrm{e}}(\mathrm{z}), \mathbf{M}^{\mathrm{e}}(\mathrm{z})] \tag{3-13}$$

This one-dimensional solution allows us to return to a three-dimensional solution in the case of beam displacement and stress.

Three-dimensional solution (3D stress field):

The 3D stress field, on the right side of the section in Fig. 3.3, is a linear combination of the 1D equilibrium internal forces solution $(\mathrm{T}_{\mathrm{x}}^{\mathrm{e}}(\mathrm{z}), \mathrm{T}_{\mathrm{y}}^{\mathrm{e}}(\mathrm{z}), \mathrm{N}^{\mathrm{e}}(\mathrm{z}), \mathrm{M}_{\mathrm{x}}^{\mathrm{e}}(\mathrm{z}), \mathrm{M}_{\mathrm{y}}^{\mathrm{e}}(\mathrm{z}), \mathrm{M}_{\mathrm{t}}^{\mathrm{e}}(\mathrm{z}))$.

The three-dimensional stress field at equilibrium can be written using the linear property, denoted as $\sigma^{e}(\mathrm{x}, \mathrm{y}, \mathrm{z})$ in the form:

$$\begin{aligned} \boldsymbol{\sigma}^{\mathrm{e}}(\mathrm{x}, \mathrm{y}, \mathrm{z}) = \mathrm{T}_{\mathrm{x}}^{\mathrm{e}}(\mathrm{z}).\, \boldsymbol{\sigma}^{1}(\mathrm{x}, \mathrm{y}) + \mathrm{T}_{\mathrm{y}}^{\mathrm{e}}(\mathrm{z}).\, \boldsymbol{\sigma}^{2}(\mathrm{x}, \mathrm{y}) + \\ \mathrm{N}^{\mathrm{e}}(\mathrm{z}).\, \boldsymbol{\sigma}^{3}(\mathrm{x}, \mathrm{y}) + \cdots \\ \mathrm{M}_{\mathrm{x}}^{\mathrm{e}}(\mathrm{z}).\, \boldsymbol{\sigma}^{4}(\mathrm{x}, \mathrm{y}) + \mathrm{M}_{\mathrm{y}}^{\mathrm{e}}(\mathrm{z}).\, \boldsymbol{\sigma}^{5}(\mathrm{x}, \mathrm{y}) + \mathrm{M}_{\mathrm{t}}^{\mathrm{e}}(\mathrm{z}).\, \boldsymbol{\sigma}^{6}(\mathrm{x}, \mathrm{y}) \end{aligned} \tag{3-14}$$

Or in a compact form:

$$\boldsymbol{\sigma}^{\mathrm{e}}(\mathrm{x}, \mathrm{y}, \mathrm{z}) = \sum_{\mathrm{i}=1}^{6} \mathrm{X}_{\mathrm{i}}^{\mathrm{e}}(\mathrm{z}) \boldsymbol{\sigma}^{\mathrm{i}}(\mathrm{x}, \mathrm{y}) \tag{3-15}$$

The six (06) internal forces are symbolized by X_i^e. They have been obtained from one-dimensional (1D) equilibrium equations, where each internal force contributes to a specific stress field and $\sigma^i(x,y)$ corresponds to the contribution of X_i^e=1(unity) within the stress field. The six (06) unit stress fields of $\sigma^i(x,y)$ are only dependent on the nature of the section (shape and materials). It represents the characteristics of the cross-section [50].

For illustration, Figs.3.3 and 3.4 show an isotropic homogeneous rectangular section, respectively, the typical axial stress fields σ_{zz} associated with the bending moments M_x and M_y. And the typical shear fields τ associated with the shear force T_y and the torsional moment M_t.

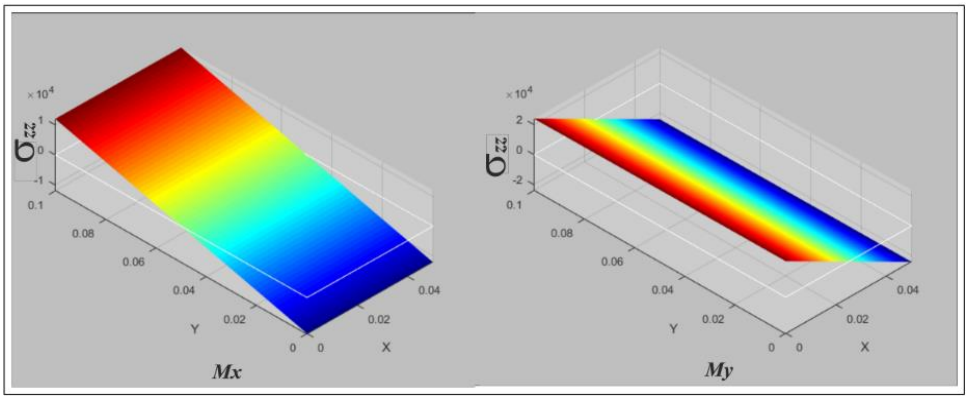

Fig 3. 3: Typical axial stress fields σ_{zz} associated with the bending moments M_x *and* M_y of an isotropic homogeneous rectangular section.

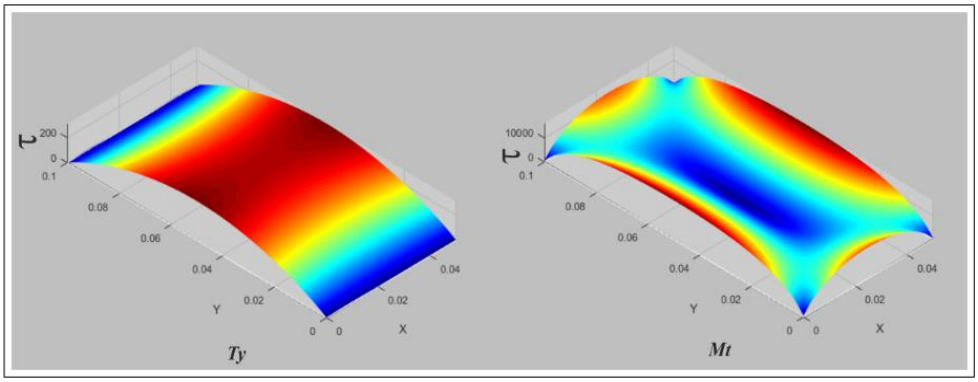

Fig 3. 4: Typical shear fields τ associated with the shear force T_y and the torsional moment M_t of an isotropic homogeneous rectangular section.

Three-dimensional solution (3D displacement field):

It is established that, for a beam far from the edges, the exact 3D solution (in displacement and in stress) is described by the 3D SV's solution. and, from the expression of this solution, the set of equations of the present classical beam theory follows.

The expression of the displacement field is obtained from the 3D SV's solution as follows:

$$\boldsymbol{\xi}_{\mathrm{SV}}(\mathrm{x},\mathrm{y},\mathrm{z}) = \mathbf{u}^{\mathrm{e}}(\mathrm{z}) + \boldsymbol{\omega}^{\mathrm{e}}(\mathrm{z}) \wedge \mathbf{GM} + \mathrm{T}_{\mathrm{x}}^{\mathrm{e}}(\mathrm{z}).\mathbf{U}^{1}(\mathrm{x},\mathrm{y})..$$
$$+\mathrm{T}_{\mathrm{y}}^{\mathrm{e}}(\mathrm{z}).\mathbf{U}^{2}(\mathrm{x},\mathrm{y}) + \mathrm{N}^{\mathrm{e}}(\mathrm{z}).\mathbf{U}^{3}(\mathrm{x},\mathrm{y}) + \cdots$$
$$\mathrm{M}_{\mathrm{x}}^{\mathrm{e}}(\mathrm{z}).\mathbf{U}^{4}(\mathrm{x},\mathrm{y}) + \mathrm{M}_{\mathrm{y}}^{\mathrm{e}}(\mathrm{z}).\mathbf{U}^{5}(\mathrm{x},\mathrm{y}) + \mathrm{M}_{\mathrm{t}}^{\mathrm{e}}(\mathrm{z}).\mathbf{U}^{6}(\mathrm{x},\mathrm{y}) \tag{3-16}$$

When $\mathrm{X}_{\mathrm{i}}^{\mathrm{e}}$ is represented by the internal force, the expression of the displacement is as follows:

$$\boldsymbol{\xi}^{SV}(x,y,z) = \overbrace{u^{e}(z) + \omega^{e}(z) \wedge X}^{\text{rigid motion of the section}} + \overbrace{\sum_{i=1}^{6} X_{i}^{e}(z)U^{i}(x,y)}^{sectional\ strain} \tag{3-17}$$

The first term translates the total movement of the section, while the second expresses its deformation. (u) and (ω) are the cross-section translation and rotation vector, respectively. $U^{i}(x,y)$ are the six (06) cross-section displacement modes of 3D SV's solution that correspond to each of the unit internal forces X_{i}^{e} = 1 (unity), where each of the six 3D SV's modes $U^{i}(x,y)$ contributes to sectional deformation by internal forces. This makes it possible to describe the Poisson's effects and out-of-plane warping, knowing that the characteristics of the cross-section $U^{i}(x,y)$ depend on the nature of the section only (its shape and materials).

For illustrations: Fig.3.5 shows, for a homogeneous isotropic rectangular section, from left to right, the Poisson's effect associated with the normal force N, and the warpings associated respectively with the shear force Ty and the torsional moment M_T.

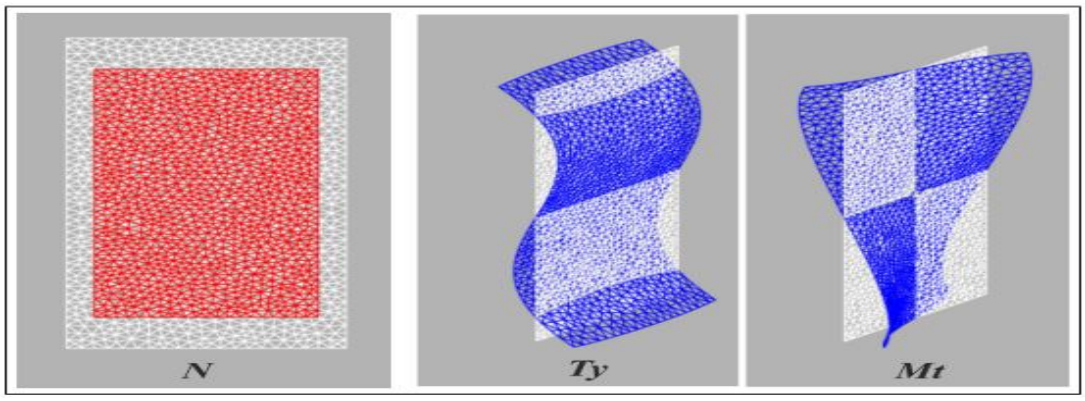

Fig 3. 5: Typical deformation modes for an isotropic rectangular section: Poisson effect associated with the Normal force N, and warping associated respectively with the shear force T_y and the torsion moment M_T.

3.5.4 Properties of the SV's solution

- The SV's solution is linear with respect to the internal forces which depend only on the torsion of the actions applied to the end sections.

- It is shown that the quantities $\boldsymbol{U}_{sv}^{i}, \boldsymbol{\sigma}_{sv}^{i}, \boldsymbol{\Lambda}_{sv}$ depend only on the nature of the section (shape and materials) and do not depend on the loading. As for the field $\boldsymbol{D}_{sv}$, it depends on the nature of the section and the type of uniform loading $[\boldsymbol{f}, \boldsymbol{F}]$ (El Fatmi [51]).
- The 3D SV's solution only verifies the extremity conditions in terms of resultants (forces and moments); it will only be correct away from the edges. In this respect, it is shown that the 3D exact solution tends asymptotically towards the 3D SV's solution when moving away from the edges. This property gives a special status to the SV's solution, i.e., it represents the 3D exact solution in the inner zone of the beam (provided that the length of the beam is greater than that characterising the edge effects). the SV's solution is often referred to as the central solution of the beam.

3.6 Mechanical characteristics of the cross-section

3.6.1 Homogeneous isotropic case

The stiffness operator $\boldsymbol{\Gamma}$ (matrix 6×6) is used to solve and define a one-dimensional (1D) problem, which depends only on the nature of the cross-section (shape, material). Where The flexibility operator is indicated by $\boldsymbol{\Lambda} = \boldsymbol{\Gamma}^{-1}$.

The structural flexibility is defined as follows:

$$\boldsymbol{\Lambda} = \begin{bmatrix} \frac{1}{GS_x} + \frac{y_c^2}{GJ} & \frac{-x_c y_c}{GJ} & 0 & 0 & 0 & \frac{y_c}{GJ} \\ \frac{-x_c y_c}{GJ} & \frac{1}{GS_y} + \frac{x_c^2}{GJ} & 0 & 0 & 0 & \frac{-x_c}{GJ} \\ 0 & 0 & \frac{1}{ES} & 0 & 0 & 0 \\ 0 & 0 & 0 & \frac{1}{EI_x} & 0 & 0 \\ 0 & 0 & 0 & 0 & \frac{1}{EI_y} & 0 \\ \frac{y_c}{GJ} & \frac{-x_c}{GJ} & 0 & 0 & 0 & \frac{1}{GJ} \end{bmatrix} \tag{3-18}$$

x_c and y_c are the coordinates of the shear centre C, J is the torsional inertia, G is the shear modulus, S_x and S_y are the reduced sectional connected to the shear forces T_x and T_y. I_x is the inertia moment with relation to x, and I_y is the inertia moment with relation to y. E is Young's

modulus. The constants [S; I_x; I_y; J; S_x; S_y; x_c; y_c] are only determined by the nature of the cross-section (shape and material). They can be specified once and for all for a particular section.

$$\boldsymbol{\sigma}^e(x,y,z) = \begin{bmatrix} 0 & 0 & \sigma_{xz}^e \\ 0 & 0 & \sigma_{yz}^e \\ \sigma_{xz}^e & \sigma_{yz}^e & \sigma_{zz}^e \end{bmatrix} \tag{3-19}$$

where the axial stress (σ_{zz}^e) is a function of $[\mathrm{N^e}, \mathrm{M_x^e}, \mathrm{M_y^e}]$ only. And the shears stress (σ_{yz}^e, σ_{xz}^e) are a function of $[\mathrm{T_x^e}, \mathrm{T_y^e}, \mathrm{M_t^e}]$ only. The axial stress, being a linear combination of $[\mathrm{N^e}, \mathrm{M_x^e}, \mathrm{M_y^e}]$, is written as follows:

$$\sigma_{zz}^e(x,y,z) = N^e(z,y) \cdot \left(\frac{1}{A}\right) + M_x^e(z,y) \cdot \left(\frac{y}{I_x}\right) - M_y^e(z,y) \cdot \left(\frac{x}{I_y}\right) \tag{3-20}$$

Different kinds of pressure fields σ_i associated with $[\mathrm{N^e}, \mathrm{M_x^e}, \mathrm{M_y^e}]$ that decrease the axial stress which can be obtained by:

$$\sigma^3(x,y) = \begin{bmatrix} 0 & 0 & 0 \\ 0 & 0 & 0 \\ 0 & 0 & \frac{1}{A} \end{bmatrix} . N^e$$

$$\sigma^4(x,y) = \begin{bmatrix} 0 & 0 & 0 \\ 0 & 0 & 0 \\ 0 & 0 & \frac{y}{I_x} \end{bmatrix} . M_x^e \tag{3-21}$$

$$\sigma^5(x,y) = \begin{bmatrix} 0 & 0 & 0 \\ 0 & 0 & 0 \\ 0 & 0 & -\frac{x}{I_y} \end{bmatrix} . M_y^e$$

These fields (σ^i) are only based on the cross-sectional properties $[A, I_x, I_y]$.

It should be mentioned that the SVBT leads to the same analytical description of the axial stress in the case of an isotropic homogeneous beam.

Shear stresses which are a linear combination of $[\mathrm{T_x^e}, \mathrm{T_y^e}, \mathrm{M_t^e}]$ are written as:

$$\sigma_{xz}^e(x,y,z) = f_x^x(x,y) \cdot T_x^e(z) + f_x^y(x,y) \cdot T_y^e(z) + f_x^t(x,y) \cdot M_t^e(z) \tag{3-22}$$

$$\sigma_{yz}^e(x,y,z) = f_y^x(x,y) \cdot T_x^e(z) + f_y^y(x,y) \cdot T_y^e(z) + f_y^t(x,y) \cdot M_t^e(z) \tag{3-23}$$

However, no analytical formulae are available to display the functions of the vectors (f_x, f_y, f_t) with relation to the special case of the circular section. Nevertheless, it is necessary to note that these functions only depend on the nature of the section (shape and material).

Three-dimensional (3D) displacement field:

For the case of the homogeneous and isotropic section, the SVBT of the 3D displacement field has been illustrated as follows:

- normal effort and bending moments $[N, M_x, M_y]$, only contribute to Poisson's ratio effects $[U^3(x,y), U^4(x,y), U^5(x,y)]$. are thus planes (the component along z is zero).
- Shear forces and torsional moments $[T_x, T_y, M_t]$, only contribute to warping. $[U^1(x,y), U^2(x,y), U^6(x,y)]$ They are therefore out-of-plane (their components, in relation to x and y, are zero).

3.6.2 Composite section (Any type of composite)

One-dimensional (ID) behaviour law:

There are many couplings between tension, bending and torsion in the composite section, due to the material being anisotropic. Besides, the stiffness operator Γ in a (6 × 6) matrix indicates the possibility that it is full. Also, every non-zero term out of the diagonal reflects a type of coupling. For the homogeneous case, the asymmetric cross-section results in bending and torsional coupling.

According to the compound homogeneous case, the various stiffness constants are expressed by:

$\widetilde{G_y S_x}$ the shear force stiffness /x

$\widetilde{G_y S_y}$ the shear force stiffness /y

$\widetilde{E_y S}$ the axial stiffness

$\widetilde{E_y I_x}$ the bending stiffness /x

$\widetilde{E_y I_y}$ the bending stiffness /y

$\widetilde{G_y J}$ the torsional stiffness.

The cross-sectional constants involved in the constitutive relations are the six classical composite cross-sectional constants $[\widetilde{G_y S_x}, \widetilde{G_y S_y}, \widetilde{E_y S}\ \widetilde{E_y I_x}, \widetilde{E_y I_y}, \widetilde{G_y J}\ ]$. The cross-sectional

constants are designated by these terms by analogy with the isotropic and homogeneous case; each term is to be considered as a symbol and is not separable (more details by El Fatmi and Ghazouani [52]).

Three-dimensional stress field:

For each composite section, the components (σ_{xx}; σ_{yy}; σ_{xy}) of the stress field are not null (see Eq. (3-19)). In the homogenous case, it is null (see Eq. (3-21)).

The variation in Poisson's ratio between materials is sufficient to produce stresses in the cross-section plane.

$$\boldsymbol{\sigma} = \begin{bmatrix} \sigma_{xx} & \sigma_{xy} & \sigma_{xz} \\ \sigma_{xy} & \sigma_{yy} & \sigma_{yz} \\ \sigma_{xz} & \sigma_{yz} & \sigma_{zz} \end{bmatrix} \tag{3-24}$$

Three-dimensional displacement field:

In the homogeneous isotropic case, $[N, M_x, M_y]$ lead only to Poisson's ratio effects, while [Tx, Ty, Mt] lead only to warping. in the composite case, any of the 6 internal forces $(T_x, T_y, N, M_x, M_y, M_t)$ can be responsible for both Poisson's effects and out-of-plane warping (Khebizi et al [28]).

3.7 Saint-Venant beam theory (SVBT)

Saint-Venant beam theory is the version of the beam theory proposed by Ladevèze and Simmonds [38].

Saint-Venant Beam Theory is the exact version of the classical beam theory. That is to say, the one that does not concede any additional assumptions to the initial modelling of the external and internal effects. This theory is governed by a system of equations involving quantities which have the particularity of being specific to the nature of the section (shape and material). SVBT, originally established for the homogeneous isotropic case, has been extended to the composite anisotropic case [53].

For a beam (Fig.3.6) it is established that away from the edges, the exact 3D solution (in displacement and stress) is described by the 3D SV's solution; and, it follows from the expression of this solution the set of equations of the present classical beam theory; or simply Saint Venant beam theory.

The relationship must be understood in both directions: SVBT can be traced back to the 3D SV's solution, which represents the exact 3D solution away from the edges.

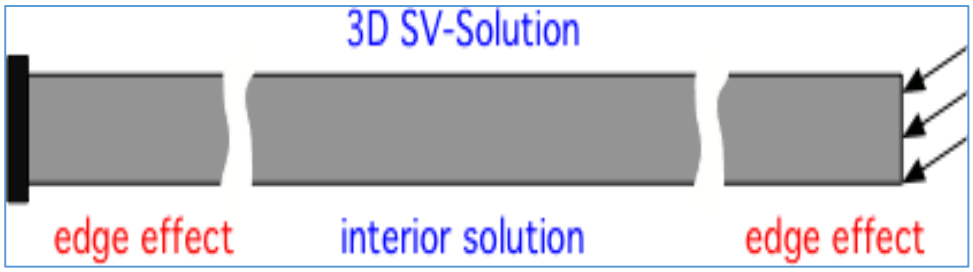

Fig 3. 6: 3D SV's solution and edge effects [54]

3.7.1 3D solution and one-dimensional equilibrium

The Saint-Venant beam theory is described by the following 1D equilibrium:

Equilibrium equations (1D):

$$\begin{aligned} \mathbf{R}' + \mathbf{p} &= \mathbf{0} \\ \mathbf{M}' + \mathbf{z} \wedge \mathbf{R} + \boldsymbol{\mu} &= \mathbf{0} \end{aligned} \tag{3-25}$$

The behaviour law (1D):

$$\begin{bmatrix} \mathbf{R} \\ \mathbf{M} \end{bmatrix} = \boldsymbol{\Gamma} \begin{bmatrix} \mathbf{u}' + \mathbf{z} \wedge \boldsymbol{\omega} \\ \boldsymbol{\omega}' \end{bmatrix}; \text{ and } \boldsymbol{\Lambda} = \boldsymbol{\Gamma}^{-1} \tag{3-26}$$

The boundary conditions:

$$\begin{bmatrix} \mathbf{u} \\ \boldsymbol{\omega} \end{bmatrix} \text{ or } \begin{bmatrix} \mathbf{R} \\ \mathbf{M} \end{bmatrix} \tag{3-27}$$

The solution (R, M, u, ω) leads to the displacement and stress fields:

$$\boldsymbol{\xi}^{SV}(x,y,z) = \overbrace{u^e(z) + \omega^e(z) \wedge X}^{\text{rigid motion of the section}} + \overbrace{\sum_{i=1}^{6} X_i^e(z) U^i(x,y)}^{sectional\ strain} \tag{3-28}$$

$$\boldsymbol{\sigma}^{e}(x,y,z) = \sum_{i=1}^{6} X_i^e(z) \boldsymbol{\sigma}^{i}(x,y) \tag{3-29}$$

3.7.2 Difference between Saint-Venant solution and Saint-Venant beam theory concerning boundary conditions

The difference between the Saint-Venant solution and the Saint-Venant beam theory that is important for us here is the imposition of boundary conditions. In actuality, the Saint-Venant solution is the Saint-Venant problem's solution whose fixed boundary conditions are the understanding of the force and moment resultants (F_0, C_0) and (F_L, C_L) on the end sections S_0

and S_L, respectively. On the other hand, the Saint-Venant beam theory allows to take into consideration other boundary conditions such as displacement conditions. This is done by knowing the kinematic quantities (u, ω). For example, an embedding at a section can be modelled with the condition (u, ω) = (0, 0). Note that the nullity of (u, ω) does not imply that the section deformations are null, since the deformations are related to the internal forces {Fi} and not to (u, ω), according to Eq (3-27).

3.8 Vlasov's hindered torsion

The case of an isotropic homogeneous section is restricted to the presentation because it allows to explain analytical results and clearly show the contribution of the hindered torsion compared to that of SV.

Vlasov only treated the special (practical) case of thin open sections. The developments will however be made for any section in order to justify Vlasov's equations for the particular case of open thin sections.

3.8.1 Saint Venant 's torsion questioned

First, it is useful to recall the basics of the SV torsion and to specify its limit.

SV's torsion properties:

- Apart from the circular case, a section warps under torsion and this warp is given by the warp function $\psi(x, y)$ which, in the sense of SV is a characteristic of the section
- The torsional behavior is governed by the relation $M_t = GJ\omega'$ where J, which the torsion constant, is given by: $J = \int_S \left(y\psi_{,x} - x\psi_{,y} - x^2 - y^2\right)dS$ where $(.)_{,x}$ and $(.)_{,y}$ denotes the partial derivatives with respect to *x* and *y*.
- A torsional moment only causes shear stresses, whose expressions are as follows:

$$\tau_{xz} = \frac{M_t}{J}\left(\psi_{,x} - y\right) \quad , \quad \tau_{xz} = \frac{M_t}{J}\left(\psi_{,y} + x\right) \tag{3-30}$$

Also, from a practical point of view:

- A section with a small warp results in a large torsion constant J; this is the case for solid or thin closed sections;
- A section with a large warp results in a small torsion constant J; this is the case for thin open sections;

For instance, the ratio of the torsion constant of a closed circular section (J_F) of radius R and thickness e to that of the same open section (J_O) is given by:

$$\frac{J_F}{J_O} \approx \frac{(2\Pi R^3 e)}{\left(\frac{2\Pi R e^3}{3}\right)} = 3\left(\frac{R}{e}\right)^2 \tag{3-31}$$

which leads, for R=10e, to a ratio of 300!

Limit of the SV's torsion

For the common thin beam and for any shape of the section, the SV torsion is correct to describe the behaviour of the beam when the end sections are free to warp (i.e. when the edge conditions are those of the SV problem). However, it can fail when warping is prevented, and this is especially true when the cross-section is thin open; i.e., when the warping of a section is potentially large.

The fact that warping is avoided (for instance at a recess) leads to axial stresses (σ_{zz}) and to a significant stiffening of the torsional behaviour of the beam, which the SV torsion cannot predict.

The so-called hindered torsion theory is a higher-order theory that has been developed to solve this problem. For example, it is of great interest in the field of steel construction since, for reasons of economy and assembly, almost all profiles are thin and open.

3.8.2 Hindered torsion theory

For the purposes of this theory, we assume that a cantilever beam is only ever subjected to $\boldsymbol{H}$ loading in S_L and that higher order kinematics are only ever limited to torsional motion. The two-parameter displacement model is provided by:

$$\boldsymbol{\xi}_{HT}(x,y,z) = \boldsymbol{\xi}(\omega,\eta) = \omega \boldsymbol{z} \wedge \boldsymbol{GM} + \eta\psi(x,y)\boldsymbol{z} \tag{3-32}$$

where η is the parameter used to control the section's torsional warp as determined by SV's solution to the warp function. The local 1D equations generated by this model are as follows:

$$\begin{aligned} M_t' &= 0 \\ M_\psi' - M_t^s &= 0 \end{aligned} \quad \text{Et} \quad \begin{bmatrix} M_t \\ M_t^s \\ M_\psi \end{bmatrix} = \begin{bmatrix} G(I_z - J) & -G(I_z - J) & 0 \\ -G(I - z - J) & G(I_z + J) & 0 \\ 0 & 0 & E^* I_\psi \end{bmatrix} \begin{bmatrix} \omega' \\ \eta \\ \eta' \end{bmatrix} \tag{3-33}$$

And the boundary conditions:

$$\begin{matrix}[\omega,\eta] & = [0,0] & \text{en } z=0 \\ [M_t, M_\psi] & = [C,Q] & \text{en } z=L\end{matrix} \quad \text{avec} \quad \begin{matrix}C = \int_S \left(xH_y - yHx\right)dS \\ Q = \int_S (xH_z\psi)dS\end{matrix} \tag{3-34}$$

Where $E^* = \frac{(1-\nu)}{(1-2\nu)(1+\nu)}E, I_\psi = \int_S \psi^2 dS, Q$ is a new external force and M_t^s and $M_\psi$two new internal forces called respectively the secondary torsion moment and the bi-moment, and they are defined as follows.

$$M_t^s = \int_S \left(x\sigma_{yy} + y\sigma_{xx}\right)dS \qquad M_\psi = \int_S (\psi\sigma_{zz})$$

The components of the 3D stress field corresponding to this model are given by the relations:

$$\begin{aligned}\sigma_{zz} &= \frac{M_\psi}{I_\psi}\psi \\ \tau_{xz} &= \frac{M_t}{J}\left(\psi_{,x} - y\right) + \left(\frac{y(I_z+J) + Iz\psi_{,x}}{J(I_z-J)}\right)M_t^s \\ \tau_{yz} &= \frac{M_t}{J}\left(\psi_{,y} + x\right) + \left(\frac{x(I_z-J) + Iz\psi_{,x}}{J(I_z-J)}\right)M_t^s M_t^s\end{aligned} \tag{3-35}$$

And also $\sigma_{xx} = \sigma_{yy} = \frac{\nu}{1-\nu}\sigma_{zz}$ et $\tau_{xy} = 0$

Torsion equation

Equations (3.29) and (3.3) demonstrate that the torsional motion is governed by the equations:

$$-E^* I_\psi \frac{Iz}{Iz-J}\omega''' + GJ\omega' = C \tag{3-36}$$

For SV torsion, this equation would have given $GJ\omega' = C$. The factor $E^* I_\psi \frac{Iz}{Iz-J}$ is called the warp stiffness and I_ψ is called the warp constant.

Comments

In comparison, at SV torsion, the hindered torsion led to axial stresses σ_{zz} via the contribution of the bi-moment M_ψ, different shears due to the contribution of the secondary torsional moment M_t^s , and the torsional behaviour of the beam was stiffened via the warp constant I_ψ (the objective is achieved).

Vlasov's theory

In reality, Vlasov's theory was only created for the specific (practical) case of open thin sections, and it results in the equation:

$$-EI_{\phi}\omega''' + GJ\omega' = C$$

where $\phi(s)$ is an approximation of $\psi(x,y)$ on the profile of the section (of abscissa s); $\phi(s)$ has the advantage of being analytically computable for any open thin section.

Furthermore, the factor $\left(\frac{Iz}{Iz-J}\right)$ is absent, this is justified for open sections because their torsion constant checks $J \ll I_z$. Finally, E appears in place of E^*: this is an (artificial) correction in order to put back the Poisson effect that the kinematic model excludes (and by the same token cancel the stresses σ_{xx} et σ_{yy}).

3.9 Conclusion

Beam theories are models of the continuous medium that simplify the solution of the mechanical problem and provide approximations of the required solution. There are three main approaches:

- Saint-Venant's beam theory which follows from Saint-Venant's solution
- The asymptotic approach
- The cinematic approach

This chapter includes many theories related to beam computation, "classical beam theories". When talking about classical beam theories, Timoshenko and Bernoulli are systematically put forward, depending on whether or not one wishes to account for shear forces. In Euler – Bernoulli beam theory, shear deformations are neglected, and plane cross-sections remain plane and normal to the longitudinal axis. In the Timoshenko beam theory, plane cross-sections still remain plane but are no longer normal to the longitudinal axis.

In addition, Saint Venant Beam Theory (SVBT) is one of the classical beam theories that leads to the 3D SV's solution, which has the special status of representing the exact 3D solution away from the edges. The SV's solution allows, even in complex cases, to account for the nature of the cross-section (shape and materials) and to give access to the state of stress in each of the materials that form the cross-section; this is fundamental when dealing with a heterogeneous beam.

However, the SV solution is still limited by the SV principle or the extent of the edge effects, which are not necessarily confined to the edges. The extremity solution is a decreasing solution that represents the edge effects, whereas the Saint-Venant's solution $\boldsymbol{s}^{SV}$ is z-polynomial and provides the exact interior solution, far enough away from the singularity zones. The presentation of the SV's solution has shown the existence of a set of section

operators that account for its mechanical behaviour with respect to the six classical interior forces. These operators are only dependent on the section (shape and materials) and can be computed once and for all. They are formed by:

- six displacement fields $\mathcal{U}_{SV}$ types associated with the six internal forces;
- six stress fields $\mathcal{S}_{SV}$ types associated with the six interior forces.

In particular, the displacement fields of the $\mathcal{U}_{SV}$, called section deformation modes, will be used to define the kinematics of the beam models in this work (next chapter).

The Vlasov hindered torsion (used in metal construction) must take precedence over the SV's torsion for the torsion of thin open profiles of common lengths. If for the homogeneous isotropic case, the only known practical case concerns the torsion of thin open profiles, it is quite different for the composite case. The extent of the edge effects depends on the loading, the type of edge condition and the nature of the section (shape and material(x)).

4 A refined beam theory and boundary conditions

4.1 Introduction

This chapter includes two higher-order beam theories built on the Saint Venant solution, called Refined Beam Theory (RBT) and Refined Beam Theory using Distortion Modes (RBT*). They are referred to as RBT/SV (as in the refined beam theory built on the SV solution). The RBT/SV models appear as a hybrid theory that combines the displacement model and the SV solution. The role of these theories is to find the 3D Saint Venant solution away from the edges because the displacement model contains the shape of the displacement of the Saint Venant solution, and to better take into account the edge effects because the boundary conditions can be better satisfied (in force and displacement). The RBT/SV models can be seen as a very extensive generalisation of Vlasov's theory; the latter is only concerned with torsional warping for the special case of homogeneous and isotropic open thin sections, whereas RBT addresses any cross-section (shape and material) and considers all types of cross-sectional deformations (warping, Poisson's effects, distortions).

The study or application of RBT/SV models can only be done numerically (finite element). A tool called CSB (CSection & CBeam) developed under Matlab and to which this work contributes is presented. It provides a systematic calculation method whatever the nature of the section: any shape (solid, thin/thick, closed/open), homogeneous, or composite (freely arranged materials and anisotropic in the broad sense).

In this chapter, boundary conditions and edge effects are also taken into account. in order to a better treatment of the boundary conditions, the proposed approach consists in partitioning the beam into two domains: the inner area (1D finite elements) and the edges zone (3D finite elements). This approach allows the boundary conditions in the 3D areas to be imposed exactly and to dispense with their modeling in the 1D or generalized sense. This part aims at coming back to the treatment of CBs in the generalized sense (1D) and to propose the RBT/SV theory on which this thesis is based. Moreover, the RBT* theory allows to get rid of the 1D modelling of the BCs by imposing them in an exact way. This theory allows the avoidance of a complete 3D computation of the beam by better consideration of the BCs and access to the 3D solution of the beams at the edges.

4.2 Higher-order beam theories (RBT and RBT*)

RBT and **RBR*** are higher-order beam theories mainly based on the 3D SV’s solution.

- Refined Beam Theory **RBT**: includes the edge effects, where only the 6 Saint-Venant cross-section deformation modes are taken into account.

- Refined Beam Theory Using the Distortional Modes **RBT***: includes edge effects, where all available cross-section deformation modes are taken into account.

The Reference problem:

As in SVBT, we show the equilibrium of a cantilever beam (Fig.4.1) with constant indefinite cross-section S, axis z and length L. The beam fixed at $z = 0$. is subjected to a surface force H at $z = L$ and a volume force f.

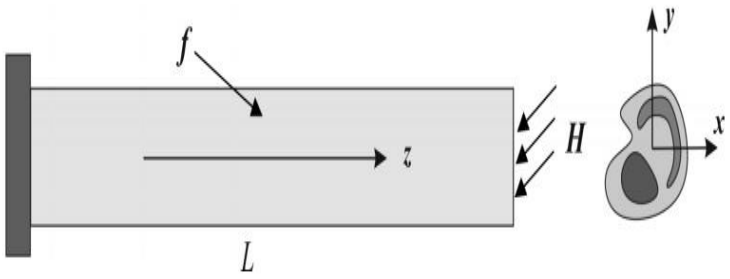

Fig 4. 1: Cantilever composite beam subjected to a body force and tip traction.

4.2.1 RBT displacement model

The displacement field of a coordinate point (x, y, z) belonging the beam is given as follows:

$$\boldsymbol{\xi}(x,y,z) = \overbrace{\boldsymbol{u}(z) + \boldsymbol{\omega}(z) \wedge \boldsymbol{X}}^{\text{rigid montion of the section}} + \overbrace{\sum_{k=1}^{p} \eta_k(z) M^k(x,y)}^{enrichment} \tag{4-1}$$

The cross-section translation and rotation vectors are respectively (u; ω), and X is the cross-section vector position. The second term is used to deform the section depending on the modes $M^k(x, y)$, (the displacement field of the cross-section), considered to be defined, and where each parameter $\eta_k(z)$ determines the amplitude of the mode $M^k(x, y)$.

The kinematic parameters $\{u_x, u_y, u_z, \omega_x, \omega_y, \omega_z, \dots, \eta_k, \dots\}$ related to the general model constitute (6 + P) degrees of freedom of the section's motion. (u_x, u_y, u_z) is used to control the translations of the section, $(\omega_x, \omega_y, \omega_z)$ uses the rotations of the section, and $\{\eta_k\}$ associated to the sectional modes M^k used to control the deformation modes of the section.

The formulation of higher displacement model faces a difficult in selecting the modes. in order of number (not too large) as well selection (the most relevant to describe the deformation of the section) [55].

4.2.2 RBT* displacement model

The mode M^k is mainly selected according to the six modes of cross-section deformation associated with the six internal forces that characterize cross-section deformations $U^i(x,y)$, according to SVBT. $D^j(x,y)$ are the additional distortion modes taken into account when the section is thin. These deformation modes are the first natural modes of vibration of the section [56].

In the RBT* model, the displacement vector is given by:

$$\boldsymbol{\xi}(x,y,z) = \overbrace{\boldsymbol{u}(z) + \omega(z) \wedge \boldsymbol{X} + \sum_{i=1}^{6} \alpha_i(z)\boldsymbol{M}_{sv}^{i}(x,y)}^{\textbf{shape of SVBT displacement}} + \sum_{j=1}^{m} \beta_j(z)\boldsymbol{D}_{v}^{j}(x,y) \tag{4-2}$$

4.2.2.1 The one-dimensional equilibrium equations of the beam

The equations governing the equilibrium of the beam according to RBT and RBT* are:

Equilibrium equations (1D):

$$\left.\begin{array}{ll} \boldsymbol{R}' + \boldsymbol{p} & = 0 \\ \boldsymbol{M}' + \boldsymbol{x} \wedge \boldsymbol{R} + \boldsymbol{\mu} & = 0 \\ A^{k\prime} - A_s^k + \ k^k & = 0(\forall k) \end{array}\right\} \tag{4-3}$$

The behaviour law (1D):

$$\begin{bmatrix} \boldsymbol{R} \\ \boldsymbol{M} \\ \vdots \\ A_s^k \\ A_k \\ \vdots \end{bmatrix} = \boldsymbol{\Gamma}_{RBT} \begin{bmatrix} \boldsymbol{u}' + \boldsymbol{z} \wedge \boldsymbol{\omega} \\ \boldsymbol{\omega}' \\ \vdots \\ \eta_k \\ \eta_k' \\ \vdots \end{bmatrix} \tag{4-4}$$

Once again, A_s^k and A_k are M^k connected and characterised by internal efforts (El fatmi [51]).

$$\left.\begin{array}{l} A^k = \int_S \left(\sigma_{xz}M_x^k + \sigma_{yz}M_y^k + \sigma_{zz}M_z^k\right)dS \\ A_s^k = \int_S \left(\begin{array}{c} \sigma_{xx}M_{x,x}^k + \sigma_{yy}M_{y,y}^k + \sigma_{xy}\left(M_{x,y}^k + M_{y,x}^i\right) \\ +\sigma_{xz}M_{z,x}^k + \sigma_{yz}M_{z,y}^k \end{array}\right)dS \end{array}\right\} \tag{4-5}$$

$[\sigma_{xx}; \sigma_{yy}; \sigma_{xy}; \sigma_{xz}; \sigma_{yz}; \sigma_{zz}]$ are the stress tensor components.

For the problem of the cantilever in Fig 4.1, the boundary conditions (1D) are as follows:

$$x = 0\ (\boldsymbol{u}, \boldsymbol{\omega}) = (\mathbf{0}, 0) \text{et}\ \{\eta\} = \mathbf{0}(\forall k)$$
$$x = L[\boldsymbol{R}, \boldsymbol{M}] = [\boldsymbol{F}, \boldsymbol{C}]\ \text{et}\ A^k = Q^k(\forall k) \tag{4-6}$$

Where $\boldsymbol{R}$ and $\boldsymbol{M}$ are the classical internal forces (1D).

$$\left.\begin{aligned} \boldsymbol{R} &= \int_S \boldsymbol{\sigma} \cdot \boldsymbol{z} dS \\ \boldsymbol{M} &= \int_S (\boldsymbol{X} \wedge \boldsymbol{\sigma} \cdot \boldsymbol{z}) dS \end{aligned}\right\} \tag{4-7}$$

The external forces (1D) are described by:

$$\left.\begin{aligned} p &= \int_S f dS & P &= \int_{S_L} H dS \\ \mu &= \int_S GM \wedge f dS & F &= \int_{S_L} GM \wedge H dS \\ \kappa^k &= \int_S f \cdot M^k & Q^k &= \int_{S_L} H \cdot M^k dS \end{aligned}\right\} \tag{4-8}$$

(p, μ, P, C) indicates the classical 1D external forces related to translation and rotation, and (κ^k, Q^k) expresses new external forces related to the M^k modes.

The 1D behaviour operator is given by:

$$\boldsymbol{\Gamma}_{RBT} = \int_S \boldsymbol{B}^t(x,y) \boldsymbol{K}(x,y) \boldsymbol{B}(x,y) dS \tag{4-9}$$

Where K is the matrix (6 × 6) related to the elastic tensor and B is expressed as follows:

$$\boldsymbol{B} = \begin{bmatrix} 0 & 0 & 0 & 0 & 0 & 0 & \dots & M^k_{x,x} & 0 & \dots \\ 0 & 0 & 0 & 0 & 0 & 0 & \dots & M^k_{y,y} & 0 & \dots \\ 0 & 0 & 0 & 0 & 0 & 0 & \dots & M^k_{x,y} + M^k_{y,x} & 0 & \dots \\ 1 & 0 & 0 & 0 & 0 & -y & \dots & M^k_{z,x} & M^k_x & \dots \\ 0 & 1 & 0 & 0 & 0 & x & \dots & M^k_{z,y} & M^k_y & \dots \\ 0 & 0 & 1 & y & -x & 0 & \dots & 0 & M^k_z & \dots \end{bmatrix} \tag{4-10}$$

Where $(\cdot)_{,x}$ and $(\cdot)_{,y}$ denote the partial derivation relative to x and y [51].

4.2.2.2 Three-dimensional solution

For the displacement $[u^e(z), \omega^e(z), \{\eta^\varepsilon(z)\}]$, the 1D solution permits a return to the 3D solution using the 3D displacement field:

$$\boldsymbol{U}^e(x,y,z) = \boldsymbol{U}(\boldsymbol{u}^e, \boldsymbol{\omega}^e, \{\eta\}^e) = \boldsymbol{u}^e(z) + \boldsymbol{\omega}^e(z) \wedge \boldsymbol{X} + \dots \eta^e_k(z) M^k(x,y) \tag{4-11}$$

This produces the 3D stress tensor field:

$$\boldsymbol{\sigma}^e(x,y,z) = \boldsymbol{K}(x,y) : \boldsymbol{\varepsilon}(\boldsymbol{U}^e(x,y,z)) \tag{4-12}$$

Where:

$$\varepsilon(\boldsymbol{U}) = \frac{1}{2}(\nabla^t \boldsymbol{U} + \nabla \boldsymbol{U}) \tag{4-13}$$

Provides the deformation tensor attached to **U**.

4.2.2.3 Comment for refined beam theories

Refined beam theories (RBTs) models that allow him to:

- To better satisfy the support conditions, because its displacement model allows to control the movements of the section (u, ω) but also its deformations $\{\eta_k\}$; thus, for example, a real embedding can be imposed.
- To better model the external effects, since they are no longer reduced, at the current section, to only a force and a moment ($[\boldsymbol{F}, \boldsymbol{C}]$, $[p, \mu]$); other forces come into play (Q^k, k^k) which are due to the projection of the external effects on the modes M^k.
- To **find** the **3D SV's solution** away from the edges because the displacement model contains the displacement shape of the Saint Venant solution; and **to better account for edge effects** because the boundary conditions can be better satisfied (in force and displacement).
- Finally, RBT can be seen as a very extensive generalisation of Vlasov's theory; the latter only concerns torsional warping for the special case of homogeneous and isotropic open thin sections, whereas RBT addresses any section (shape and material) and considers all types of cros-section deformations (Poisson's effects, warping distortions).

4.2.2.4 Advantages of RBT/SV model compared to other models

The Saint Venant or Timoshenko/Bernoulli beam theories are classical beam theories. It should be remembered that the Timoshenko/Bernoulli beam theories are based on simplifying assumptions. i.e., the starting point is a displacement model which supposes that the section is undeformable (they do not take into account beam cross-section deformation), and the 3D computation time is too heavy (a large number of finite elements). Saint Venant's beam theory follows from the 3D SV's solution, where the section is free to deform. It also owes its justification to the fact that the resolution according to the SV beam theory leads to the 3D

SV's solution which represents, far from the edges, the exact 3D solution of the equilibrium of the beam (more details about beam models [57]).

RBT/SV is a higher-order beam theory built (mostly) on SV's solution; which allows it: to better satisfy the support conditions, better model the external actions, and find far from the edges the 3D SV's solution because the displacement model contains the shape of the displacement of the SV's solution; and to better account for edge effects, because the boundary conditions can be better satisfied (in terms of force and displacement). Finally**,** RBT can be seen as a very extended generalization of Vlasov's theory; this only concerns torsional warping for the special case of homogeneous and isotropic open thin sections, whereas RBT/SV addresses any section (shape and material) and considers all types of section deformation (warping, Poisson's effects, distortions).

4.3 Distortion modes

The distortion of a thin section is a deformation of its profile. Fig.4.2 shows an example of distortion for an I-section. The distortion is practically due to the low bending stiffness of the legs of the section profile.

In RBT/SV, it is considered that a distortion of any shape can be approximated by the combination of n simple distortion modes.

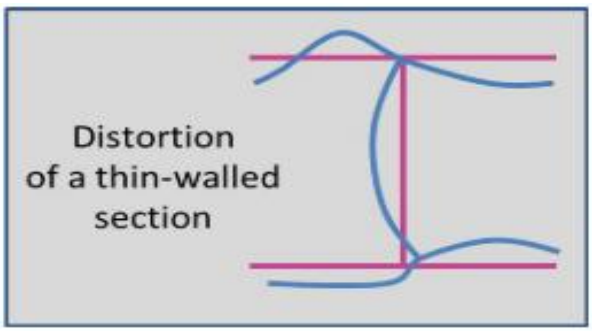

Fig 4. 2: Distortion of I-thin section [51]

In order to determine a simple distortion mode, SV’s problem is considered for a beam in equilibrium under end loading and uniform lateral loading; for example, for an I-section, the case of linear lateral loading specified in Fig.4.3 (warp).

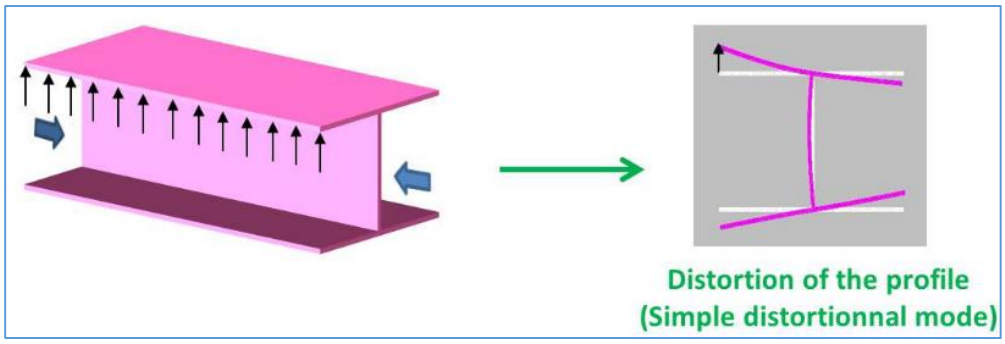

Fig 4. 3: Uniform lateral loading: I-beam and cross-section distortion [51]

For this problem, the displacement field of SV gives rise to the term D_{sv}^{j}, whose contribution to the deformation of the section is illustrated by the distortion described on the right-hand side of figure.4.3 This mode is considered as a simple distortion mode.

In order to consider n modes of simple distortions requires to consider (separately) n cases of lateral uniform loadings for the beam.

For example, figure.4.4 shows 5 loading cases to get 5 simple distortion modes. These 5 cases are gathered on a figure.4.5(left) section; but a richer model could use more modes by considering the 11 cases specified figure.4.5 (right)

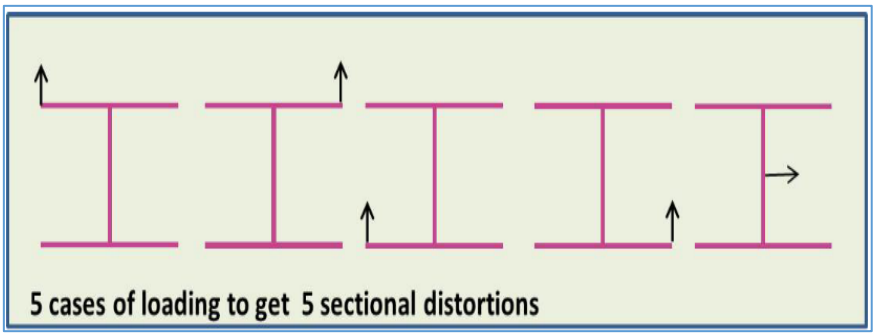

Fig 4. 4: 5 load cases for an I-section.

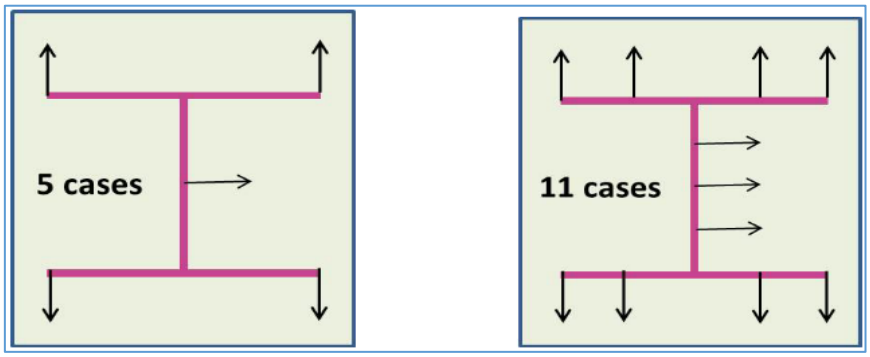

Fig 4. 5: Different load cases (5 and 11) for the I-section [51]

4.4 Cross-section beam analysis (CSB) package

CSB (Cross-Section and Beam analysis) is a numerical tool dedicated to the computation of beams with a cross-section of any shape, made of isotropic or anisotropic materials freely arranged. It allows to solve, in the standard framework of linear elasticity, the equilibrium of a beam subjected to any loading and support conditions.

The beam theory (RBT/SV) proposed by El Fatmi [51] is a higher order beam theory whose originality is to use as section deformation modes the section specific modes that reflect the physical nature of the section (shape and materials). These modes are part of the Mechanical Characteristics of the Section (MCS) provided by the 3D SV's solution. It thus appears that this RBT/SV theory adapts to the (physical) nature of the section.

4.4.1 The functioning of CSB

To solve a beam problem through RBT/SV, two steps are required:

- Calculate the section modes M^k. This task is performed with the numerical tool **CSection**. Starting from the definition of the cross-section (shape and materials), **CSection** provides the calculation of the cross-section modes by 2D finite elements.
- Formulate the corresponding higher order theory (RBT/SV) and solve the 1D beam problem. The complementary tool to **CSection**, named **CBeam**, already operational to compute the 3D solution of SV, has been extended to perform this task automatically (regardless of the number of modes chosen for the section). **CBeam** uses the section modes provided by **CSection** and calculates the beam problem according to the variational and 1D finite element formulation.

Important: The calculation of the Mechanical Characteristics of the Section (MCS) is performed by 2D finite elements. However, CSection does not provide a 2D mesher, but imports a section whose geometry and mesh have been previously made. Currently, the meshing is assumed to be done using the Gmsh generator.

This combination of 2D and 1D calculations that leads to a 3D solution that is fully comparable to a real 3D finite element calculation.

The **CSection** and **CBeam** numerical tools form the **CSB** package required for the application of RBT/SV (see Fig.4.6). The computation time for **CSB** is of the order of a few seconds on a standard PC; this time is mainly consumed by **CSection**; a complex section may require a large 2D mesh.

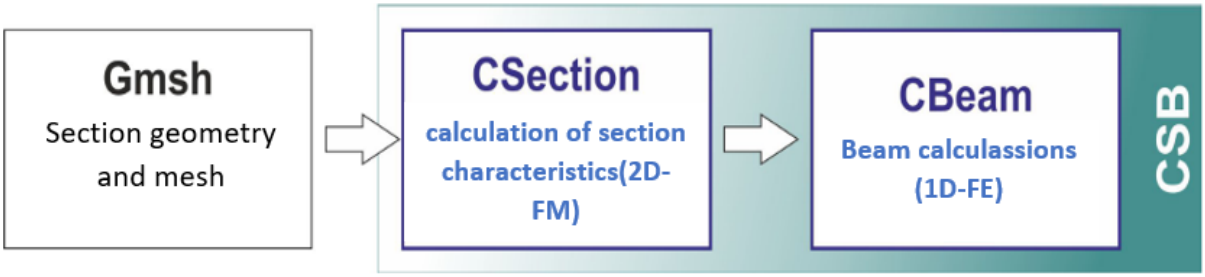

Fig 4. 6: The functioning of CSB

4.5 On boundary conditions and edge effects

The properties of the edge effects are related to the treatment of the Boundary Conditions (BCs) in the generalised (1D) sense that is associated with the beam model used. This treatment, which can be seen as a modeling (or an approximation) of the BCs, necessarily leads to a loss of information about the reality or the exact 3D data of these BCs. when the extent of the edge effect is large, it can dominate the mechanical behaviour of the beam and call into question the behaviour described by the beam theory used: both the inner 3D solution and the global 1D behaviour.

The objective of this part is to come back to the treatment of BCs in the generalized sense (1D) and to propose, for the RBT/SV theory on which this thesis work is based. in addition, RBT* theory allows getting rid of the 1D modelling of BCs by imposing them in an exact way. This theory, which avoids the need for a full 3D calculation of the beam, will offer two things:

- better consideration of BCs: this sometimes allows for an improved inner solution associated with RBT theory.
- access to the 3D solution of the beams at the edges.

4.5.1 Boundary conditions and edge effects

For the sake of exposition, let us consider the equilibrium of a beam subjected to the conditions of support and loading at its ends S_0 and S_L as shown in figure.4.7.

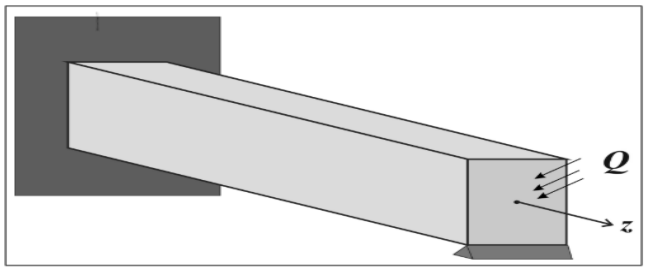

4. 7: Clamped and simply supported beam subjected to surface force Q

For instance, let us consider the application of the Saint Venant Beam Theory (SVBT), which is considered here as the reference for representing the classical theories (by classical we mean those governed by the 6 classical internal forces).

The SVBT has the advantage of a clear status: the inner $3D$ solution to which it leads corresponds to the solution towards which the exact $3D$ solution tends when one moves away from the edges. And it is now established that the edge effects associated with it depend on the BC and the nature of the section (shape and materials).

For the application of SVBT to the above beam problem, the treatment of the boundary conditions is as follows:

- In S_0, the embedding is carried out by blocking the translations and rotations of the section;
- in S_L, the support is made by blocking the vertical translation and the loading considered is the torsor $\mathcal{Q}$ associated with the applied force **Q**.

This is an exact $3D$ BC model. Indeed:

- In S_0, the embedding thus achieved leaves the section free to deform;
- in S_L, the simple support as modelled does not block the vertical translation of all the points of the lower edge of the section, and the torsor $\mathcal{Q}$ does not allow to account for the exact way in which the force **Q** is applied.

Let d_0 and d_L be the distances from the sections S_0 and S_L for which the $3D$ SV's solution represents (almost) the exact $3D$ solution. Figure.4.8 this assumes that the dimension that characterises the length of the beam (L) is (sufficiently) larger than the dimension that will simply be noted as d that characterises the extent of the edge effects.

Let us note formally:

- $\langle \boldsymbol{\xi}, \boldsymbol{\sigma} \rangle$, the exact $3D$ solution.
- $\langle \boldsymbol{\xi}_{sv}, \boldsymbol{\sigma}_{sv} \rangle$, the $3D$ SV's solution, the one valid in the inner area of the beam.
- $\langle \boldsymbol{\xi}_{\text{bords}}, \boldsymbol{\sigma}_{\text{bords}} \rangle$, the $3D$ solution at the edges, i.e., the restriction of the exact $3D$ solution to the areas relative to d_0 and d_L.

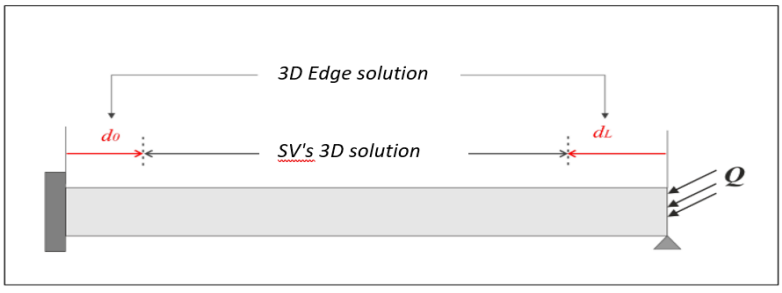

Fig 4. 8: Edge solution and SV's solution.

SVBT is only of interest if $L \gg d$; i.e., if the corresponding edge effects appear to be confined to the edges; if this is the case, the $1D$ beam theory correctly describes the global (macrocospic) behaviour of the beam and the associated $3D$ solution correctly describes the equilibrium state of the inner zone; this is what is expected from a beam theory.

Otherwise, if d appears of the same order as L, the beam theory is questioned, and a finer beam theory becomes necessary. Beyond the SVBT, this discourse is valid for any beam theory. What changes from one beam theory to another is the quality and extent of the $3D$ solution that the theory provides for the inner zone and thus the extent of the edge effects. For example, RBT has been shown to be a beam theory that goes beyond the SVBT to incorporate a significant portion of the edge effects that are associated with the SVBT; it is satisfactory in a larger interior area and the corresponding edge effects manifest themselves in a smaller area than for the SVBT.

Beyond the extreme sections of the beam, edges are in fact any singularity of the restriction of the exact $3D$ solution in the areas around the singularities (Fig.4.9). By loading, support, change of section, ... and by solution at the edges $\langle \boldsymbol{\xi}_{\text{bords}}, \boldsymbol{\sigma}_{\text{bords}} \rangle$ elsewhere, L will continue to characterise the dimension of the beam or structure and d the dimension that characterises the extent of the edge effects.

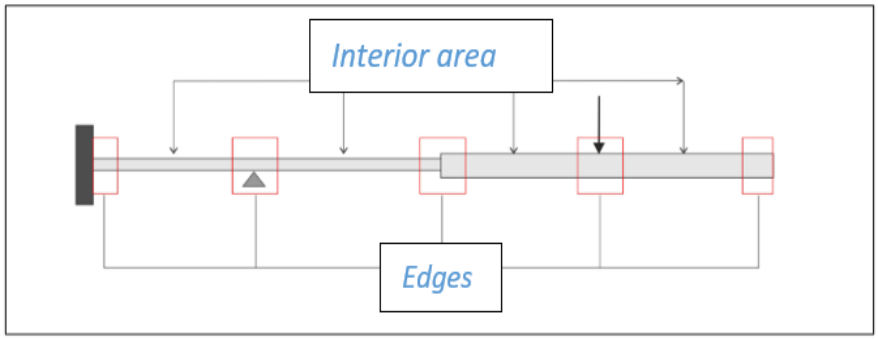

Fig 4. 9: Edges: any area around a support singularity, loading, change in section, etc.

The bottom line is that:

- The objective of a beam theory is to describe correctly the global $1D$ macroscopic behaviour of the beam and to provide a correct $3D$ solution in displacement and stresses in an inner zone of the beam whose dimension is much larger than that characterising the associated edge effects.
- Whatever $1D$ beam theory is used, there will always be a deviation from the exact $3D$ solution, especially at the edges.
- when the extent of edge effects is large (d of the order of L), the results of beam theory ($3D$ interior solution and $1D$ global behaviour) can be questioned.

- whatever the extent of the edge effects, it may still be necessary to supplement the inner 3D solution with the calculation (at least a sufficient approximation in the engineering sense) of the 3D solution at the edges, because it may be dimensional.

4.5.2 Applications

The two examples that will be analysed are the beams, shown in Figure.4.10, that were analysed in detail in (El Fatmi [51]):

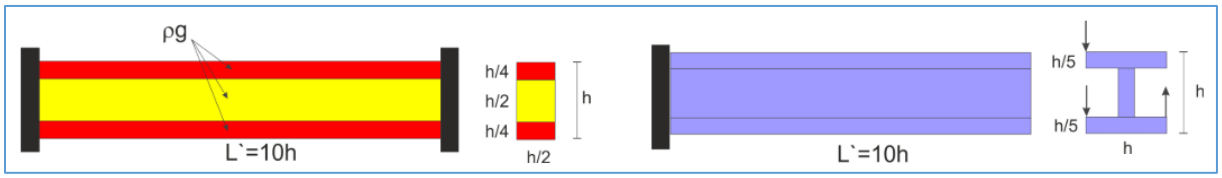

Fig 4. 10: The two examples as analysed [51]

- Simple bending (under self-weight ($\rho \boldsymbol{g}$)) of a bi-clamped beam whose sandwich section with isotropic phases is strongly contrasted (1/200);
- The bending-torsion (loading concentrated at the free end) of an isotropic homogeneous I-beam;

The section geometries are shown in Fig.4.10 and the materials in Table.4.1.

These two cases, which were analyzed to validate the RBT theory, led respectively to an extremely significant shear force effect and a hindered warping effect.

Table 4. 1 Material properties

sandwich/skin, Mat_s sandwich/core, Mat_c	E_s= 200 Gpa E_c= 1 Gpa	V_s = 0.25 V_c = 0.25
I-profile, Mat	E = 200 Gpa	V_c = 0.25

However, these validation tests were carried out for BCs (embedded and free sections) which are particularly well suited to the RBT displacement model. This is an opportunity to confront the RBT theory with conditions that are less obvious to satisfy, such as the simple support specified in 3D in Figure.4.11 We will see that this is where the RBT* connection is a way forward to better capture the reality of the edge condition.

For this purpose, the same beam will be analysed for the case embedded on one side and simply supported on the other Fig.4.11.

- the profile whose thickness is here (t=h/10) is maintained in torsional-bending but for a loading imposed eccentrically on the upper flange; the slenderness is maintained at L/h=10.

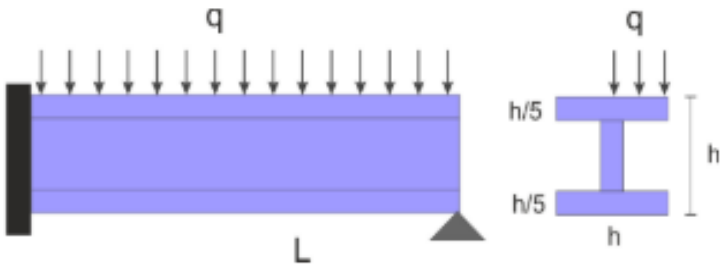

Fig 4. 11: An example that will be analysed according to an RBT* calculation

But before performing this RBT* analysis, it is useful (for the following) to recall the main results obtained in (El Fatmi [51]) regarding the shear and general buckling effects led to by the simple bending of the sandwich and the torsion-bending of the profile, respectively, both of which have been treated for a relatively small release (L/h=10).

4.5.2.1 On the shear effect

It was shown that the simple bending of the bi-encased sandwich beam led to a shear effect which increases with the ratio of the stiffness contrast ($r = E_s/E_c$) between the skin and the core. This shear effect can be seen at two levels:

- by the value of the reduced cross-section coefficient $\left(k_y = \frac{GSy}{\langle GS \rangle}\right)$ which decreases sharply with the stiffness contrast r Table.4.2; ($\langle GS \rangle$ is the average over the section of GS).

Table 4. 2 The coefficient k_y according to the ratio $r = E_s/E_c$ for the sandwich section [51]

r	1	10	50	100	200
k_y	0.8330	0.2087	0.0469	0.0238	0.0120

- by the contribution of the shear force in the displacement u_y of the mean line of the beam; the figure illustrating this displacement for the case r =200 compares the SV results of RBT and 3D-FE.

Comment: The displacement of SV already accounts (via the reduced cross-section) for the shear effect:

$$u_y(L/2) = \underbrace{\frac{qL^4}{384EIx}}_{\text{effet du moment}} + \underbrace{\frac{qL^2}{8GSy}}_{\text{effet de l'effort tranchant}} \tag{4-14}$$

where q is the clean weight. However, the SVBT leaves the shear forces at the right of the embedding free; this leads (Fig.4.12) to a significantly larger deflection than the reality illustrated by the 3D-FEM result, which the RBT theory correctly describes because shear forces are prevented.

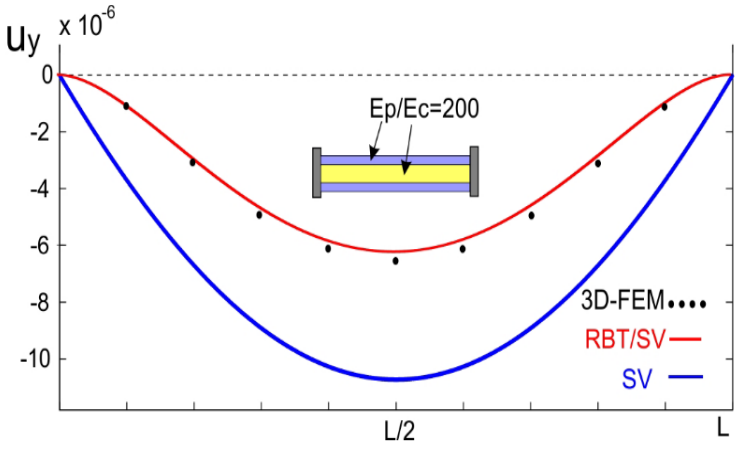

Fig 4. 12: Deflection of the mean line [51].

The fact that the solution of SV leaves free warpings of shear force at the ends thus leads to a more flexible behavior.

4.5.2.2 On the effect of the hindered warp

Fig.4.13. shows the variations of the axial stresses σ_{zz} for two points A and B of the upper flange: for the SVBT, the RBT theory and via an 3D-FEM calculation. In addition, Fig.4.14 (right) gives the distributions of the axial stress at the level of the embedding.

For this section in torsional-bending, the SV's solution fails because the warping, which is free to occur at the free edge, is prevented at the level of the embedding. The warping of the section is here due to the torsion moment and the shear force. This warping prevented at the level of the embedding leads to an axial stress σ_{zz} that the solution of SV cannot predict.

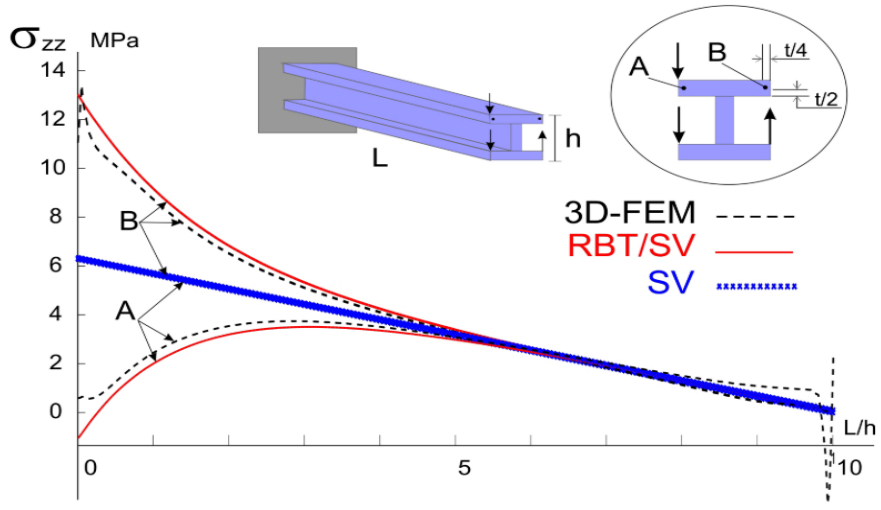

Fig 4. 13: Bending-torsional of a thin open beam treated [51]

It will be seen that the stress field has the same shape (up to a sign) as the torsional warping of the section (Fig.4.14 (left)), which confirms that the torsional warping is dominant here.

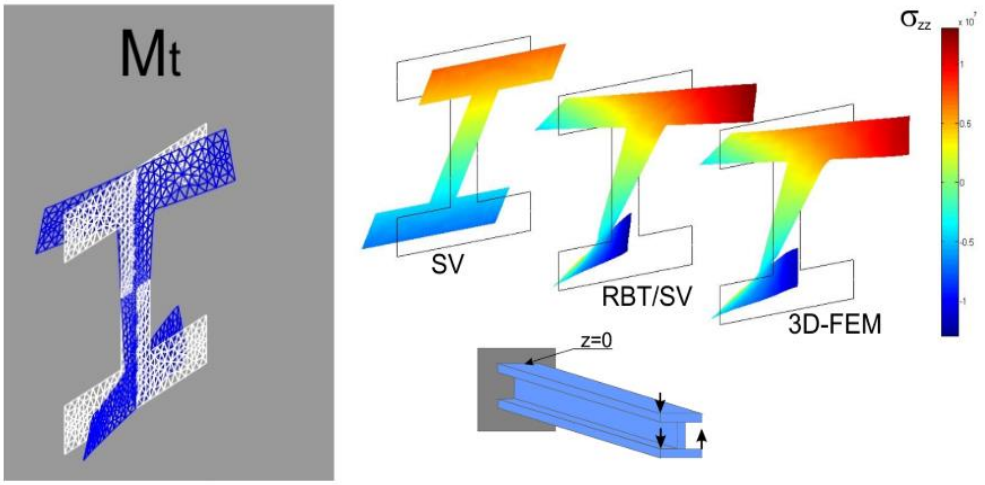

Fig 4. 14: Torsional warping and stress distribution σ_{zz} near the embedment

For the calculation of the two selected examples, the application of the RBT theory requires, for each case, a section calculation so that the section modes are determined beforehand. The deformation modes of the two sections are given in Fig.4.15 only those modes that correspond to Poisson's effects and warping will be used. Because they are fundamental in the analysis of the 3D results in the following, we will note, for the sandwich section, the shape of the warp associated with the shear force Ty and for the thin open section, the shape of the warp associated with the torsional moment Mt.

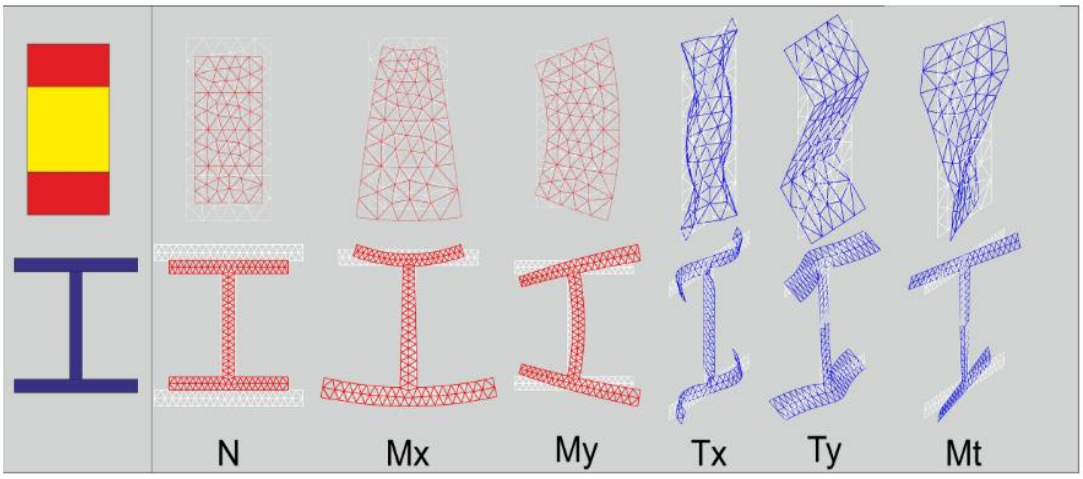

Fig 4. 15: Modes of deformation of the two sections

4.5.2.3 Bending-torsional of an open profile, clamped /supported

For the example (Fig.4.11) to which the RBT* calculation will be applied, and in order to properly account for the effect of the boundary conditions on the overall behaviour of the beam, on the 3D solution inside and near the edges, we will compare it with SVBT, RBT, and 3D-FEM (The 3D-FEM reference results by "**Abaqus**"),

The 3D results will focus on the axial (σ_{zz}) and shear (τ) stress fields:

- At the middle section of the beam.
- To the rights of the sections in the vicinity of the extremities.
- Along the axis of the beam for significant points of the section.

The distribution of stresses σ_{zz} and τ along the beam axis and at the midsection is shown in Fig.4.16 It is noted here that the SV's solution is completely defaulted.

The RBT solution also deviates (but to a much lesser extent) from the 3D-FEM solution; it captures the stress pattern but quantitatively the error is significant. On the other hand, the RBT* solution coincides with the 3D-FEM solution over almost the entire length of the beam. It is clear here, that the 3D-FEM modelling of the support, has led to a clear improvement of the inner solution associated with the RBT theory.

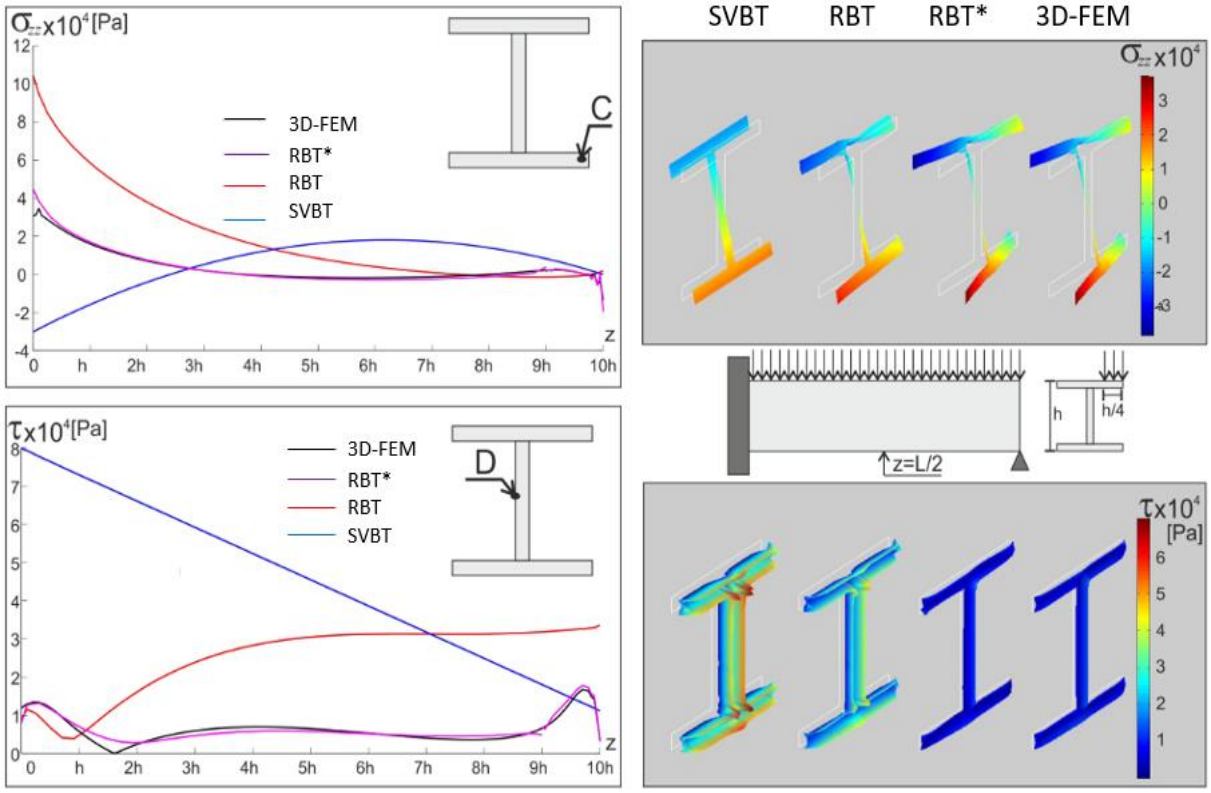

Fig 4. 16: Stress distribution σ_{zz} and τ at the middle section

Furthermore, Fig.4.17 which shows the sectional constraints near the two edges, indicates that the RBT* solution is able to correctly describe the 3D-FEM solution.

Thus, for this bending-torsion profile, taking into account the 3D nature of the simple support via a 3D zone located near the support (h) will have allowed here:

- A remarkable improvement of the 3D inner solution associated with RBT, which was

not apparent in the previous example (sandwich beam); this means that the 1D modelling of this support was sufficient for the sandwich section, but not for an I-shaped section;

- To access the 3D solution at the edge of the support, in a completely correct manner.

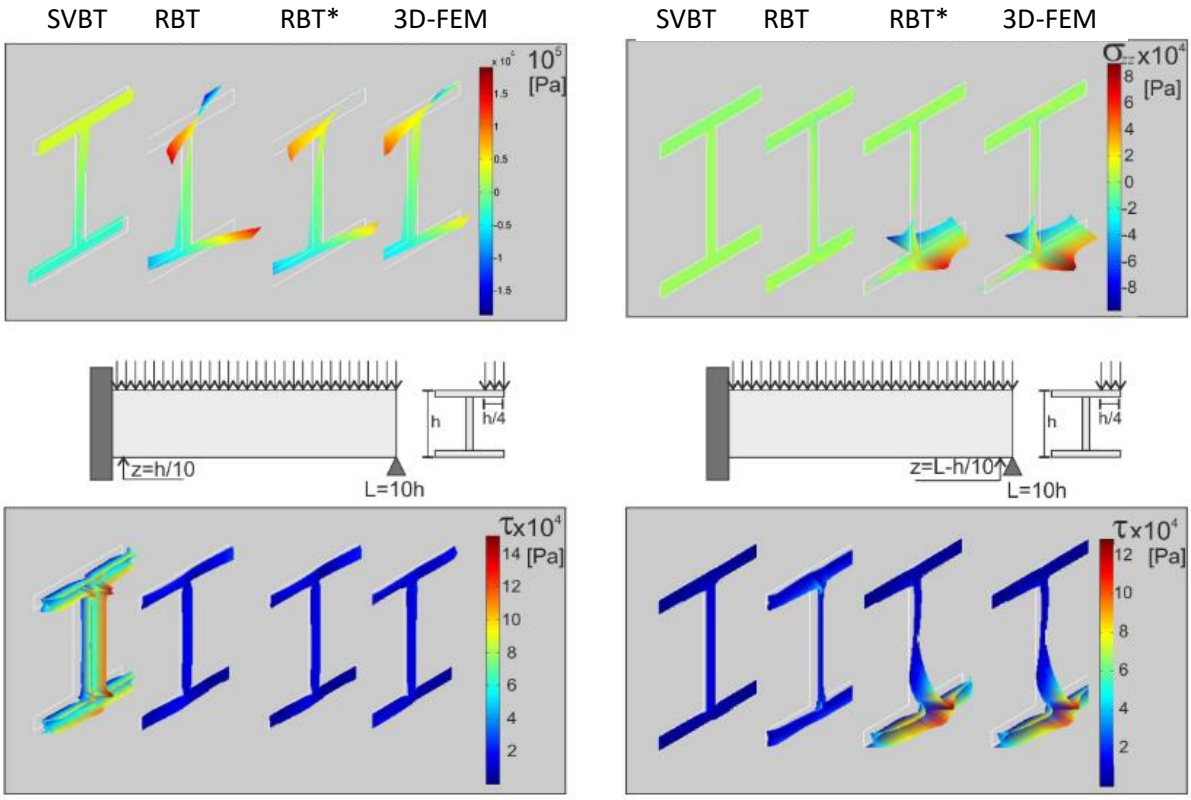

Fig 4. 17: Stress distribution σ_{zz} and τ at sections near the ends

4.6 Connections

The most commonly used method for a displacement approach is to impose the continuity of the displacement field at the boundaries [58].

Another method is to combine 1D and 3D calculations[59]: the solution in the 1D domain is based on beam theory, and the results obtained at the boundary are used as imposed conditions to solve the problem in the 3D area.

A less direct method whose application has been adapted to other types of connection (1D-2D or 2D-3D) and to other types of behaviour is the so-called Aarlequin method proposed by Ben [60]: This method introduces an overlap or transition zone in which the two models (1D and 3D) assigned different weighting functions coexist; these weighting functions make it possible to decide the preponderance of one model over the other in the calculation of the whole structure.

4.7 Conclusion

Refined beam theory models built on the 3D SV's solution (RBT/SV) are presented (The theories on which the thesis mainly focuses). The kinematic model includes, other than the rigid motion of the section, two sets of section deformation modes that account for its mechanical behavior: The first group $\{\boldsymbol{u}_{SV}^{i}\}$, which is the basis of the model, is extracted from the Saint-Venant solution and essentially translates the warping and Poisson's effects related to the six classical interior forces. The second group $\{\boldsymbol{D}_{v}^{j}\}$, , introduced especially when thin or complex croos-sections are treated, takes as section deformation modes the vibration modes of the cross-section. These modes essentially reflect the section distortions.

RBT models aim to satisfy the support conditions and better explain the edge effects. In addition, finding the 3D SV’s solution away from the edges because the displacement model contains the displacement shape of the Saint Venant solution. Also, the RBT models treat any section in terms of shape and material and take into account all kinds of deformations of the cross-section (warping, Poisson's effects, deformations).

The theory of RBT/SV was introduced by a tool called CSB (Cross-section and Beam Analysis). CSB is proposed as a set of two complementary numerical tools CSection and CBeam, where CSection calculates the Mechanical Characteristics of the cross-Section by 2D finite elements, then CBeam uses these Mechanical Characteristics of the cross-section to calculate the beam by 1D finite elements.

Finally, for a better treatment of the boundary conditions, the proposed approach consists in partitioning the beam into two domains:

- An inner area, for which the solution can be treated by beam theory and 1D finite elements (1D-FE);
- A zone at the edges, for which the strongly 3D solution is intended to be treated by 3D finite elements (3D-FE).

This approach allows the boundary conditions in the 3D areas to be imposed exactly and to dispense with their modelling in the 1D or generalized sense. This approach is only of interest (in terms of calculation cost) if the area to be calculated by 1D-FE is much larger than the area to be treated by 3D-FE.

5 Analysis of beams: Applications

5.1 Introduction

This chapter is dedicated to the numerical applications of the beam theories proposed in the previous chapter and denoted RBT/RBT*. The objective here is to highlight the ability of the RBT models to account for the static bending-torsional problem of functionally graded beams. the analysis focuses on the effects of bending-torsional, which is the main objective of this work. For this, a significant set of FGM beams subjected to different cases of loads or support conditions is treated.

In these theories, the displacement models include Poisson's effects, out-of-plane deformations and distortions. For a given section, the sectional displacement modes are derived from the computation of the particular 3D Saint-Venant's solution. These modes, which reflect the mechanical behaviour of the cross-section, lead to a beam theory that actually corresponds to the cross-section type in terms of shape and material. In addition, the models take into account edge effects to predict a 3D solution in a larger internal region to better describe the overall behaviour of FGM beams.

The mechanical and physical characteristics of the FGM beams vary continuously, according to a power-law distribution, through the thickness of the beams.

For each example, beyond the 1D results, the 3D solution resulting from the application of the RBT models are systematically compared to the solution obtained in the literature, 3D-FEM (which we also consider as a reference) and those provided by the full Saint-Venant beam theory (SVBT) calculations

5.2 Numerical results and discussion

5.2.1 Numerical implementation

In this work, the theory of RBT/SV was introduced by a tool called CSB (Cross-section and Beam Analysis) (Naccache and El Fatmi [55]).

CSB is a numerical tool dedicated to the computation of beams with any cross-sectional shape, made of freely arranged isotropic or anisotropic materials. It is used to solve in the standard framework of linear elasticity and the equilibrium of a beam subjected to any loading and support conditions. CSB is proposed as a set of two complementary numerical tools CSection and CBeam:

- CSection calculates the mechanical characteristics of the cross-section ($\boldsymbol{M}_{sv}^{i}$) and a set of $\boldsymbol{m}$ distortion modes ($\boldsymbol{D}_{V}^{j}$) by 2D finite element method (2D-FEM).
- CBeam uses these mechanical characteristics of the cross-section to calculate the beam

by 1D finite element method (1D-FEM).

5.2.2 Validation example: Vibration

In order to validate the current RBT models, a square cross-section laminated composite beam $[90/0/0/90]$ with Simply-Supported (S-S) at both ends is investigated. The length and width of the beam are $l = 6.35\,m$ and $a = 0.28\,m$, respectively. The material properties for this composite beam are taken from Ref. (Li *et al* [61], Yang *et al* [62]) and are given as follows:

$$E_1 = 241.5 \times 10^9 \text{Pa}, \qquad E_2 = E_3 = 18.98 \times 10^9 \text{Pa}$$
$$G_{12} = G_{13} = 5.18 \times 10^9 \text{Pa}$$
$$G_{23} = 3.45 \times 10^9 \text{Pa}, \qquad \nu_{12} = \nu_{13} = 0.24, \qquad \rho = 2015 \text{kg/m}^3$$

The fundamental natural frequency of the Simply-Supported laminated composite beam is calculated using the present RBT models as shown in table. 5.1. This natural frequency is compared with higher-order beam theories TSDBT , ESDBT by Li *et al* [63] and FSDBT by *Li et al* [61] where these theories refer to the first-order, exponential , and trigonometric shear deformation beam theories, respectively. We also compared our results with those obtained by CUF-1D (Carrera unified formulation) beam models with Lagrange Expansion functions (denoted as CUF-LE), the CUF-1D is highlighted because it is able to capture cross-section deformations Yang *et al* [62]. Some beam has been studied by the classical beam theories such as the EBBT (Euler Bernoulli's Beam Theory) and TBT (Timoshenko's Beam Theory) from the literature Yang *et al* [62]. Table. 5.1 shows a good agreement with the natural frequency value obtained by our models (RBT models) and that obtained by other models. Moreover, the natural frequency obtained by EBBT is greater than the value of other models due to the kinematic approximation introduced by EBBT.

Table 5. 1 fundamental natural frequency (Hz) of the square composite beam with simply-supported (S-S) conditions based on the RBT models and the literature

Mode number	**RBT**	**RBTd**	**Abaqus**	**TSDBT**	**FSDBT**	**ESDBT**	**EBBT**	**TBT**	**CUF-LE**
Mode 1	14.99	14.99	14.95	14.97	14.90	14.97	15.13	15.00	14.87

5.2.3 Validation example: RBT models with 3D FEM

In order to illustrate the performance of the RBT/SV models, a thin-walled non-symmetric homogeneous profile subjected to clamped-simply supported (CS) boundary conditions is studied. In this example (Fig. 5.1) the beam length L = 2 m and b1= 0.04, b2= 0.02, h= 0.1 and t= 0.005. The mechanical properties of this beam are (E= 70 MPa, v = 0.3). The stress results for the RBT models are extracted by the CSB tool, based on an initial set of cross-

section problems solved by 2D FEM (using exclusively 6-node triangular finite elements), and then the beam problem is solved by 1D FEM calculations. Also, the commercial code Abaqus is used to perform the 3D-FEM computations (using the 15-nodes quadratic triangular prism (C3D15)).

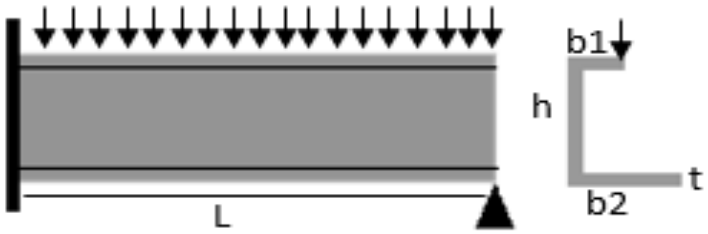

Fig 5. 1: The equilibrium beam problem

Cross-sectional analyses

The cross-sectional analyses of this beam are performed by 2D FEM using the CSection tool. Figure 5.2 shows the out-of-plane deformations (group 1) related to the shear forces (T_x, T_y) and the torsional moment (M_t), while the latter are the Poisson's ratio deformations (group 2) related the axial force (N) and the bending moments (M_x, M_y). in addition group 3 shows 15 additional deformation modes, 10 in-plane (pink colour) and 5 out-of-plane (blue colour) for the cross-section of the homogeneous beam. These deformation modes lead to a beam theory that really corresponds to the type of cross-section (shape and material).

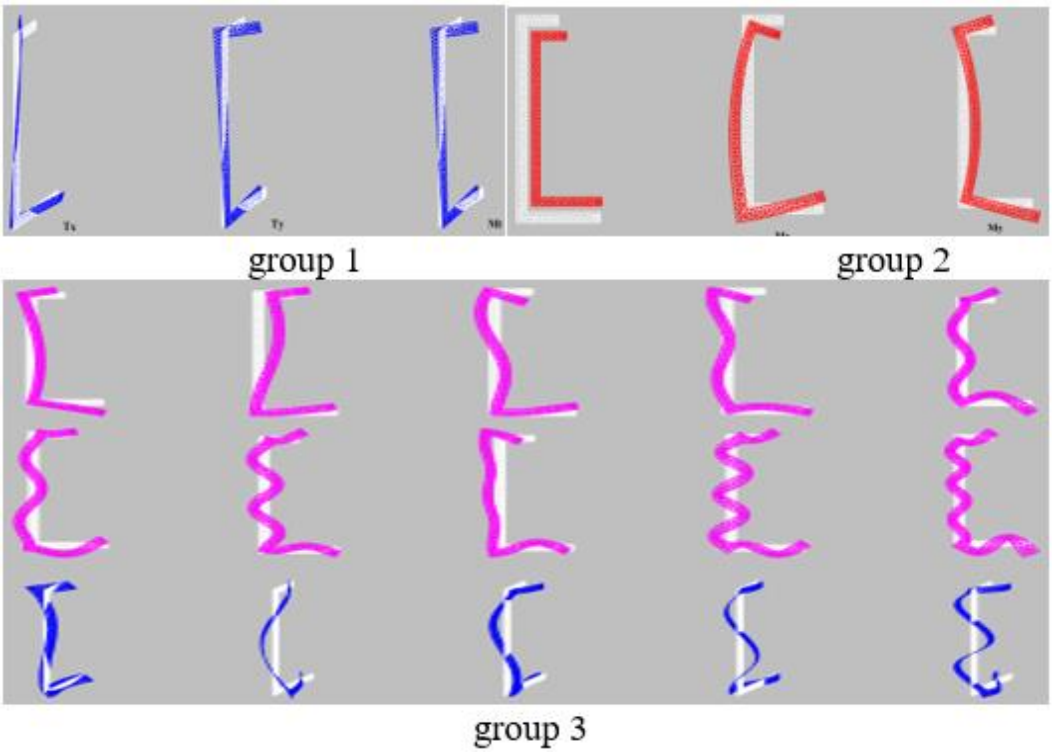

Fig 5. 2: Cross-section deformations: out of plane warpings (group1), Poisson's effects (group 2) and distortions (group 3) for the homogeneous sections

Bending-torsional of a clamped-simply supported beam

Figure 5.3 presents the stress distribution fields for axial stress σ_{zz} and shear stress τ near to the two supports. The results obtained near the edges indicate a good agreement between the RBT models and those obtained by 3D FEM (especially between RBT* and 3D FEM) in terms of the numerical results and section deformations. Thus, for this Flexural-torsional profile, taking into account the 3D nature of the simple support via a 3D zone located near the support will have allowed here: A remarkable improvement of the 3D inner solution associated with RBT models, and to access the 3D solution at the edge of the support, in a completely correct manner.

RBT models aim to satisfy the support conditions and better explain the edge effects. In addition, finding the 3D SV's solution away from the edges because the displacement model contains the displacement shape of the Saint Venant solution. Also, the RBT models treat any section in terms of shape and material and take into account all kinds of deformations of the cross-section (warping, Poisson's effects, deformations).

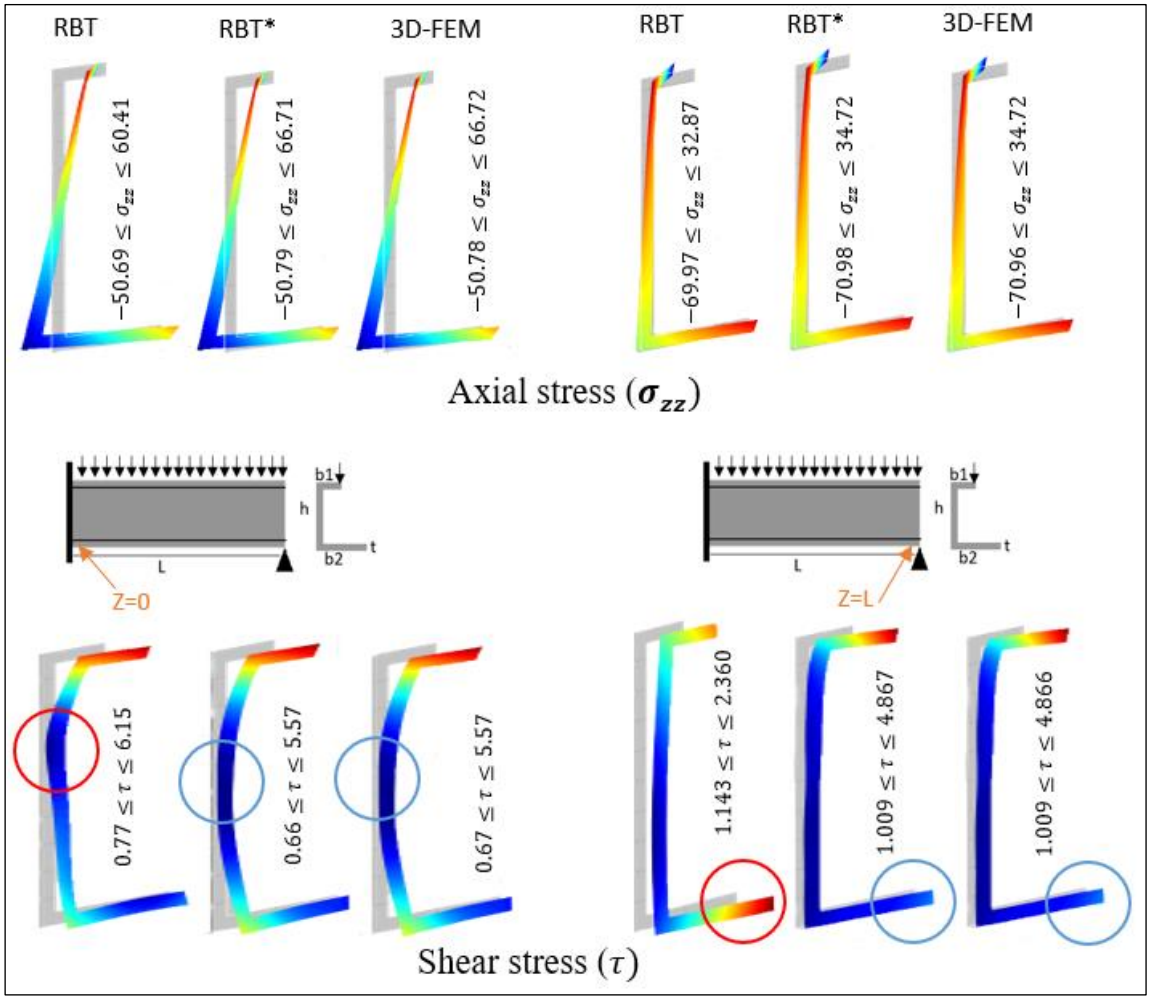

Fig 5. 3: Stress distribution σ_{zz} and τ at sections near the ends

5.2.4 Validation example: Bending analysis (Equilibrium)

In this section, in order to validate the current theory, we study a simply-supported FGM beam (L=1.6m, h=0.1m, b=0.1m) subjected to a uniformly distributed load q (see Fig 5.4).

Through the study this beam, the most important results obtained based on the 3D displacement fields are presented. The beam is composed of aluminum (AL: Em =70 GPa, v=0.3); and Zirconia (Zero2: Ec= 200 GPa, v = 0.3). The mechanical properties of the FGM beam change through the thickness. The top surface of the beam (y = + *h*/2) is pure Aluminum, whereas the bottom surface of the beam (y = − *h*/2) is pure Zirconia.

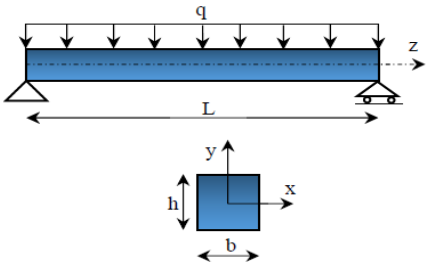

Fig 5. 4: Simply supported FGM beam

Figs 5.5 and 5.6 show the non-dimensional transverse displacements (w/w_{static}) along the length of the FGM beam. The static deflection of a completely aluminium beam under uniformly distributed load is calculated as follows:

$$w_{\text{static}} = \frac{5\times q\times L^4}{384\times E_m\times I} \tag{24}$$

The non-dimensional deflections (Fig 5.5), obtained by a refined beam theory (RBT), are compared with those provided by Şimşek [64] (Fig 5.6) using the higher-order shear deformation theory (HOSDT). It can be seen that the present results are in excellent agreement with HOSDT. It can also be seen that the deflection of full metal is greater than that of full ceramic, this can be explained by the fact that Young's modulus of ceramic is higher than that of metal. The non-dimensional deflection of the FGM beam (P ≠ 0) is between those of the metal and ceramic beams. For the FGM beam, the non-dimensional transverse deflection decreases as the power-law exponent P increases. This is due to the fact that an increase in the power-law exponent leads to a decrease in the bending stiffness of the beam.

The axial stresses σ_{zz} are computed at the mid-span of the beam. The axial stress field obtained by 3D RBT, is shown in Figs 5.7 and 5.8. The shape of the 3D stress distribution is plane in the homogeneous case and passes through the middle axis of the cross-section while in the FGM beam it is not plane and does not pass through the middle axis of the cross-section.

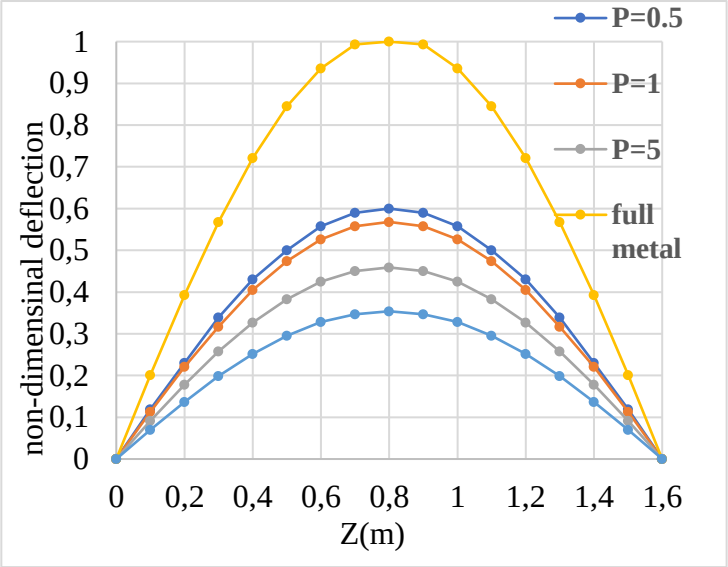

Fig 5. 5: Non-dimensional deflections distributions by RBT

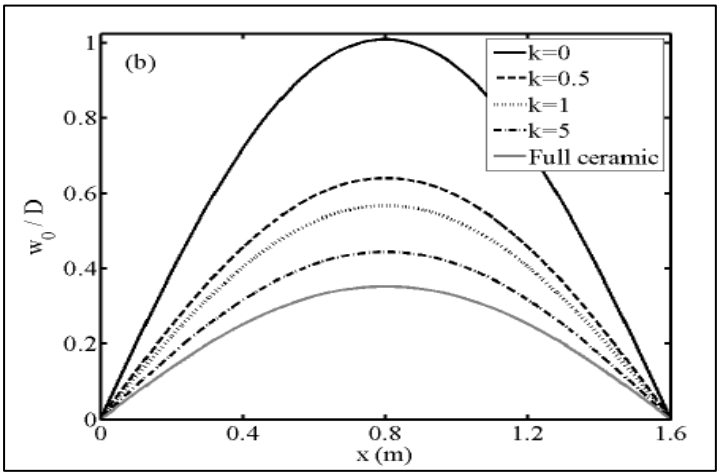

Fig 5. 6: Non-dimensional deflections distributions by Şimşek [64]

Fig 5.9 shows the distribution of non-dimensional axial stress through the thickness in mid-span of the FGM beam for different values of P. The results obtained with RBT show good agreement with those obtained with HOSDT by Şimşek [64] Fig 5.10.

The axial stress is normalized by:

$$\bar{\sigma}_{zz} = \frac{\sigma_{zz} \times b \times h}{q \times L} \tag{25}$$

In Figure 5.9 we can see that the axial stress distribution is only linear for full metal, but for other cases ($P \neq 0$) the axial stress distribution is not linear, and also the tensile stress values are greater than the compressive stresses in the case of FGM beam. on the other hand, we can note for the full metal, the value of axial stress is zero (σ_{zz}) at the mid-plane ($h/y = 0$), while for the other cases ($P \neq 0$) the axial stresses are not zero. This is due to the variation of the Young's modulus across the thickness of the FGM beam.

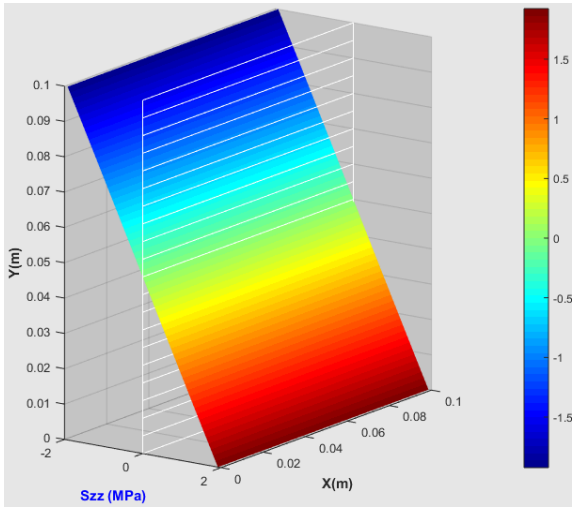

-1.924e6 Pa≤ σ_{zz}≤ 1.924e6 Pa

Fig 5. 7: (a) Axial stress distributions obtained by RBT (P=0)

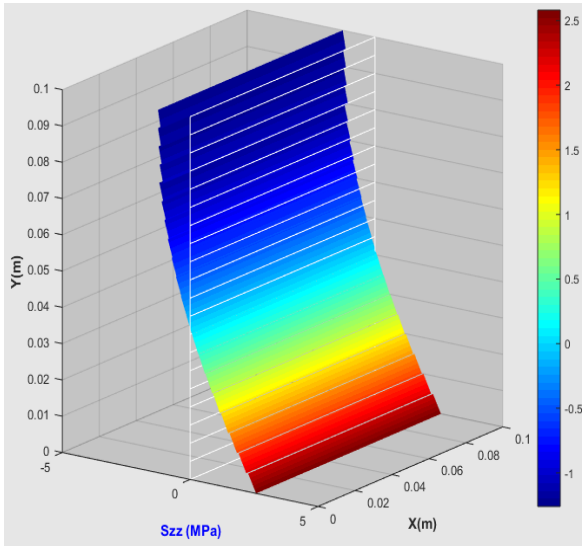

-1.260e6 Pa≤ σ_{zz}≤ 2.581e6 Pa

Fig 5. 8: (b) Axial stress distributions obtained by RBT (P=5)

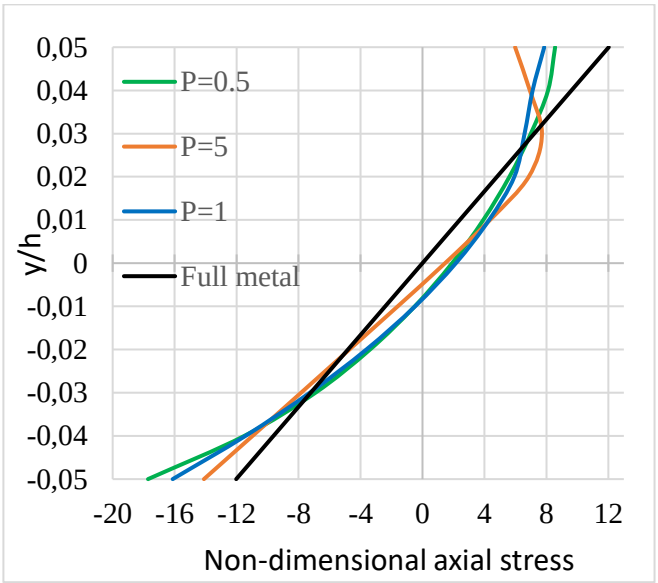

Fig 5. 9: Non-dimensional deflection obtained by RBT

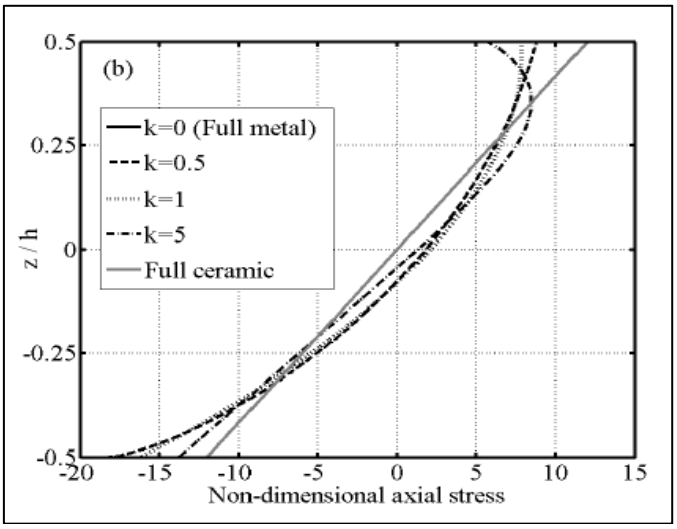

Fig 5. 10: Non-dimensional deflection obtained by Şimşek [64]

5.3 Bending-torsional Analysis

In order to illustrate the performance of RBT/SV and the numerical tools CSection and CBeam, the most important 1D/3D results are given based of 3D displacement fields, in the inner region and near the edge of the beams. In order to compare the results of the different theories, we studied the cantilever FGM beams shown in Fig 5.11. The first beam (I-section) is subjected to bending-torsional with three loads, for the second beam (square-section) it is subjected to torsional behavior resulting from two loads, all these loads are identical (1KN Per-Force) and applied at the free end of the beams (see Fig 5.11). These beams are composed of aluminum (AL: E_m =70 GPa, v=0.3); and Zirconia (Zro2: E_c= 200 GPa, v = 0.3). The mechanical properties of FGM beams change through their thickness according to power-law and exponential distribution. The top surface of the beams (y = + h/2) is pure aluminum, whereas the bottom surface of the beams (y = − h/2) is pure zirconia.

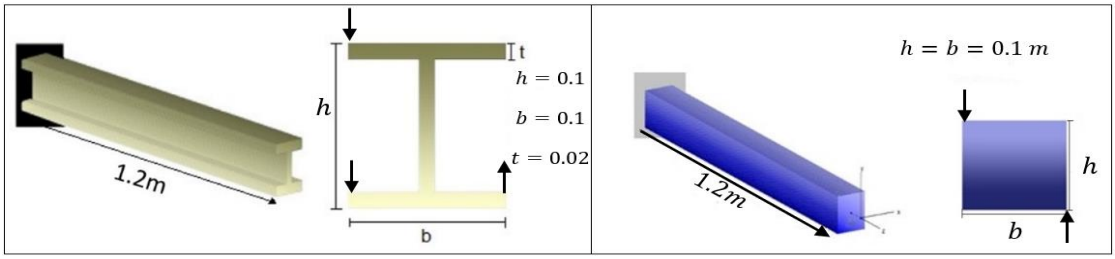

Fig 5. 11: FGM beams and sections description.

5.3.1 Cross-section analysis

By using the C-Section tool, 2D-FEM analyses of FGM beam cross-sections are performed. This tool provides for each section: the six cross-section modes ($\boldsymbol{M}_{sv}^{i}$) and a set of $\boldsymbol{m}$ distortion modes ($\boldsymbol{D}_{V}^{j}$) related to the natural vibration of the section.

Figs 5.12 and 5.21 (next exemple) present the six (6) transverse modes [T_x, T_y, N, M_x, M_y, M_t] associated with the classical transverse stresses of each section. the deformation modes in red color indicate the Poisson's effects related to the axial force (N) and the bending moments (M_x, M_y), while the deformations in blue color indicate the out-of-plane warpings related to the shear forces (T_x, T_y) and the torsional moment (M_t). In addition, certain additional sectional distortions are considered for I-Section and square-section: 10 in-plane (pink color) and 5 out-of-plane (blue color) shown in Figs 5.13 and 5.22 (next exemple).

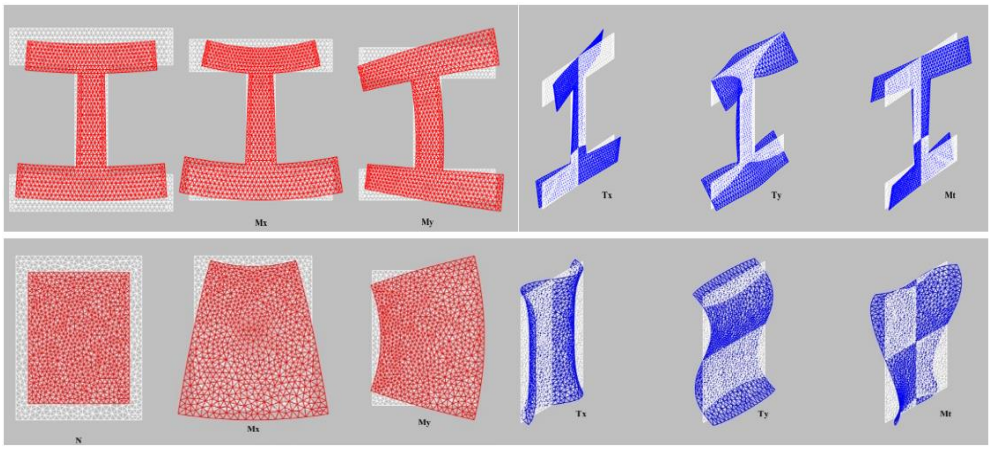

Fig 5. 12: Cross-sections deformations: Poisson's effects (N, M_x, M_y) and out-of-plane warpings (T_x, T_y, M_t) for the FGM sections (for P=1)

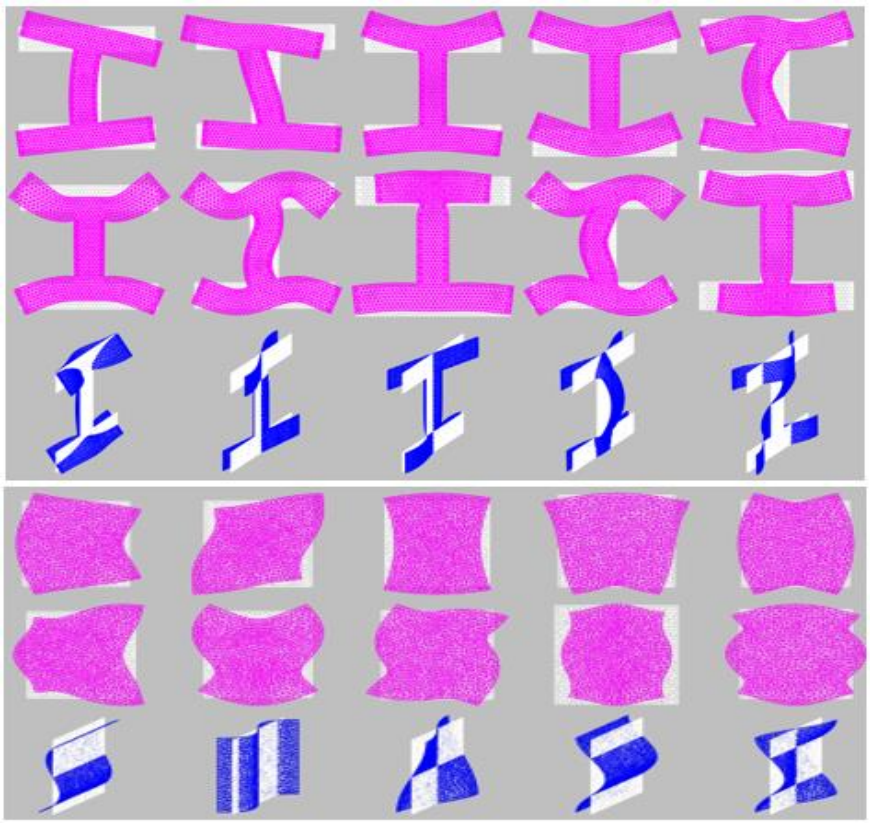

Fig 5. 13: Cross-section deformations: distortions modes $\boldsymbol{D}_V^j$ of the FGM sections (for P=1)

5.3.2 1D/3D Results

5.3.2.1 Bending-torsional Analysis with FGM cantilever beam (I-section)

The analysis performed focuses on the effect of embedding on 3D stresses and the general behaviour of the FGM beam. Table 5.2 shows the maximum transverse deflection of the cantilever beam (I-section) for different values of power law exponent, using the different theories. The deflection of the metal beam (P = 0) is found to be higher than the deflection of the ceramic beam (**P** → ∞). This is illustrated by the fact that the Young's modulus of ceramic is greater than that of metal. For the FGM beam, the deflection is located between the deflections of metal and ceramic beams. Consequently, when the power-law exponent P is increased, the transverse deflection decreases in the case of the FGM beam. This is explained by an increase in the exponent of the power-law resulting in an increase in the bending rigidity of the FGM beam. It can also be seen that the value of the transverse deflection of the SVBT is comparatively higher than the other theories.

Table 5. 2 The maximum transverse deflection of an FGM cantilever beam (I -section) for various values of the power law exponent (mm).

Power-low Exponent	RBT	RBT*	SVBT
Full metal	1.2074	1.2081	1.2207
P=0,5	0.7713	0.7714	0.7799
P=1	0.7255	0.7259	0.7336
P=2	0.6705	0.6709	0.6780
P=3	0.6384	0.6390	0.6435
P=4	0.6120	0.6124	0.6188
P=5	0.5934	0.5937	0.6000
Full ceramic	0.4226	0.4228	0.4273

The maximum torsional rotation for an FGM cantilever beam depending on the different theories is given in Table. 5.3. We notice an approximate similarity of the RBT, RBT* values, and a small difference to the SVBT theory. According to the deflection and torsional rotation for the FGM cantilever beam, we conclude that the RBT, RBT* behaviour is stiffer than expected by SVBT.

Table 5. 3 Maximum torsional rotation of FGM cantilever beam (I-section) for various values of the power law exponent (rad 10^{-3}).

Power-low Exponent	RBT	RBT*	SVBT
Full metal	8,1096	8,1372	9,2776
P=0,5	4,7417	4,7589	5,3371
P=1	4,2986	4,3159	4,8557
P=2	3,9397	3,9547	4,4434
P=3	3,7698	3,7855	4,2534
P=4	3,6698	3,7855	4,1445
P=5	3,6008	3,6832	4,0708
Full ceramic	2,8383	2,8480	3,24471

Systematically, the comparison between the theories was carried out out by considering the main stress components for the FGM beam, the axial stress σ_{zz}, and the shear stress modulus $\tau = \sqrt{\tau_{xz}^2 + \tau_{yz}^2}$ in the different regions of the beam. Fig 5.14 shows the axial stress fields at the embedding and in the mid-span of the beam, both for the homogeneous and FGM beam models. The results obtiened by SVBT are quite different from RBT and RBT* at embedding, while they converge at the mid-span of the beam. In addition, it can be seen that the axial stress distribution for the homogeneous case is linear. it shows that the axial stresses of the SVBT due to bending only, while for the FGM beam, the axial stress is nonlinear. similarly, the axial stresses of RBT and RBT* are very different from those obtained by the SVBT. Moreover, the difference results from the effect of the bending-torsion stress (clearly the torsion is important) resulting from the enrichment of the displacement field of RBT models. For the FGM beam P ≠ 0, the axial stress distribution is nonlinear and does not pass along the neutral axis (the line passing the z-axis of the center of gravity). This is caused by the variation of Young's modulus in the thickness of the FGM beam.

Fig 5.15 shows the variations of the axial stress (σ_{zz}) along the span for 2 points, **A** and **B**, that belong to the top flange of the FGM beam. The results as shown in Figure 5.15 have been obtained using the present assumption, i.e. a non-deformable cross-section at the embedding for the SVBT and deformable for RBT and RBT*. It can be seen a large difference between the stress results of the three theories at the embedding level, and a convergence between the results is seen far from the embedding (The internal effect propagates over a distance of about d ≈ L/2). If the section is taken as undeformable for both RBT and RBT*, the same results as for SVBT are found. we can see that RBT and RBT* take into account edge effects in order to predict a 3D solution in a larger internal region to better describe the overall behaviour of the

beam. In SVBT, the 3D solution is an integral part and it describes the correct solution in the internal region of the beam.

Fig 5.16 displays the comparison between the shear stress distributions at the embedding (Z=0) and (Z=L). One can see that the shear stress fields are definitely different in terms of shape and materials for the three theories in the embedding area (Z=0). The results of the shear stresses given by the SVBT are based on the shear force (T_y) and the torsional moment (M_t). The deformations avoided in the case of RBT and RBT* at the embedding level (Z=0), led to totally different shear stresses than those given by SVBT. Far from the embedding ($Z \neq 0$), the shear stress results are similar for SVBT and RBT but different for RBT* (Some differences can be observed in the locations designated by the circles in Fig 5.16). This is due to the enrichment of the displacement field through higher modes (additional deformation modes " distortion modes").

5.3.2.2 FGM cantilever beam (With square-section)

Table. 5.4 Shows the maximum rotation for the FGM cantilever beam according to various values of the power-law exponent. The results obtained show a good description of the mechanical behaviour of the FGM beam in terms of rotation for all theories. It can be noted that the rotation of the full ceramic beam is lower than the full metal in both theories, while the FGM beam rotation is between the ceramic and metal beams.

The effect of restricted warping is known to be significant for a square-section subjected to torsion. In this section, a comparison of the results between SVBT and RBT are systematically made for the shear effects of the FGM beam. Fig 5.17 illustrates a comparison between the shear stress field at the embedding and at the mid-span of homogeneous and FGM beams. We can observe the clear difference of the shear stress fields provided by the SVBT and RBT results at the embedding (Z=0) in terms of shape and values, due to the enrichment of the displacement fields of the RBT (taking into account the edge effects), while the stress results presented by SVBT and RBT are consistent far from the embedding (mid-span of the beam).

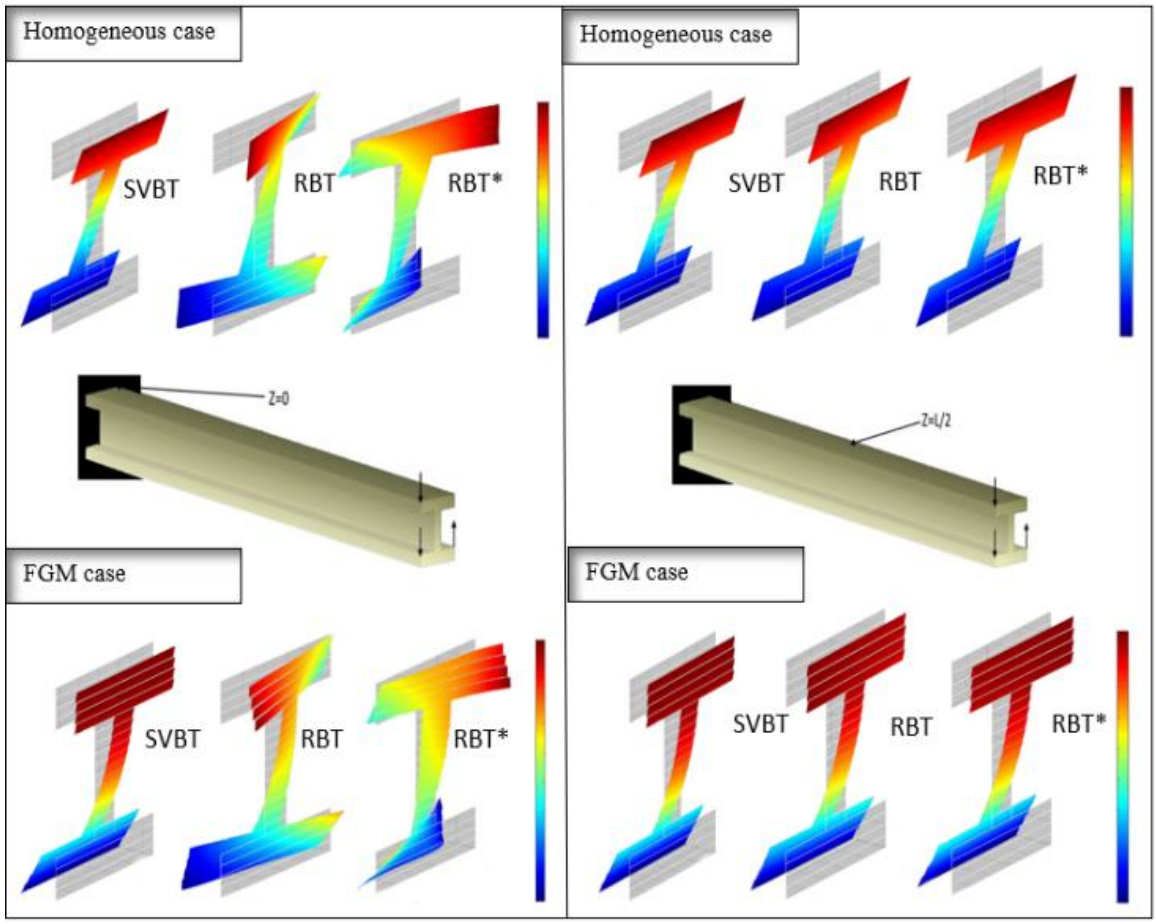

Fig 5. 14: Axial stresses distributions at embedding (Z=0) and at mid-span (Z=L/2). Comparison of RBT, RBT* and SVBT

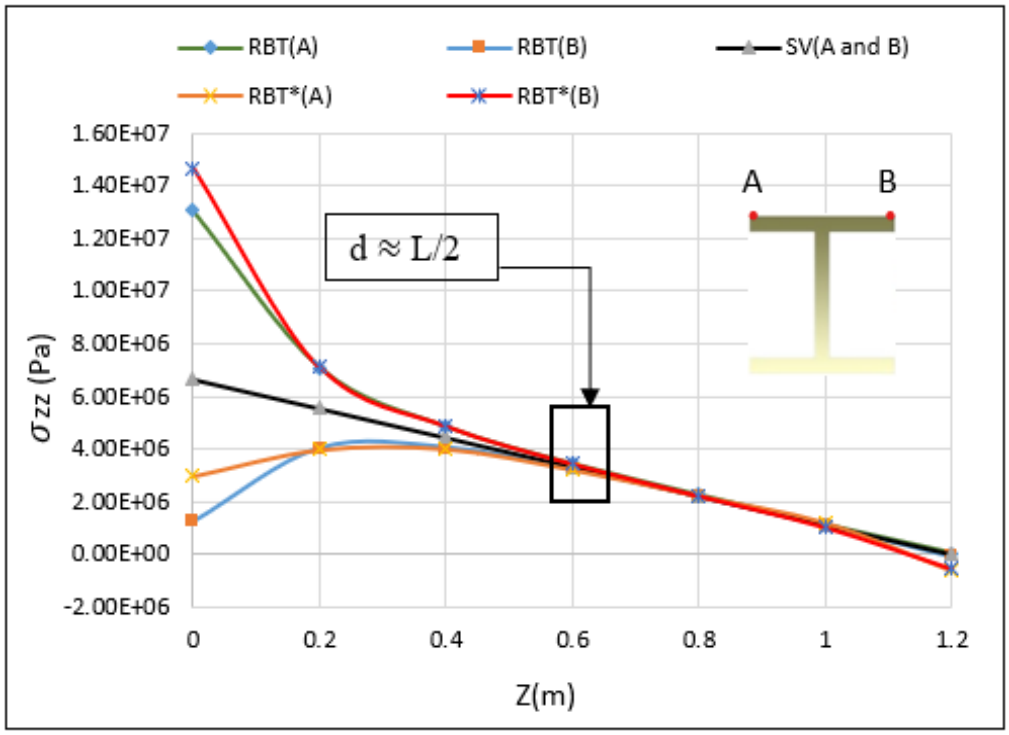

Fig 5. 15: Axial stress variations along the FGM beam for two points (A and B) belonging to the upper flange. Comparison of RBT, RBT* and SVBT

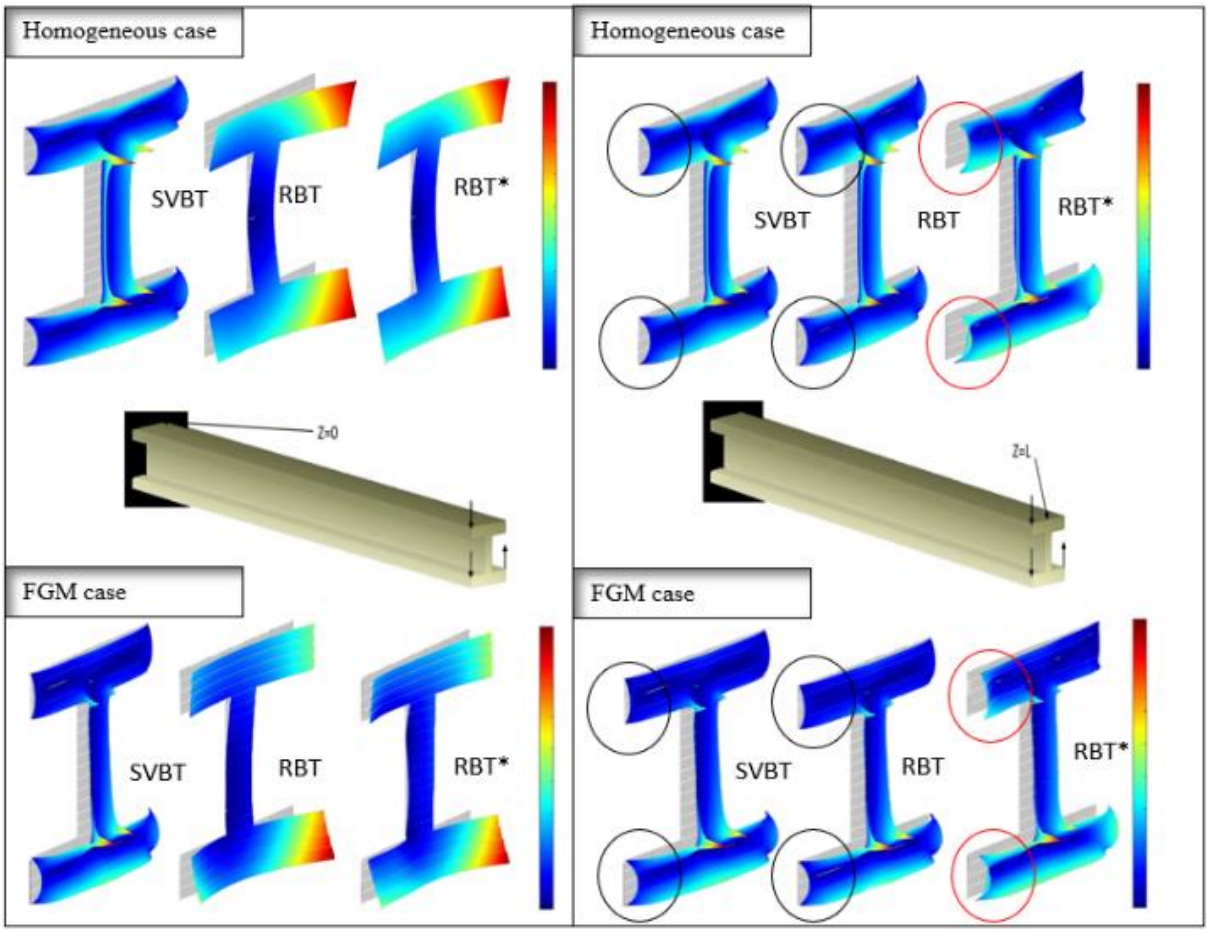

Fig 5. 16: Shear stresses distributions at embedding (Z=0) and free end (Z=L). Comparison of RBT, RBT* and SVBT

Figs 5.18 and 5.19 show the variation of the axial stress σ_{zz} along the beam for a point **A** close to the edge of the cross-section, and the variation of the shear stress for point **B** (the maximum shear point for the SVBT torsion) in the middle of the cross-section along the beam. Moving from the free end of the beam, we can observe an opposite relationship between the shear stresses and the axial stresses, where a decrease in shear follows an increase in axial stress or the reverse. These results show that the internal effect of the RBT propagates along the beam for this square-section, while the SVBT solution is no longer efficient to represent the central solution.

Table 5. 4 Maximum rotation of FGM cantilever beam (with square-section) for various values of the power law exponent (rad ad 10^{-3}).

power-low exponent	RBT	RBT*	SVBT
full metal	0.3163	0.3163	0.3171
P=0,5	0.2120	0.2121	0.2129
P=1	0.1695	0.1695	0.1699
P=2	0.1489	0.1489	0.1493
P=3	0.1401	0.1402	0.1405
P=4	0.1352	0.1353	0.1356
P=5	0.1242	0.1321	0.1248
full ceramic	0.1107	0.1107	0.1110

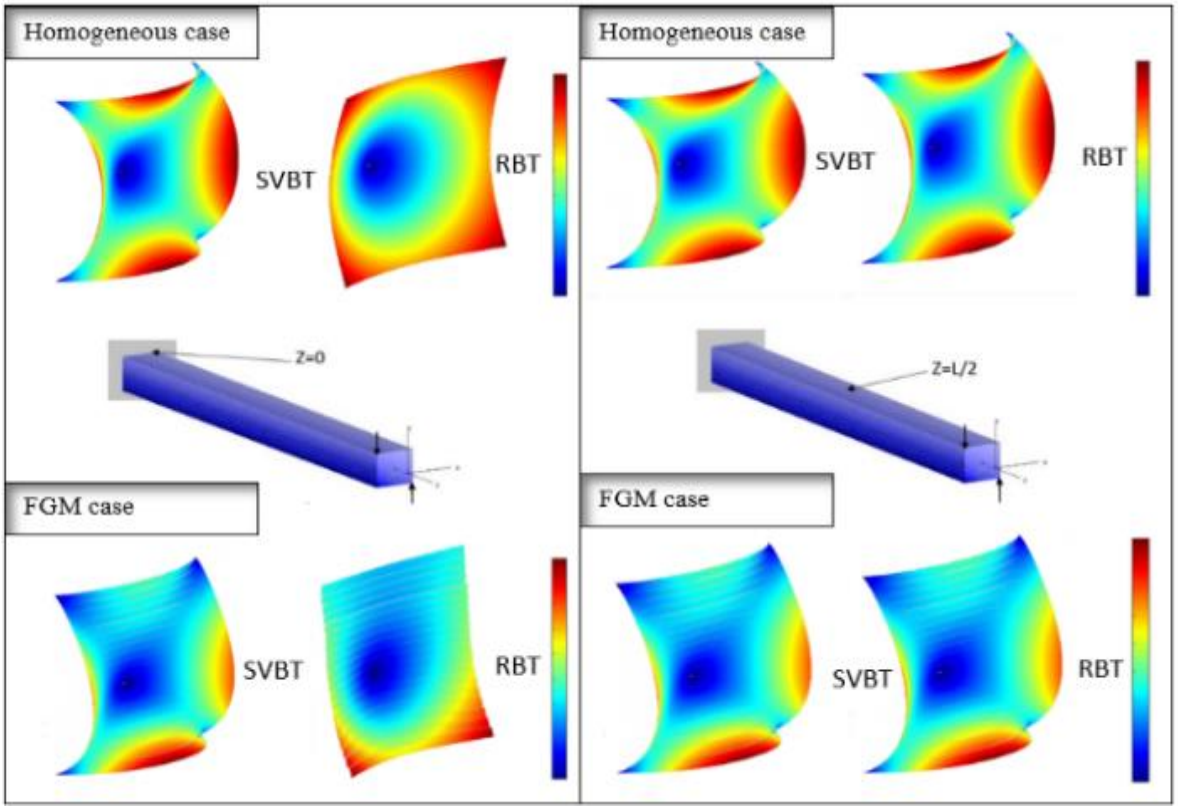

Fig 5. 17: Shear stress τ fields at Z=0 and midspan Z=L/2. Comparison of SVBT and RBT results

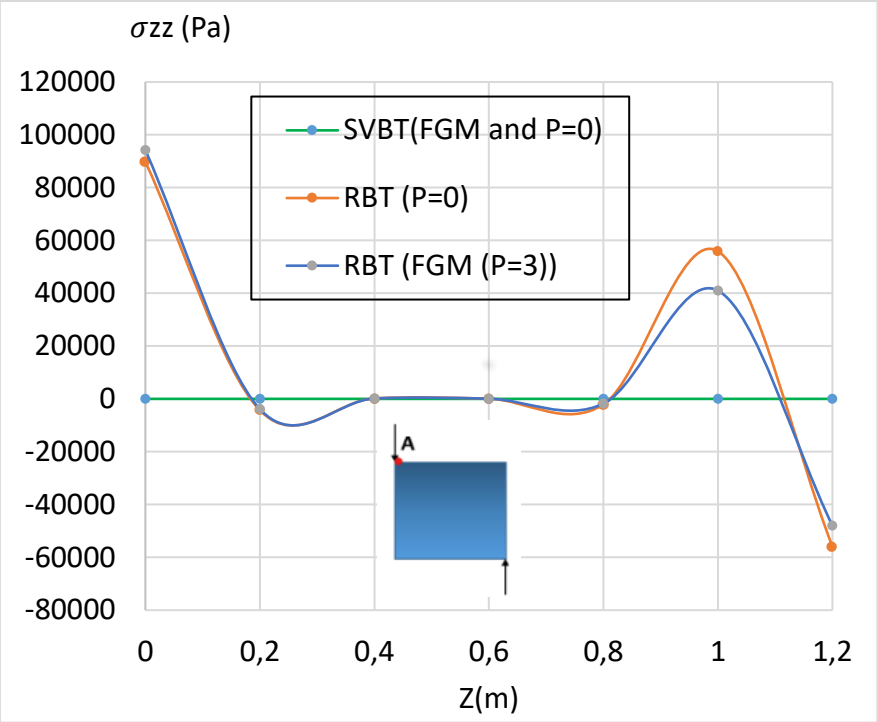

Fig 5. 18: Axial σ_{zz} stress variation along the FGM and homogeneous (P=0) beam for the point A

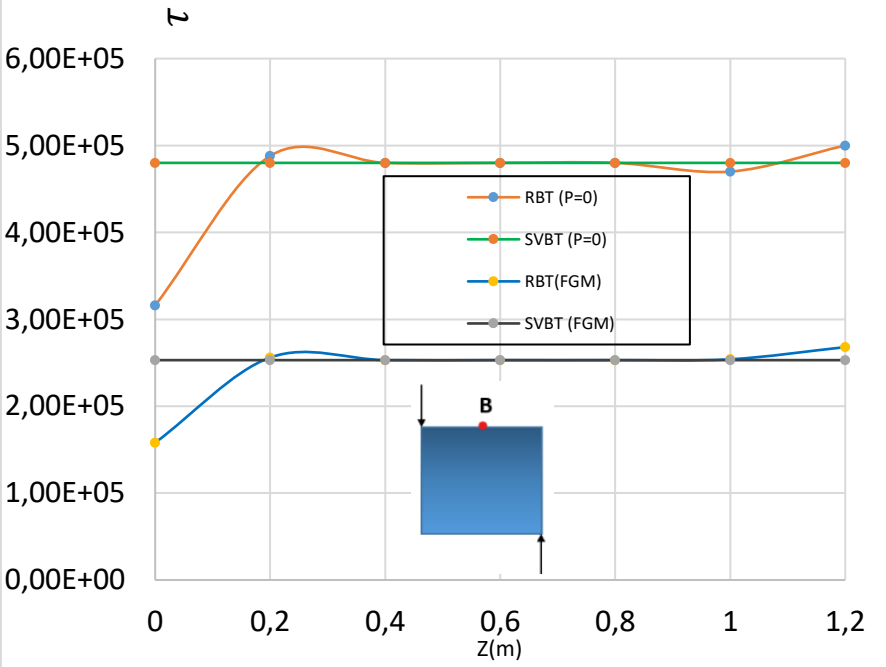

Fig 5. 19: shear τ stresses variation along the FGM and homogeneous (P=0) beam for the point B

5.3.2.3 Bending-torsional analysis with FGM cantilever beam (A channel section)

To illustrate the efficiency of RBT/SV and the numerical tools CSection and CBeam, the most significant 1D/3D findings are presented based on 3D displacement fields, in the interior area of the beam and close to the edge. To compare the results of the theories, we studied an FGM cantilever beam (UPE 200 channel, L = 1 m), subjected to bending-torsional behaviour provided by a load applied at the free end of the beam (F=1KN). The beam was composed of zirconia (Zero2: Ec= 200 GPa, v = 0.3) and aluminium (AL: Em = 70 GPa, v = 0.3). Its properties varied through the thickness of the beam. The bottom surface of the beam (y = − h/2) was pure zirconia, whereas the top surface of the beam (y =+ h/2) was pure aluminium. The geometric properties and characteristics of the FGM beam are seen in Fig 5.20.

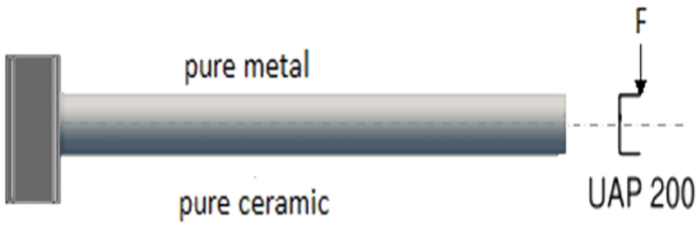

Fig 5. 20: Geometric characteristics and properties of the FGM beam

The analysis performed focuses on the effect of embedding on 3D stresses and the general behaviour of the FGM beam.

Table. 5.5 indicates the maximum transverse deflection of the cantilever beam for the various values of the power-law exponent, subject to the load on its free side, through three theories (SVBT, RBT and RBT*). It can be seen that the deflection of the metal beam (P = 0) is greater than the deflection of the ceramic beam ($p \to \infty$). This can be demonstrated by the fact that the Young's modulus of ceramics is greater than that of metal. The deflection of the FGM beam (P ≠ 0) is located between the deflection of ceramic and metal beams. Therefore, as the power-law exponent P is raised, the transverse deflection decreases for the FGM beam. This is attributed to the fact that an increase in the exponent of the power-law causes an increase in the bending stiffness of the beam. Also, it can be seen that the value of the transverse deflection of SVBT is twice that of the other theories. The reason for this difference is that RBT and RBT* behaviour is stiffer than expected in SVBT. Fig 5.23 shows the 3D deformation of the tested FGM beam.

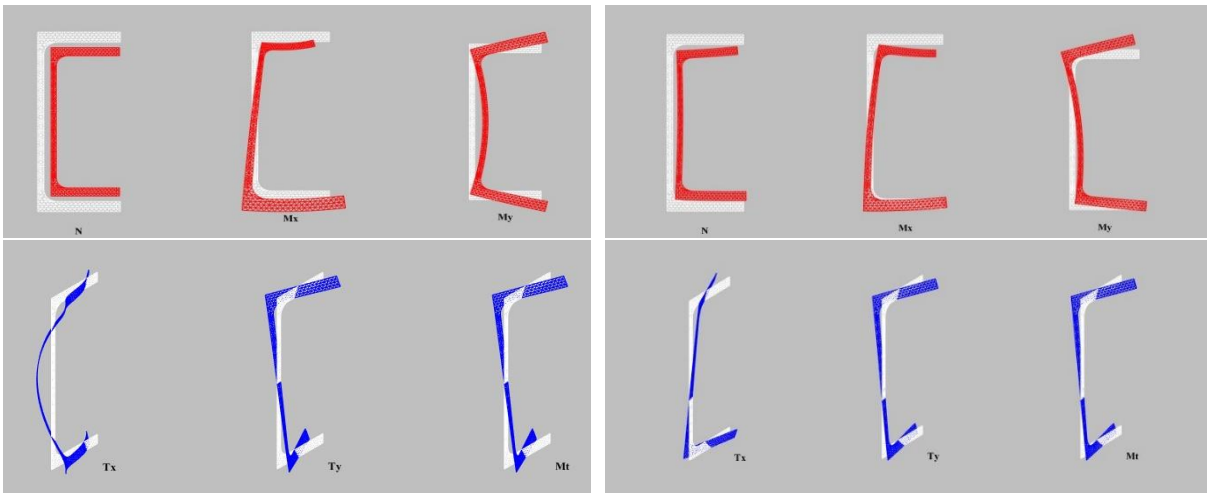

(a) Homogeneous case (b) FGM P=5

Fig 5. 21: Cross-section deformations: (Poisson effects and out-of-plane Warping) for the Homogeneous case (left side) and FGM P=5 (right side)

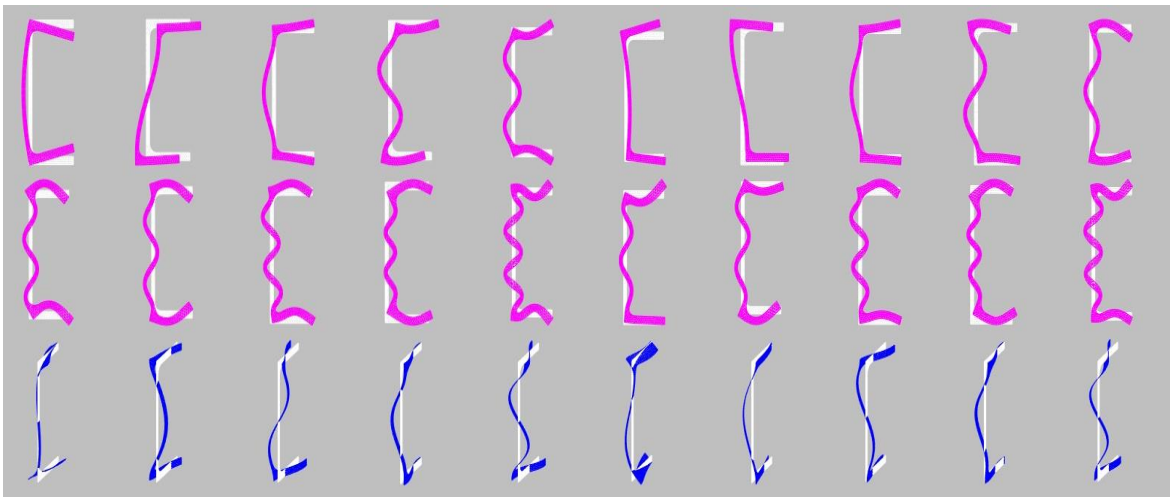

(a) Homogeneous case (b) FGM P=5

Fig 5. 22: Cross-section deformations: Distortion modes for the U-sections (Homogeneous case; left side), and (FGM P=5; right side): 10 in-plane (Pink colour) and 5 out-of plane (blue colour).

Table 5.6 shows the maximum torsional rotation for an FGM cantilever beam according to the three theories. We can see an approximate similarity in the RBT and RBT* values and an overall difference with respect to SVBT theory. Fig 5.24 shows the torsional rotation comparison differences for P=1, we find that RBT and RBT* values are much smaller than SVBT values (ω_z^{CBT} = -2.26e^{-2}) (ω_z^{RBT} = - 9.56e^{-3}, $\omega_z^{RBTd} = -9.37e^{-3}$) (see table. 5.6). We conclude that RBT and RBT* behaviour is stiffer than that expected by SVBT.

The comparison between the theories was systematically carried out for the most important components of the stresses for the FGM beam case, the axial stress σ_{zz} and the modulus shear stress $\tau = \sqrt{\tau_{xz}^2 + \tau_{yz}^2}$ in the various regions of the beam. Fig 5.25 shows the axial stress

fields when embedding and at the midspan of the beam, for the homogeneous and FGM beam cases. It can be observed that the SVBT results are completely different from the RBT and RBT* results at the embedding, and the results converge in the midspan. Moreover, we notice that the axial stress distribution is linear for the homogeneous case.

Table 5. 5 Maximum transverse deflection of an FGM cantilever beam for various values of power-law exponents, subject to loading on its free side (mm).

	Theory				
Power-law Exponent	SVBT	RBT	RBT*	Deflection Difference	
Full metal	-2.61E-03	-1.18E-03	-1.20E-03	CBT≈ 2.2 RBT	CBT≈ 2.16 RBT*
0.5	-1.23E-03	-5.94E-04	-5.87E-04	CBT≈ 2 RBT	CBT≈ 2 RBT*
1	-1.32E-03	-6.54E-04	-6.44E-04	CBT≈ 2 RBT	CBT≈ 2 RBT*
2	-1.42E-03	-7.10E-04	-7.01E-04	CBT≈ 2 RBT	CBT≈ 2 RBT*
3	-1.46E-03	-7.29E-04	-7.21E-04	CBT≈ 2 RBT	CBT≈ 2 RBT*
4	-1.49E-03	-7.41E-04	-7.25E-04	CBT≈ 2 RBT	CBT≈ 2 RBT*
5	-1.51E-03	-7.50E-04	-7.32E-04	CBT≈ 2 RBT	CBT≈ 2 RBT*
$p \to \infty$	-9.13E-04	-4.12E-04	-4.20E-04	CBT≈ 2.2 RBT	CBT≈ 2.17RBT*

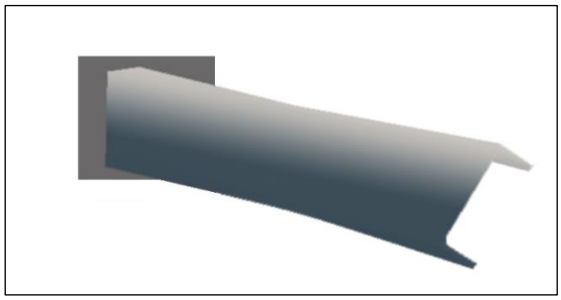

Fig 5. 23: 3D deformation of the FGM beam

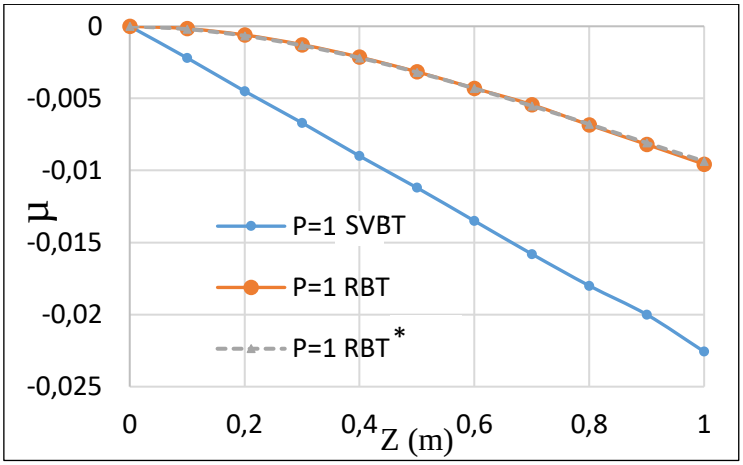

Fig 5. 24: Torsional rotation comparison for FGM cantilever beam according to SVBT, RBT and RBT* at P=1

Table 5. 6 Maximum torsional rotation for FGM cantilever beam according to SVBT, RBT, and RBT* (Unit rad)

Power-law Exponent	Theory		
	SVBT	RBT	RBT*
Full metal	-4.44E-02	-1.72E-02	-1.76E-02
P=0.5	-2.44E-02	-1.03E-02	-1.08E-02
P=1	-2.26E-02	-9.56E-03	-9.37E-03
P=2	-2.15E-02	-9.05E-03	-9.38E-03
P=3	-2.45E-02	-1.04E-02	-1.03E-02
P=4	-2.49E-02	-1.06E-02	-1.03E-02
P=5	-2.52E-02	-1.07E-02	-1.03E-02
$p \to \infty$	-1,56E-02	6.03E-03	-6.16E-03

This indicates that the axial stresses of SVBT only occur from the bending, but for the FGM case the axial stress is nonlinear. While the axial stresses of RBT and RBTd are completely different from those obtained by the SVBT theory. This diference results from the effect of both the bending- torsion warping stress (it is clear that torsion is of great importance) obtained by enrichment of the displacement field (higher-order beam theory). We also note that the axial stress results for RBT and SVBT differ from those of the RBTd at the mid-plane for the homogeneous case. In the FGM case P ≠ 0, the axial stress distribution is nonlinear and does not pass from the neutral axis (the line passing through the centre of gravity of the section z-axis). This is due to the variation in Young's modulus through the thickness of the FGM beam.

Fig 5.26 shows the axial stress (σ_{zz}) variations along the span for two points, A and B, belonging to the upper flange for the FGM beam. The results in Fig 5.26 were obtained through the present hypothesis, i.e. a non-deformable section at the level of the embedding for the SVBT model and deformable for RBT and RBT*. We can see a large difference between the stress results of the three theories at the level of embedding and a certain convergence between the results is observed far from the embedding. If the section is considered as being non-deformable for both models RBT and RBT*, the results are identical to those of SVBT. We conclude that RBT and RBT* theory takes into account edge effects in order to predict a 3D solution in a larger internal region to better describe the overall beam behaviour. According to SVBT, the 3D solution is an integral part and it describes the exact solution in the inner area of the beam. Fig 5.27 shows the comparison of the shear stress distributions at

embedding (Z=0) and (Z=L) through the three theories. We can see that the shear stress fields are clearly different (shape and values) for the three theories at the embedding area (Z=0). The shear stress results obtained in the CBT theory are due to the shear force (T_y) and the moment torsion (M_t). The deformations prevented in the case of RBT and RBT*, at the level of the embedding (Z=0), gave shear stresses that were totally different from the one obtained by the SVBT. Far from the embedding ($Z \neq 0$), the shear stress results are identical for SVBT and RBT but different for RBT* because of the enrichment of the displacement field by higher modes (distortion modes of the cross-section).

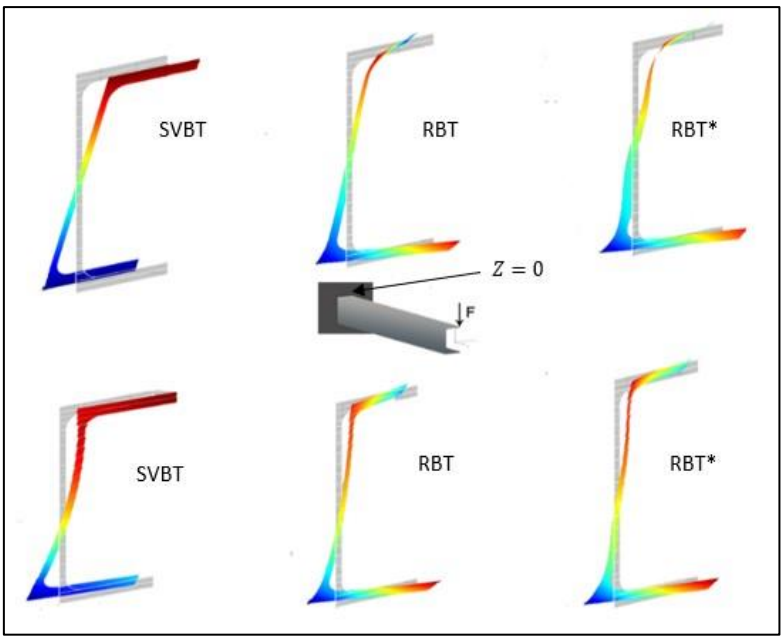

(a) Axial stress at Z=0

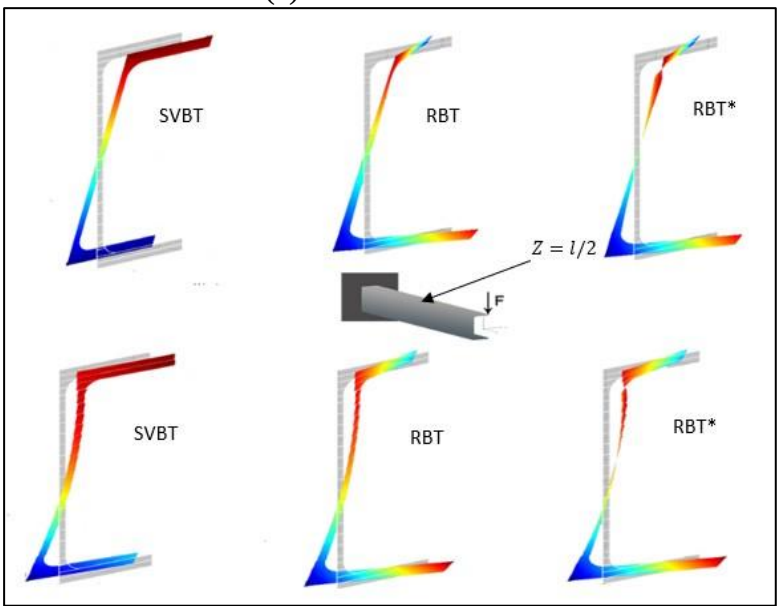

(b) Axial stress at Z=L/2

Fig 5. 25: Comparison of the axial stresses distributions at embedding (Z=0) and Z=h/2 obtained by SV's solution (SVBT), RBT and RBT*

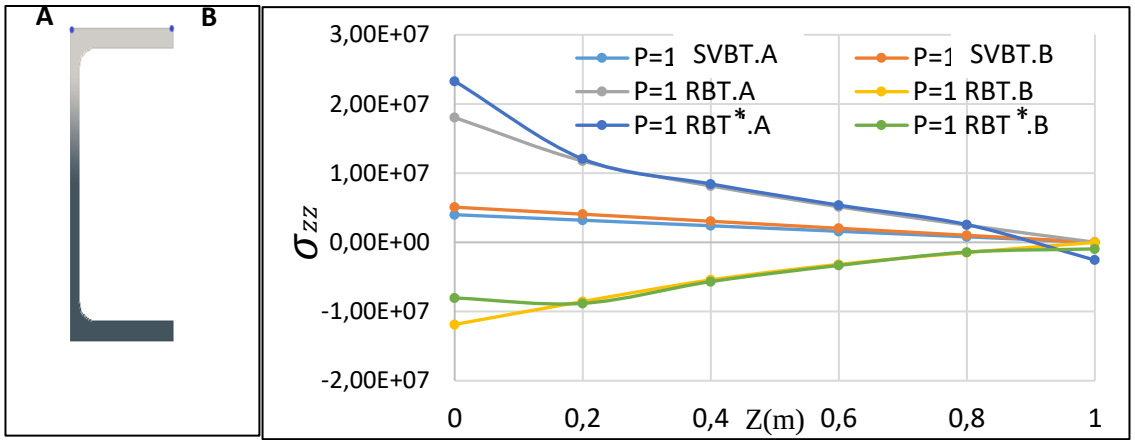

Fig 5. 26: Axial stress σ_{zz} variations along the span for two points A and B belonging to the upper flange for FGM at P=1

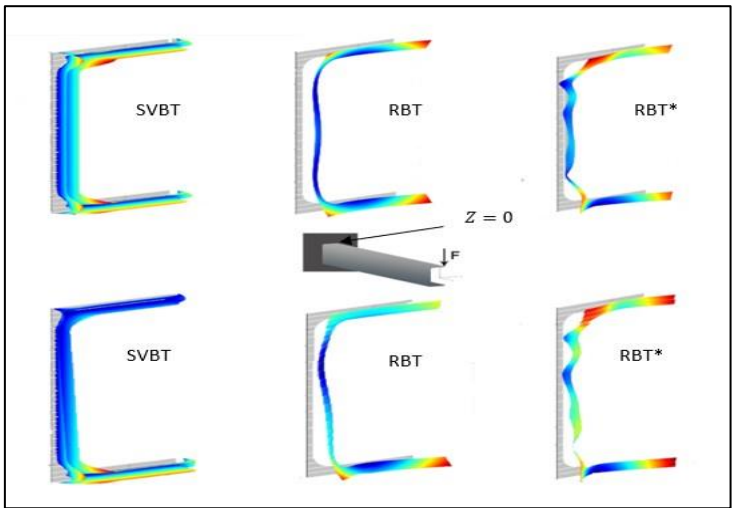

(a) shear stress at Z=0

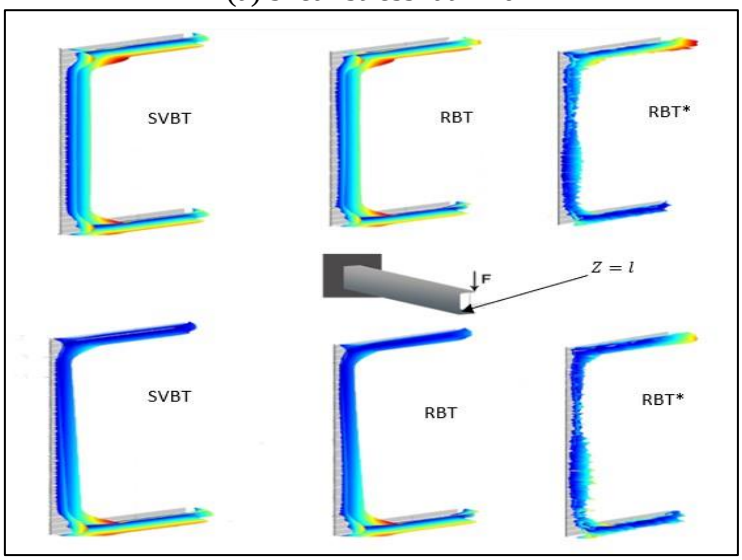

(b) shear stress at Z=L

Fig 5. 27: Comparison of the Shear stress distributions at embedding (Z=0) and (Z=L) obtained by SV's solution (SVBT), RBT and RBT*

5.1 Conclusion

The bending-torsional behaviour analysis of the functionally graded materials (FGMs) beams has been studied using a refined 1D/3D beam theories (RBT and RBT* built on the 3D SV's solution). The results include the main deformation modes of the cross-section (Poisson's effects, out-of-plane deformations and distortions), These cross-section modes are extracted from the associated 3D SV's solution for any given section and lead to a beam theory that really reflects the nature of the cross-section (shape and materials). which is important for FGM beams. In order to apply RBT/SV, a CSB package is used which has two tools, C-section and C-beam (complete each other). C-section calculates the mechanical characteristics of the cross-section by 2D FEM, then C-beam uses these mechanical characteristics to calculate the FGM beam by 1D FEM. Using the cross-section and beam problems , a 3D solution is given in more detail in terms of 3D displacements and deformations to analyze FGM cantilever beams.

The results of RBT models have shown that it is free of all the hypothesis of the classical beam and is applicable for an arbitrary cross-section. It is evident that RBT/SV is not only capable of describing the elastic structural performance of FGM beams, but also of providing a 3D solution in the major internal zone of the beam in terms of displacements and stresses (takes into account the edge effect). The axial stresses are the result of the bending stress and those induced by the torsional warping (actually the shear stress too, but it is clear that the torsional stress is more significant). As for SVBT, the axial stresses are those resulting from the typical SV's stresses in bending.

The shear stress field is completely different for the theories (shape and values) at embedding. For SVBT, the shear stresses are due to shear force and bending, while for RBT and RBT*, the inhibition stress resulted in a completely different shear field (degree of enrichment of cross-section strain modes). On the other hand, the results obtained by SVBT lead to a more flexible torsion behavior this is due to the fact that the embedding leaves the deformation of the cross-section free. The fact that this deformation may be blocked in RBT and RBT*, when compared to SVBT, to a stiffening of the torsional behavior (The rotation at the end is twice as small).

6 General Conclusion

A refined beam theories built on the 3D Saint-Venant's solution (RBT/SV) is presented and validated for equilibrium analysis of elastic beams of any homogeneous or FGM cross-section (shape and materials).

The kinematic model based on the RBT/SV allows the cross-section to deform in and out of plane depending on the cross-sectional deformation modes. These modes, which reflect the behaviour of the cross-section given its shape and the materials of which it is made, can be divided into two main groups:

- the first group, fundamental, is extracted from the 3D SV's solution; it reflects the warping and Poisson effects related to the six classical internal forces $(T_x, T_y, N, M_x, M_y, M_t)$.
- The second group, additional, is extracted from the natural vibrations of the cross-section and is introduced as cross-section distortion.

One of the unique features of RBT/SV is that it is free from all assumptions generally accepted for beams and is based only on the model displacement field's shape. Integrating from the outset deformation modes specific to the nature of the section (shape and materials), The application of RBT/SV is systematic and no distinction is made between homogeneous or heterogeneous, solid or thin, open or closed, symmetrical or not, isotropic or anisotropic material sections.

It is important to note that the kinematics adopted contains the shape of the 3D Saint Venant displacement field solution. This allows the suggested theory to find the 3D Saint Venant solution in the inner region of the beam and to better capture some of the edge effects. Furthermore, by using all the available Saint Venant functions to include the warps and Poisson's effects related to the six classical interior forces, RBT/SV can be seen as a very broad extension of Vlasov's theory, which is restricted to the hindered torsional warping of homogeneous and isotropic open thin cross-section beams.

The application of such a general beam theory, which aims to account for the complexity of the 3D mechanics of the section (anisotropic composite), is only possible numerically. This is why RBT/SV is accompanied by the CSB (Cross-section and Beam analysis) software (dedicated to the engineer) which allows its implementation and modeling of different FGM

beams. CSB also allows static thermoelastic calculations, natural vibration and buckling problems to be solved, and is currently being developed to solve corostion problems.

For a better treatment of the boundary conditions, the suggested approach consists in partitioning the beam into two domains: an inner zone for which the solution can be treated using beam theory and 1D finite elements (1D-FE), and another zone at the edges, for which the strong 3D solution is intended to be treated using 3D finite elements (3D-FE). This method allows to impose boundary conditions in the 3D zones precisely in 3D and liberates one from modeling them in a 1D or generalized sense. This approach is only useful (in terms of calculation cost) if the area to be used for 1D-FEM calculations is much larger than the area to be treated by 3D-FEM.

To illustrate the relevance of the refined beam theories, a significant set of examples is considered for the static analysis and vibration: several configurations of homogeneous or FGM cross-sections and different support conditions are treated. The results obtained for RBT models are systematically compared with other models in the literature, 3D-FEM which we also consider as a reference, and those provided by the full Saint-Venant beam theory (SVBT) calculations. Based on the comparisons, it can be concluded that the suggested beam theory (RBT/SV) is able to predict the global behaviour of beams satisfactorily while having access to local phenomena, for the static behaviour of FGM beams; and with a single formulation and systematic treatment, for a very large class of homogeneous, composites or FGM cross-sections.

Finally, it is important to remember that a beam theory remains a simplified approach whose objective is to approximate as well as possible the 3D reference solution for a low computational cost. Currently the CSB tool is operational and its extension has allowed to solve and illustrate all the problems (equilibrium, static thermoelastic, vibration and buckling).

References

[1] H.-S. Shen, *Functionally graded materials: nonlinear analysis of plates and shells*. CRC press, 2016.

[2] J. N. Reddy, "Analysis of functionally graded plates," *Int. J. Numer. Methods Eng.*, vol. 47, no. 1–3, pp. 663–684, 2000, doi: 10.1002/(SICI)1097-0207(20000110/30)47:1/3<663::AID-NME787>3.0.CO;2-8.

[3] J. Murin, M. Aminbaghai, J. Hrabovsky, R. Gogola, and S. Kugler, "Beam finite element for modal analysis of FGM structures," *Eng. Struct.*, vol. 121, pp. 1–18, 2016, doi: 10.1016/j.engstruct.2016.04.042.

[4] K. Yoon, P. S. Lee, and D. N. Kim, "Geometrically nonlinear finite element analysis of functionally graded 3D beams considering warping effects," *Compos. Struct.*, vol. 132, pp. 1231–1247, 2015, doi: 10.1016/j.compstruct.2015.07.024.

[5] V. Z. Vlasov, "Thin-walled elastic beams," *PST Cat.*, vol. 428, 1959.

[6] J. Yao, Z. Zhou, and H. Zhou, "Highway engineering composite material and its application," *Highw. Eng. Compos. Mater. Its Appl.*, pp. 1–163, 2019, doi: 10.1007/978-981-13-6068-8.

[7] P. Z. Tang, "Composite Material and Its Application Technology." Chongqing university press, Chongqing, 1998.

[8] Ever J. Barbero, *Introduction to Composite Materials Design 2nd Edition*. 2011.

[9] M. Maria, "Advanced composite materials of the future in aerospace industry," *Incas Bull.*, vol. 5, no. 3, pp. 139–150, 2013, doi: 10.13111/2066-8201.2013.5.3.14.

[10] S. J. Park and M. K. Seo, *Intermolecular Force*, vol. 18. 2011.

[11] Y. Zhou, M. Fan, and L. Chen, *Interface and bonding mechanisms of plant fibre composites: An overview*, vol. 101. Elsevier Ltd, 2016.

[12] V. Cech, E. Palesch, and J. Lukes, "The glass fiber-polymer matrix interface/interphase characterized by nanoscale imaging techniques," *Compos. Sci. Technol.*, vol. 83, pp. 22–26, 2013, doi: 10.1016/j.compscitech.2013.04.014.

[13] J. Payan, "Etude du comportement de composites stratifiés sous chargement statique et de fatigue." Université de la Méditerranée-Aix-Marseille II, 2004.

[14] K. Friedrich, “Fractographic analysis of polymer composites,” in *Composite Materials Series*, vol. 6, Elsevier, 1989, pp. 425–487.

[15] M. Koizumi, “The concept of FGM, ceramic transaction, functionally graded materials 34,” 1993.

[16] B. Kieback, A. Neubrand, and H. Riedel, “Processing techniques for functionally graded materials,” *Mater. Sci. Eng. A*, vol. 362, no. 1–2, pp. 81–106, 2003.

[17] J. S. Moya, A. J. Sanchez-Herencia, J. Requena, and R. Moreno, “Functionally gradient ceramics by sequential slip casting,” *Mater. Lett.*, vol. 14, no. 5–6, pp. 333–335, 1992.

[18] I. M. El-Galy, B. I. Saleh, and M. H. Ahmed, “Functionally graded materials classifications and development trends from industrial point of view,” *SN Appl. Sci.*, vol. 1, no. 11, pp. 1–23, 2019, doi: 10.1007/s42452-019-1413-4.

[19] D. Mahmoud and M. A. Elbestawi, “Lattice structures and functionally graded materials applications in additive manufacturing of orthopedic implants: a review,” *J. Manuf. Mater. Process.*, vol. 1, no. 2, p. 13, 2017.

[20] D. Almasi, M. Sadeghi, W. J. Lau, F. Roozbahani, and N. Iqbal, “Functionally graded polymeric materials: A brif review of current fabrication methods and introduction of a novel fabrication method,” *Mater. Sci. Eng. C*, vol. 64, pp. 102–107, 2016.

[21] A. K. Singh, “A novel technique for manufacturing polypropylene based functionally graded materials,” *Int. Polym. Process.*, vol. 33, no. 2, pp. 197–205, 2018.

[22] S. N. S. Jamaludin, F. Mustapha, D. M. Nuruzzaman, and S. N. Basri, “A review on the fabrication techniques of functionally graded ceramic-metallic materials in advanced composites,” *Sci. Res. Essays*, vol. 8, no. 21, pp. 828–840, 2013.

[23] B. Saleh, J. Jiang, A. Ma, D. Song, D. Yang, and Q. Xu, “Review on the influence of different reinforcements on the microstructure and wear behavior of functionally graded aluminum matrix composites by centrifugal casting,” *Met. Mater. Int.*, vol. 26, no. 7, pp. 933–960, 2020.

[24] R. S. Parihar, S. G. Setti, and R. K. Sahu, “Recent advances in the manufacturing processes of functionally graded materials: a review,” *Sci. Eng. Compos. Mater.*, vol. 25, no. 2, pp. 309–336, 2018.

[25] S. K. Bohidar, R. Sharma, and P. R. Mishra, “Functionally graded materials: A critical review,” *Int. J. Res.*, vol. 1, no. 4, pp. 289–301, 2014.

[26] Z. Y. Liu, C. Li, X. Y. Fang, and Y. B. Guo, “Energy consumption in additive manufacturing of metal parts,” *Procedia Manuf.*, vol. 26, pp. 834–845, 2018.

[27] H. Ziou, H. Guenfoud, and M. Guenfoud, “Numerical modelling of a Timoshenko FGM beam using the finite element method,” *Int. J. Struct. Eng.*, vol. 7, no. 3, pp. 239–261, 2016, doi: 10.1504/IJSTRUCTE.2016.077719.

[28] M. Khebizi, H. Guenfoud, M. Guenfoud, and R. El Fatmi, “Three-dimensional modelling of functionally graded beams using Saint-Venant’s beam theory,” *Struct. Eng. Mech.*, vol. 72, no. 2, pp. 257–273, 2019, doi: 10.12989/sem.2019.72.2.257.

[29] G. Ilies, G. Hamza, G. Mohamed, K. Mourad, and R. El, “Bending-torsional behavior analysis using a refined beam theory,” vol. 39, no. 1, pp. 2019–2022, 2021.

[30] H. GUENFOUD, “Modélisation par éléments finis spéciaux des structures en matériaux à gradient fonctionnel.” 2019.

[31] I. Guendouz, M. Khebizi, H. Guenfoud, M. Guenfoud, and R. El Fatmi, “Analysis of torsional-bending FGM beam by 3D Saint-Venant refined beam theory,” *Struct. Eng. Mech.*, vol. 84, no. 3, p. 423, 2022.

[32] S. Chi and Y.-L. Chung, “Cracking in coating–substrate composites with multi-layered and FGM coatings,” *Eng. Fract. Mech.*, vol. 70, no. 10, pp. 1227–1243, 2003.

[33] I. Guendouz, M. Khebizi, H. Guenfoud, and M. Guenfoud, “Analysis of FGM Cantilever Beams under Bending-torsional Behavior Using a Refined 1D Beam Theory,” *Period. Polytech. Civ. Eng.*, vol. 66, no. 4, pp. 1262–1277, 2022, doi: 10.3311/ppci.20595.

[34] L. Trabucho and J. M. Viano, “Mathematical modelling of rods,” *Handb. Numer. Anal.*, vol. 4, pp. 487–974, 1996.

[35] M. K. Ferradi, A. Lebée, A. Fliscounakis, X. Cespedes, and K. Sab, “A model reduction technique for beam analysis with the asymptotic expansion method,” *Comput. Struct.*, vol. 172, pp. 11–28, 2016.

[36] J.-S. Kim and K. W. Wang, “Vibration analysis of composite beams with end effects

via the formal asymptotic method," *J. Vib. Acoust.*, vol. 132, no. 4, 2010.

[37] V. L. Berdichevsky, "Variational-asymptotic method of shell theory construction," *PMM*, vol. 43, no. 4, pp. 664–687, 1979.

[38] V. V Volovoi, D. H. Hodges, V. L. Berdichevsky, and V. G. Sutyrin, "Asymptotic theory for static behavior of elastic anisotropic I-beams," *Int. J. Solids Struct.*, vol. 36, no. 7, pp. 1017–1043, 1999.

[39] V. V Volovoi and D. H. Hodges, "Theory of anisotropic thin-walled beams," *J. Appl. Mech.*, vol. 67, no. 3, pp. 453–459, 2000.

[40] W. Yu, D. H. Hodges, V. Volovoi, and C. E. S. Cesnik, "On Timoshenko-like modeling of initially curved and twisted composite beams," *Int. J. Solids Struct.*, vol. 39, no. 19, pp. 5101–5121, 2002.

[41] W. Yu, D. H. Hodges, V. V Volovoi, and E. D. Fuchs, "A generalized Vlasov theory for composite beams," *Thin-Walled Struct.*, vol. 43, no. 9, pp. 1493–1511, 2005.

[42] D. H. Hodges, *Nonlinear composite beam theory*. American Institute of Aeronautics and Astronautics, 2006.

[43] V. L. Berdichevskii, "On the energy of an elastic rod," *J. Appl. Math. Mech.*, vol. 45, no. 4, pp. 518–529, 1981.

[44] W. Yu, D. H. Hodges, and J. C. Ho, "Variational asymptotic beam sectional analysis–an updated version," *Int. J. Eng. Sci.*, vol. 59, pp. 40–64, 2012.

[45] W. Yu and M. Blair, "GEBT: A general-purpose nonlinear analysis tool for composite beams," *Compos. Struct.*, vol. 94, no. 9, pp. 2677–2689, 2012.

[46] E. Carrera, A. Pagani, M. Petrolo, and E. Zappino, "Recent developments on refined theories for beams with applications," *Mech. Eng. Rev.*, vol. 2, no. 2, pp. 14–298, 2015.

[47] S. M. Han, H. Benaroya, and T. Wei, "Dynamics of transversely vibrating beams using four engineering theories," *J. Sound Vib.*, vol. 225, no. 5, pp. 935–988, 1999.

[48] P. Ladevèze and J. Simmonds, "New concepts for linear beam theory with arbitrary geometry and loading," *Eur. J. Mech.*, vol. 17, no. 3, pp. 377–402, 1998.

[49] V. Giavotto *et al.*, "Anisotropic beam theory and applications," *Comput. Struct.*, vol. 16, no. 1–4, pp. 403–413, 1983.

[50] R. El Fatmi and H. Zenzri, “On the structural behavior and the Saint Venant solution in the exact beam theory: Application to laminated composite beams,” *Comput. Struct.*, vol. 80, no. 16–17, pp. 1441–1456, 2002, doi: 10.1016/S0045-7949(02)00090-1.

[51] R. El Fatmi, “A refined 1D beam theory built on 3D Saint-Venant’s solution to compute homogeneous and composite beams,” *J. Mech. Mater. Struct.*, vol. 11, no. 4, pp. 345–378, 2016.

[52] R. El Fatmi and N. Ghazouani, “Higher order composite beam theory built on Saint-Venant’s solution. Part-I: Theoretical developments,” *Compos. Struct.*, vol. 93, no. 2, pp. 557–566, 2011, doi: 10.1016/j.compstruct.2010.08.024.

[53] D. Iesan, “Saint-Venant’s problem for inhomogeneous and anisotropie elastic bodies,” *J. Elast.*, vol. 6, no. 3, pp. 277–294, 1976.

[54] R. El Fatmi, “Probl ` eme , Solution et Principe de Saint Venant,” pp. 1–8.

[55] F. Naccache and R. El Fatmi, “Buckling analysis of homogeneous or composite I-beams using a 1D refined beam theory built on Saint Venant’s solution,” *Thin-Walled Struct.*, vol. 127, no. January, pp. 822–831, 2018, doi: 10.1016/j.tws.2018.02.028.

[56] F. Naccache and R. El Fatmi, “Numerical free vibration analysis of homogeneous or composite beam using a refined beam theory built on Saint Venant’s solution,” *Comput. Struct.*, vol. 210, pp. 102–121, 2018, doi: 10.1016/j.compstruc.2018.08.005.

[57] K.-S. Hong, L.-Q. Chen, P.-T. Pham, and X.-D. Yang, “Beam Model,” *Control Axially Mov. Syst.*, pp. 53–123, 2022, doi: 10.1007/978-981-16-2915-0_3.

[58] E. Carrera and E. Zappino, “Carrera unified formulation for free-vibration analysis of aircraft structures,” *AIAA J.*, vol. 54, no. 1, pp. 280–292, 2016.

[59] O. Allix, E. Baranger, and L. Blanchard, “An efficient strategy for the calculation of end effects on composite pipes: The thermoelastic case,” *Compos. Struct.*, vol. 76, no. 4, pp. 291–302, 2006, doi: 10.1016/j.compstruct.2005.02.005.

[60] H. Ben Dhia and G. Rateau, “The Arlequin method as a flexible engineering design tool,” *Int. J. Numer. Methods Eng.*, vol. 62, no. 11, pp. 1442–1462, 2005, doi: 10.1002/nme.1229.

[61] J. Li, H. Hua, and R. Shen, “Dynamic stiffness analysis for free vibrations of axially

loaded laminated composite beams," *Compos. Struct.*, vol. 84, no. 1, pp. 87–98, 2008, doi: 10.1016/j.compstruct.2007.07.007.

[62] H. Yang, E. Daneshkhah, R. Augello, X. Xu, and E. Carrera, "Numerical vibration correlation technique for thin-walled composite beams under compression based on accurate refined finite element," *Compos. Struct.*, vol. 280, no. October 2021, 2022, doi: 10.1016/j.compstruct.2021.114861.

[63] J. Li, X. Hu, and X. Li, "Free vibration analyses of axially loaded laminated composite beams using a unified higher-order shear deformation theory and dynamic stiffness method," *Compos. Struct.*, vol. 158, pp. 308–322, 2016, doi: 10.1016/j.compstruct.2016.09.012.

[64] M. Şimşek, "Static analysis of a functionally graded beam under a uniformly distributed load by Ritz method," *Int. J. Eng. Appl. Sci.*, vol. 1, no. 3, pp. 1–11, 2009.